

*“Remember to look up at the stars and not down at your feet.
Try to make sense of what you see and wonder about what makes the universe exist.
Be curious.
And however difficult life may seem, there is always something you can do and succeed
at. It matters that you don't just give up.”*

— STEPHEN HAWKING

University of Alberta

**Studying Structure-Nanoaggregation Relations of Polyaromatic Molecules
in the Bulk Oil Phase and at the Oil-Water Interface Using Molecular
Dynamics Simulation**

by

Robel Berhe Teklebrhan

A thesis submitted to the Faculty of Graduate Studies and Research
in partial fulfillment of the requirements for the degree of

Doctor of Philosophy

in

Chemical Engineering

Department of Chemical & Materials Engineering

© Robel Berhe Teklebrhan

Spring 2014

Edmonton, Alberta

Permission is hereby granted to the University of Alberta Libraries to reproduce single copies of this thesis and to lend or sell such copies for private, scholarly or scientific research purposes only. Where the thesis is converted to, or otherwise made available in digital form, the University of Alberta will advise potential users of the thesis of these terms.

The author reserves all other publication and other rights in association with the copyright in the thesis and, except as herein before provided, neither the thesis nor any substantial portion thereof may be printed or otherwise reproduced in any material form whatsoever without the author's prior written permission.

Dedication

**This thesis is dedicated *to the memory* of my beloved late father,
*Berhe Teklebrhan.***

Abstract

The detection, identification and characterization of early stage molecular association of polyaromatic molecules into nanoaggregates, where these nanoaggregates represent the first level of molecular clusters or building blocks are critical in areas such as design and fabrication of advanced 3-D materials, drug carriers, petroleum and crude bitumen processing, etc. Molecular association of polyaromatic molecules (e.g., asphaltenes) in petroleum and crude bitumen processing, for example, leads to precipitation and deposition, which results in blocking of reservoir rocks and transport pipes. The deposition of these polyaromatic molecules has been linked to the solubility, aggregation and colloidal interactions in the system. To probe the aggregation and adsorption mechanism of the polyaromatic molecules in an organic medium and at the oil-water interface, various well-designed and custom-synthesized perylene bisimide-based polyaromatic molecules with only a subtle structural difference in their attached hydrophilic/hydrophobic side chains were used and systematically investigated by molecular dynamics simulations.

The results showed that variation in the structure of hydrophilic/hydrophobic side chains and polarity of functional groups leads to significant variations in molecular association, dynamics of molecular nanoaggregation and network formation of nanoaggregates. The aggregates of polyaromatic molecules grow to larger sizes in aliphatic than aromatic solvents. The aromatic solvent was shown to hinder molecular association by weakening π -

π stacking, demonstrating the control of molecular aggregation by tuning solvent properties. Larger size aromatic rings in polyaromatic molecules lower the interfacial activity of the polyaromatic molecules due to stronger intermolecular π - π interactions and molecular aggregation in the bulk oil phase. The protonated polyaromatic molecules are found to preferentially adsorb at the oil-water interface in a head-on (or side-on) orientation with the aromatic core staying in the nonaqueous phase. The major findings from this work provide scientific insights in polyaromatic molecular associations in nonaqueous systems and in the design of proper chemical demulsifiers for polyaromatic mediated emulsions formed under specific process conditions of temperature, pressure and pH of heavy oil production.

Acknowledgements

First of all, I would like to thank my supervisor Dr. Zhenghe Xu for his intellectual guidance, outstanding supervision and most importantly for his unconditional support and encouragement throughout my PhD program. Dr. Xu has been an astonishing and wonderful mentor to me for the past few years and I have learnt a lot from him both in academic and non-academic aspects of life. What impressed me the most besides other qualities he own is that his dedication, multi-tasking ability, hardworking and passion to engineering research projects with a tremendous skill and intelligence in connecting to practical challenges. He always reminds me to critically evaluate my findings and to look at the bigger picture of my work. Dr. Xu, many thanks for implanting the confidence in me to be a better human being as well as researcher in my area.

I would also like to express my heartfelt gratitude and appreciation to my magnificent co-supervisor Dr. Subir Bhattacharjee for his never-ending support, encouragement and personal guidance in shaping and guiding my study. His extensive knowledge, inquisitive mind, logical way of thinking and extremely fast in finding solutions to my modeling problems helped me ease my life throughout the research project. He is one of the most intelligent, energetic, extremely caring and outstanding professors you will ever have. I am grateful for that and thank you for being an inspiring professor and engineer to me.

I am also very grateful to Dr. Johan Sjöblom from the Department of Chemical Engineering, Ugelstad Laboratory, Norwegian University of Science and Technology (NTNU), for his insightful scientific guidance, support and

discussion we had with him in person at the University of Alberta by traveling thousands of kilometres throughout the tenure of my PhD research. Special thanks to Dr. Philip Choi and Dr. Tian Tang for the many critical scientific suggestions and support in revising my thesis. Also, I would like to thank Dr. Jacob Masliyah who initially inspired me to pursue a research in the oil sands. I also would like to thank Dr. Lingling Ge and Dr. Duo Wei of Yangzhou University (China) for their support in planning and executing numerous experimental techniques (DLS and 2D-NOSEY NMR).

I will forever be thankful to my colleagues and friends Dr. Louxiang Wang, Moise Dion, Dr. Alexandre Hahn Englert, Cuiying Jian, Dr. Qian Liu, Dr. Tanya Kuznicki, Teresa Bisson, Marjan Tamiz, Tenny Thomas, Zelalem Mekonnen, Dr. Wondim Teferi, Anand Natarajan and Dr. Plamen Tchoukov for their assistance during my graduate studies. I want to acknowledge and thank my friend Dr. Tesfalidet Asfaha from the University of Guelph for his unlimited support and motivation during my PhD program. Also, special thanks to Jonathan Clark, Jim Skwarok, Lisa Carreiro and Lily Laser for all their administrative and computational support. I am also grateful to the financial and material support from NSERC Industrial Research Chair in Oil Sands Engineering and Petromaks program (Norwegian Research Council) and JIP 1 (Ugelstad Laboratory). Special thanks as well to the Oil Sands and Coal Interfacial Engineering Facility (OSCIEF) for laboratory assistance and computational resources. Finally, I would like to express my sincere and heartfelt thanks to my beloved mother for her boundless love, moral and emotional support she has poured in me throughout my

long undergraduate and graduate studies. Special thanks as well to my wonderful sisters and my brother for their love, encouragement, patience and support in my academic journey. I would like also to thank Eng. Efreem Teklemariam and his wonderful wife Nazareth in particular for their assistance and support when times got tough. I also thank students and staff members of the Chemical and Material Engineering department at the University of Alberta for their support.

Table of Contents

CHAPTER 1	1
Introduction	1
1.1 Background.....	1
1.2 Challenges in Upstream Processing of Non-conventional Oils	7
1.3 Objectives of the Current Study.....	9
1.4 Organization of the Thesis	10
CHAPTER 2	12
Literature Review	12
2.1 Crude Bitumen Production from the Oil Sands	12
2.2 Crude Bitumen Analysis.....	16
2.2.1 Asphaltene Molecular Composition	18
2.2.2 Asphaltene Molar Mass and Elemental Composition.....	19
2.3 Asphaltenes at the Oil-Water Interface.....	21
2.4 Asphaltene Aggregation and Flocculation.....	25
2.5 Proposed Asphaltene Structures	26
2.5.1 Asphaltenes Model Compounds	28
2.5.2 Perylene Bisimide Derivatives.....	34
2.6 Summary	37
CHAPTER 3	39
MD Simulation and Experimental Methods	39
3.1 MD Simulation.....	39
3.1.1 Equation of Motion	40

3.1.2	GROMOS96 Force Field	41
3.1.3	Integration of the Equations of Motion.....	43
3.1.4	MD Simulation Parameters.....	45
3.1.4.1	Thermostats.....	46
3.1.4.2	Barostat	48
3.1.4.3	Periodic Boundary Condition	49
3.2	Experimental Techniques.....	50
3.2.1	Dynamic Light Scattering	51
3.2.2	Nuclear Magnetic Resonance	53
3.3	Validation of the Simulation Parameters	53
3.4	Summary	58
CHAPTER 4	60
Probing Structure-Nanoaggregation Relations of Polyaromatic Molecules: A	Molecular Dynamics Simulation Study	60
4.1	Introduction.....	60
4.2	Simulation Method.....	62
4.2.1	Molecular Models	63
4.2.2	Simulation Setup and Conditions	65
4.3	Experimental Methods	68
4.3.1	Materials and Solution Preparations	68
4.3.2	Dynamic Light Scattering	69
4.4	Results and Discussion	69
4.4.1	Nanoaggregate Formation and Growth.....	69

4.4.2	π - π Stacking with Side Chain Terminal Groups.....	76
4.4.3	Radial Distribution Function of Solvent Molecules near Polyaromatic Core.....	80
4.4.4	Effect of Intermolecular Interactions on Diffusion.....	82
4.4.5	Aggregation Behavior of PA Molecules in Toluene Studied by Dynamic Light Scattering.....	88
4.5	Conclusions.....	92
CHAPTER 5		95
Initial Partition and Aggregation of Protonated Polyaromatic Molecules at the Oil-Water Interface		95
5.1	Introduction.....	95
5.2	Details on Molecular Models and Simulation	98
5.3	Results and Discussion	103
5.3.1	Density Profiles of Protonated PA Molecules	103
5.3.2	Partition and Aggregation of Protonated Polyaromatic Molecules at the Oil-Water Interface	110
5.3.3	Intermolecular Hydrogen Bonding of Protonated PA Molecules at the Oil-Water Interface	118
5.3.4	The Preferential Orientation of Protonated PA Molecules at the Oil- Water Interface.....	120
5.3.5	Migration of PA Molecules from the Bulk Oil Phase to the Oil-Water Interface Assisted by Anionic Side-Chain Moieties.....	127

5.3.5.1 Density Profiles of Polyaromatic Molecules with Anionic Side-Chain Moieties	128
5.3.5.2 Preferential Orientation of Deprotonated Polyaromatic Molecules at the Oil-Water Interface	134
5.4 Conclusion	136
CHAPTER 6	138
The Influence of Naphthenic Acid on the Initial Partition and Aggregation of PA Molecules at the Toluene-Water Interface	138
6.1 Introduction	138
6.2 Molecular Modeling and Simulation Methods	139
6.3 Results and Discussion	144
6.3.1 Density Profiles of PA and NA Molecules	144
6.3.2 Partition of PA and NA Molecules at the Toluene-Water Interface	150
6.3.3 The Influence of NA Molecules on the Self-Association of Polyaromatic Molecules	153
6.4 Conclusions	159
CHAPTER 7	161
Summary and Conclusions	161
7.1 Major Conclusions and Contributions	163
7.2 Suggestions for Future Research	168
References	171
Appendix A	187

List of Tables

Table 3.1. Density, self-diffusivity and enthalpy of vaporization of toluene and heptane	57
Table 4.1. Compounds, molecular weights, and structures of PA molecules	64
Table 4.2. Composition of simulation systems.....	67
Table 4.3. Radius of gyration and number of aggregated molecules of the large nanoaggregate cluster in the simulated system.....	75
Table 4.4. Mean distance between two polyaromatic cores	78
Table 4.5. Radius of gyration of a single PA molecule in bulk phase.....	87
Table 4.6. Diffusion coefficient of PA molecules in heptane and toluene	88
Table 5.1. System composition and simulation setup	101
Table 5.2. Total number of water molecules around the interface-bound PA molecules at the end of the simulation time.....	118
Table 5.3. The average number of intermolecular hydrogen bonds per PA molecule.....	119
Table 5.4. Ratio of the number of protonated to deprotonated PA molecules, the ratio of the number of PA molecules in the large nanoaggregate of at the oil-water interface, and the average number of intermolecular hydrogen bonds	133
Table 6.1. Structures of polyaromatic and naphthenic acid molecules	142
Table 6.2. System composition and setup of PA and NA molecules	144
Table 6.3. Number of aggregated molecules of the large nanoaggregate cluster and the mean aggregate number of clusters	156

Table A.1. The average number of intermolecular hydrogen bonds per C5 Pe molecule at 298 K temperature and 1 bar	189
--	-----

List of Figures

Figure 2.1. Simplified schematics of bitumen production process from oil sands ore by Hot Water-based Extraction process.....	14
Figure 2.2. A typical schematic diagram of SARA fractionation method which is used for the fractionation of crude bitumen components based on solubility behaviour.	17
Figure 2.3. Bulk asphaltenes analysis by ESI FT-ICR MS.	19
Figure 2.4. Crude oil interfacial species adsorbed at the oil-water interface	22
Figure 2.5. Yen-Mullins model	26
Figure 2.6. The two proposed and equally competing models.....	27
Figure 2.7. Typical asphaltene model compounds used to represent asphaltenes molecules	30
Figure 2.8. Perylene bisimide structure.....	35
Figure 2.9. Typical examples of perylene bisimide	36
Figure 3.1. Simplified mathematical framework of GROMOS96 force field.....	42
Figure 3.2. The mathematical framework of Verlet algorithm	44
Figure 3.3. Schematic diagram of the periodic boundary conditions.....	50
Figure 3.4. The structure of N-(1-hexylheptyl)-N'-(2-indol-3-yl-propanoic acid)-perylene-3,4,9,10-tetracar-boxylicbisimide polyaromatic surfactant molecules (TP).....	54
Figure 3.5. (a) t vs. MSD for toluene; (b) t vs. MSD for heptane; (c) $\log(t)$ vs. $\log(\text{MSD})$ for toluene; (d) $\log(t)$ vs. $\log(\text{MSD})$ for heptane.	56

Figure 3.6. The diffusion coefficient as a function of concentration for TP molecules in chloroform at 298 K	58
Figure 4.1. Initial molecular arrangement of PAP molecules in toluene and heptane	66
Figure 4.2. Snapshots of molecular configurations of the five PA surfactant molecules in heptane and toluene	70
Figure 4.3. Radial distribution functions calculated from the PA center of mass of PA molecules in toluene and heptane at 298 K.	71
Figure 4.4. PAP-PAP radial distribution functions calculated from the PAP center of mass as a function of time in toluene and heptane	73
Figure 4.5. Normalized radial distribution functions.of polyaromatic core in toluene and heptane at 298 K.....	77
Figure 4.6. The configuration and steric hinderances of polyaromatic stacking between two PA surfactant molecules: (a) BisA - BisA T-shaped or tail-to-tail association, (b) PAP - PAP π - π polyaromatic stacking, (c) C5 Pe - C5 Pe π - π polyaromatic stacking, and (d) TP - TP π - π polyaromatic stacking	79
Figure 4.7. The RDFs of solvent molecules near a polyaromatic core of the PA molecules in toluene and heptane at 298 K.	80
Figure 4.8. Solvent-accessible surface area of the PA surfactant molecules over the simulation time of 20 ns in toluene and heptane at 298 K.....	81
Figure 4.9. Mean square displacement as a function of time for PA molecules in toluene and heptane at 298 K.....	83

Figure 4.10. (a-b) $\log(t)$ vs. $\log(\text{MSD})$ for BisA in toluene and heptane; (c-d) $\log(t)$ vs. $\log(\text{MSD})$ for PAP in toluene and heptane.....	84
Figure 4.11. (a-b) $\log(t)$ vs. $\log(\text{MSD})$ for TP in toluene and heptane; (c-d) $\log(t)$ vs. $\log(\text{MSD})$ for PCH in toluene and heptane; (e-f) $\log(t)$ vs. $\log(\text{MSD})$ for C5 Pe in toluene and heptane.....	85
Figure 4.12. Intensity-intensity time correlation functions vs. PA molecules concentration in toluene.....	91
Figure 4.13. Normalized scattering intensities (I) as a function of PA molecules concentration in toluene.....	92
Figure 5.1. Two-dimensional schematic representation of the PBI-based polyaromatic molecules	102
Figure 5.2. Density profiles of toluene-water and heptane-water systems containing various protonated PA molecules	104
Figure 5.3. Radial distribution function calculated from the center of mass between the PA molecules and water (a-b), and among PA molecules in the bulk oil phase (c-d)	106
Figure 5.4. Radial distribution function calculated from the center of mass between the aromatic side chain and the water (a-b), and the carboxyl groups of PA molecules and the water (c-d) averaged over the last 2 ns of the simulation time in toluene-water and heptane-water systems at 298 K.	108
Figure 5.5. Snapshots of molecular configurations of C5 Pe and TP molecules at the end of the simulation time.....	109

Figure 5.6. A schematic diagram showing the initial molecular arrangements of the PA molecules at the oil-water systems	111
Figure 5.7. The root mean square distance of C5 Pe molecules as a function of time from the oil-water interface (along z) in heptane-water system at 298 K.....	113
Figure 5.8. The root mean square distance of each layer of C5 Pe molecules as a function of time from the oil-water interface (along z) in heptane-water system at 298 K.....	114
Figure 5.9. The root mean square distance of different PA molecules and oil-water interface as a function of time in toluene-water and heptane-water systems at 298 K.	115
Figure 5.10. Partition ratio of the PA molecules in heptane-water and toluene-water systems averaged over the last 2 ns of the simulation time at 298 K.....	117
Figure 5.11. (a-d) The distance of the individual interface-bound PA molecules from the oil-water interface as a function of time averaged over the last 2 ns of the simulations time at 298 K.....	121
Figure 5.12. The schematic representation of the angle distribution (θ) of the polyaromatic ring plane of the PA molecules at the oil-water interface.....	122
Figure 5.13. (a-b). The number fraction of polyaromatic molecules averaged over the last 2 ns of the simulation time in toluene-water and heptane-water at 298 K.	124

Figure 5.14. (a-d). Snapshots of molecular configurations of C5 Pe and PAP at the toluene-water and heptane-water interface at the end of 10 ns simulation time.....	125
Figure 5.15. (a-b). The radial distribution function of polyaromatic cores of the interfacial-bound molecules at the oil-water interface averaged over the last 2 ns of the simulation time in toluene-water system and heptane-water system at 298 K.....	126
Figure 5.16. Density profiles of toluene-water and heptane-water systems containing various deprotonated PA molecules averaged over the last 2 ns of the simulation time at 298 K.....	129
Figure 5.17. The radial distribution function between the oxygen atom of the deprotonated carboxyl functional group (O^-_{-COO}) and the oxygen atom of the water molecules (O_w) averaged for the last 2 ns of the simulation time.....	130
Figure 5.18. The number fraction of deprotonated PA molecules averaged over the last 2 ns of the simulation time in toluene-water and heptane-water at 298 K.....	135
Figure 6.1. A schematic diagram showing the initial molecular arrangements of PAP, C5 Pe and NA molecules at the toluene-water systems	143
Figure 6.2. Density profiles of various uncharged PA and NA molecules at the toluene-water systems averaged over the last 2 ns of the simulation time at 298 K.....	147

Figure 6.3. Radial distribution functions calculated from the center of mass between PA and water (a), NA and water (b), among the polyaromatic core of the PA molecules (c), among the NA molecules (d), between –COOH of NA molecules and polyaromatic core (e), and between NA and PA molecules (f).....149

Figure 6.4. The root mean square distance as a function of time of PAP (a), C5 Pe (b), NA (c) molecules from the toluene-water interface. (d) Partition ratio of PAP, C5 Pe and NA molecules in toluene-water systems.....151

Figure 6.5. Radial distribution functions calculated from the center of mass among the polyaromatic core of the PA molecules (a), between NA and PA (b), and the mean aggregate number of clusters in pure toluene phase and at the toluene-water interface (c-d).155

Figure 6.5. Snapshots of PA molecules at the end of the simulation time in toluene.....158

Figure A.1. The root mean square distance of C5 Pe molecules from the oil-water (SPC or SPC/E) interface as a function of time in toluene-water and heptane-water systems at 298 K.....188

Figure A.2. Partition ratio of the C5 Pe molecules in oil-water (SPC or SPC/E) systems.....188

List of Acronyms

AV	Accessible Volume
D	Diffusion Coefficient
DLS	Dynamic Light Scattering
ERCB	Energy Resource Conservation Board
FFT	Fast Fourier Transform
GROMOS	GRONingen MOlecular Simulation
HWE	Hot Water-based Extraction
LB	Lattice Boltzmann
LLS	Laser Light Scattering
MD	Molecular Dynamics
MSD	Mean Square Displacement
NA	Naphtanic Acid
NFT	Naphtha-based Froth Treatment
NMR	Nuclear Magnetic Resonance
NOESY	Nuclear Overhauser Effect Spectroscopy
NPT	Isothermal-Isobaric Ensemble
PA	Polyaromatic
PBC	Periodic Boundary Condition
PBI	Perylene Bisimide
PME	Particle Mesh Ewald
RDF	Radial Distribution Function
RMSD	Root Mean Square Distance

SAGD	Steam-Assisted Gravity Drainage
SAM	Surface Active Molecules
SASA	Solvent Accessible Surface Area
SPC	Single Point Charge
VAPEX	Vapor Extraction Process
VMD	Visual Molecular Dynamics

Chapter 1

Introduction

1.1 Background

Non-conventional crude oils, such as crude bitumen, heavy oils and other unconventional hydrocarbon resources rich in complex mixtures of heavy organic compounds such as asphaltenes, resins, waxes, etc., are being increasingly explored to address the dramatic rise in the demand for fossil fuel energy and petrochemical products around the world.¹⁻³ To develop new technologies and tackle the numerous challenges the petroleum industry faces in extracting and processing these resources, a comprehensive and systematic understanding of the physico-chemical properties of the crude oil, the molecular interactions among the various crude oil components, their interactions with the solvent additives (diluent) and water during extraction, influence of pressure and temperature on their phase behavior, etc., is of paramount importance.

Crude oil is a complex mixture of various hydrocarbons and many other organic and inorganic molecules.^{1,2,4} Crude oil also contains a substantial amount of heteroatoms (i.e. sulfur, oxygen, nitrogen, etc.) and molecules containing heavy metals (i.e. iron, vanadium, nickel, etc.).^{4,5} In general, heavy oils and crude bitumen from different locations and depths of the oil deposits contain different

blends at variable concentrations of these various compounds. Because of this diversity, characterization of the individual molecules associated with crude oils is challenging, if not impossible. Consequently, fractionation based on solubility classes is often used as a means to classify crude oil and bitumen into four key classes of compounds. The most common and standard method for separation of crude bitumen into different crude oil fractions is the SARA (saturates, aromatics, resins and asphaltenes) fractionation.

A more modern approach toward petroleum characterization is petroleomics,⁶⁻⁸ which involves use of high resolution analytical techniques (2D GC-GC, FT-ICR-MS, LC-MS, ESI-MS, NMR, etc.) to identify the compounds and their isomers present in a crude oil, as well as various liquids (solvents) that come in contact with crude oil. These techniques provide significant insights regarding the molecular weight distribution, functional groups, elemental distribution, isomers, and a variety of other information regarding the petroleum chemistry. The broad objective of petroleomics is to associate these structural and molecular databases to the functional behavior of the systems, for instance, solubility characteristics, propensity of aggregation, emulsification, and fractionation. Such an approach eventually connects with the process engineering databases that can provide insight regarding the upstream and downstream processing of these fluids.

As noted above, although recent advances in petroleomic technologies have enabled us to easily identify and probe the fingerprints of some polar and non-polar constituents of the crude oil, they have failed to enlighten us on the

spatial and temporal resolutions of the molecular associations and the hierarchy of interactions in molecular nanoaggregate formation in the crude oil. It is important to note that molecular associations in crude oil lead to precipitation and deposition during crude oil transportation and production, which results in blocking of reservoir rocks and transport pipes.⁹⁻¹² Moreover, molecular association in crude oil also strongly influence the solubility, viscosity, density, and other physical properties of the crude oil under specific process conditions.⁹⁻¹⁷ Therefore, molecular based computational techniques such as molecular dynamics (MD) simulations are increasingly being combined or integrated with other experimental techniques to explore the time-dependent behavior of the molecular dynamics, molecular associations and nanoaggregate formation over an enormous range of spatio-temporal domains.

Molecular dynamics (MD) is a powerful molecular simulation technique combining molecular modeling followed by classical dynamics of an ensemble of molecules. MD modeling enables us to explore molecular interactions, track rapid processes, and their collective behavior at a nano scale.¹⁸ It also provides a link between microscopic and macroscopic system behaviors. MD modeling generally allows both the static and dynamic properties of the crude oil to be predicted directly from underlying interactions between molecules.¹⁸ It is used in a wide range of applications such as in examining chemical reactions and processes, structural evolutions, and other thermodynamic properties.¹⁹ MD modeling is also used for numerous predictions prior to synthesizing a molecule or carrying out actual experiments.¹⁹ Thus, more comprehensive features of the crude oil

constituents and their molecular structure-function relations can be obtained directly by using MD simulations, where no current experimental techniques are able to detect directly at a pico scale time. MD simulation technique is also used in predicting the free energy of association between different components of the crude oil and structure refinements in X-ray crystallography and NMR spectroscopy.²⁰

MD simulation methods are governed by the system's Hamiltonian formulation of mechanics, then followed by the integration of the Hamilton's equations of motion.²¹ Given the initial coordinates and velocities for all the atoms in a given system, the evolution of the atoms in time is fully determined.^{18,21} Thus, once a precise MD methodology, force field and simulation time were defined, both the structural and dynamic properties of the system can be predicted directly from the underlying interacting atoms in the system.

Recent advances in complex algorithms, simulation methods and powerful computer hardware are now helping us in narrowing the gap between actual system behaviors and quantitative models.²¹⁻³² For example, a hybrid molecular dynamics method such as molecular dynamics-Lattice Boltzmann simulation (MD-LB) has been developed into an alternative for experimental techniques studying complex engineering systems and modeling the physical phenomena and interactions in fluids efficiently and to some extent accurately.²²⁻²⁵ The MD-LB model is well suited and has shown some success a wide range of multi-phase fluid flow applications involving interfacial dynamics.²⁵ It is important to mention that, unlike other conventional numerical methods such as finite element methods,

MD-LB method is based on the microscopic models and mesoscopic kinetic theory equations.²⁵

Over the last decades, several researchers^{33-38,39-41} in the field of petrochemistry generally use hypothetical or imaginary molecules to model selective petroleum components under various system conditions using MD simulations with purpose to understand the physico-chemical properties of the crude oil.³³⁻³⁸ From their study, several insights and findings have been elucidated such as aromatic π - π stacking associations, solvent polarity and polar functional group interactions as key driving forces of molecular aggregation in crude oils.^{33-38,39-41} For example, Kuznicki *et al.* (2008)³⁴ reported an extensive MD study on the aggregation and partition of some petroleum components using a hypothetical model compounds in toluene, heptane and water.^{34,35} Results from their intensive MD simulation work identified stacking of the polyaromatic rings of the crude oil components as the dominant structural feature of the aggregates in all the solvents. Their study also showed that when molecules are ionized they have a distinct affinity to go to the toluene-water interface in comparison to the nonionized polyaromatic molecules, highlighting the importance of the dissociation of the carboxylic acid functional groups in the crude oil. Diallo *et al.* (2000)³⁸ also conducted an extensive MD simulation study on a number of in-house computer generated hypothetical model compounds over a wide range of pressure and temperatures to estimate the thermodynamic properties of some crude oil components such as the molar volume, density, cohesive energy, solubility parameter, heat capacity, isothermal compressibility, etc. Results from

their simulation study revealed that the change in pressure does not considerably affect the molar volume, solubility parameter and enthalpy of the simulated system, which is consistent with a number of experimental observations. A linear decrease on solubility parameter with temperature was reported in their study, which is consistent with the existing experimental observations.

Although these model compounds which were employed in the MD simulation to model the petrochemistry have proven to be useful for extracting some valuable information regarding crude oil components, they are not real molecules. As a result, their actual behaviours cannot be easily verified experimentally. Additionally, none of these putative model compounds has been developed to include strategic structural functional groups for further derivatization so that we can easily alter and study different components of the crude oil separately while keeping the core aspect of the crude oil behaviour intact. Furthermore, despite being hypothetical their study is also limited to the specific properties of the crude oil, overlooking different types of molecular associations present in the complex crude oil systems.

The lack of ideal or real model compounds with strategic structural functional groups for further derivatization hampers the proper exploration on the behaviour of crude oil components in the upstream and downstream processing environments. Thus, designing and synthesizing real molecules based on the findings from the high resolution analytical techniques is crucial. In this research, the ability of these model compounds which mimics the actual crude oil behaviour under extraction and upgrading conditions will be explored by MD

simulation and various experimental techniques. Model compounds synthesized and functionalized in-house based on the findings of the high resolution analytical techniques were used to study the physico-chemical properties of the crude oil components using MD simulations coupled with experimental techniques such as dynamic light scattering and nuclear magnetic resonance. The role of various crude oil components, individually or in combination, on the influence of aggregation and emulsion stabilization in crude oil is also examined.

1.2 Challenges in Upstream Processing of non-Conventional Oils

Asphaltenes are a solubility class compound library present in crude oils, which are characterized as bulky polyaromatic molecules comprised of condensed aromatic ring cores with attached alkyl side chains.^{5,9-11,38,42-49} They are the heaviest and most polar constituents of the crude oil. Asphaltenes are characterized as molecules insoluble in *n*-alkanes such as pentane and heptane, but soluble in toluene. The aggregation, flocculation and deposition of asphaltene molecules in the refineries, upgrading processes, reservoir rock formations, oil wells, pumps, storage vessels, transfer pipelines, etc., are a big challenge in the oil field industry.^{7,50} The deposition of asphaltene molecules has been linked to the solubility molecular aggregation and colloidal interactions in the system.⁵¹

Speight *et al.* (2004)⁴⁷ have reported extensively on the problems associated or that arise as a result of asphaltenes flocculation or deposition. The authors reported that the flocculation depends primarily on the production scale of the crude oil and the solvent added during the froth treatments. They mentioned

the following challenges in the oil field industry due to the presence of asphaltenes: (i) the well bore plugging and pipeline deposition; (ii) the formation of emulsions as a result of the water contamination during wellhead storage; (iii) sedimentation during crude bitumen storage; (iv) ignition delay and poor combustion due to high percentage of heavy organic compounds in the fuel oil, etc. Therefore, it is crucial to know these bulk polyaromatic molecules with attached alkyl chains and their associations in the bulk oil phase since very little data are available about chemical and physical properties of these solubility class molecules, in particular, during crude oil production and transportation.

Another big challenge in processing high levels of asphaltene content crude oil is the formation of emulsion in the system. Water-in-oil or oil-in-water emulsions are encountered at all stages during crude oil processing and transportation in all oilfield industries. While in industries such as pharmaceutical, food and cosmetics, emulsions are usually considered as desirable, but for the most part in oilfield industries and water treatment plants they are regarded as undesirable.^{44-48,52,53} The emulsified water droplets are known to contain salts such as chlorine.⁵ Even upon the elimination of the water at high temperature ends, the salts still linger in the crude oil products, which usually cause refinery catalyst poisoning, scaling and corrosion of pipelines and upgrading equipment.⁵ Moreover, because of the dramatic increase in the volume to be handled, these salt-containing emulsified water droplets can also increase the costs of transportation and refining. Therefore, removing the water droplets from the crude

oil is of great importance to reduce the processing cost and improve the final product quality.

It is believed that asphaltenes or bulky polyaromatic molecules form a steric interfacial film covering the water drops, thereby, provide stabilization against water droplet coalescence.^{45,49,54-58} Under these circumstances, the oil-water separation becomes extremely difficult. Several studies^{44-48,33-38,59-61} have shown that once the interfacially active asphaltenes are removed, crude oil emulsion ceases to remain stable. It has also been reported in the literature that a low concentration of asphaltene in the crude oils is sufficient to form stable emulsions.^{5,45,34,35} Thus, it is imperative to explore the mechanism of emulsion formation and stabilization by asphaltenes to aid to design of appropriate chemical demulsifiers under specific process conditions.

1.3 Objectives of the Current Study

The objectives of this study are:

- i) To investigate the molecular association, nanoaggregate formation and molecular dynamics of polyaromatic molecules in a bulk nonaqueous solution with the objective to gain molecular insight into the hierarchy of interactions in molecular nanoaggregation.
- ii) To examine the adsorption and partition behavior of polyaromatic molecules at the oil water interface. The effect of different substituent functional groups on molecular orientations, interfacial layering arrangements and dynamics at the interface is also studied in detail.

- iii) To explore the interaction between naphthenic acids and polyaromatic molecules in a bulk nonaqueous solution and at the oil-water interface.

The physico-chemical properties of the in-house synthesized asphaltene-like or polyaromatic model compounds in the bulk and at the oil-water interface were studied in this thesis research by using molecular dynamic simulations, dynamic light scattering and nuclear magnetic resonance. The model systems used were not a real crude oil-water emulsion but an artificial emulsion model system developed based on the information obtained through petroleomics. The data obtained from this study will then be used in predicting the physico-chemical properties of a crude oil to gain a better understanding of the oil wells and to optimize the upstream and downstream processes conditions.

1.4 Organization of the Thesis

The thesis is organized into seven chapters and the details of each chapter are described as follows:

Chapter 1 introduces the general background of this study and then followed by reviewing the use of model compounds in the MD simulation and current industrial challenges in the upstream and downstream processes in crude oil production.

Chapter 2 provides a detailed discussion on surfactant mediated emulsion formation and stability in the oil sands industry. The associations of heavy organic molecules in crude oil during transportation and production, and their role

in emulsion formation were reviewed. The previous work on the use of model compounds in the study of emulsion formation in oil sands processing was briefly reviewed.

Chapter 3 focuses on the general mathematical description of the molecular dynamics simulation method and the experimental techniques used in this study. The assumptions made and the validations of the modeling developed are also presented in this chapter.

The detailed computational and experimental results for the objectives stated in section 1.3 are analyzed and discussed in Chapter 4, Chapter 5 and Chapter 6 of this thesis. Conclusions were drawn based on our findings. Finally, the conclusions and summary of the entire research project with possible directions for future work are presented in Chapter 7.

Chapter 2

Literature Review

2.1 Crude Bitumen Production from the Oil Sands

In the last few years, the Canadian oil sands development program has been expanded exponentially to fulfill the demand of crude oil around the world. The Canadian oil sands deposits are gigantic, with a bulk of them located in the northern part of the province of Alberta.^{2,62} According to the Energy Resource Conservation Board (ERCB ST98, 2008),^{5,63} the initial in-place volume of the crude bitumen is estimated to be around 1.712 trillion barrels (or 271.9 billion cubic meters), of which 175 billion barrels are regarded as recoverable crude oil under the current economic conditions and available technologies.

Oil sands ore consists of naturally occurring mixtures of coarse sand, fine mineral solids, clays, water, electrolytes and crude bitumen.⁵ Depending on the quality of the oil sands ore, the amount of crude bitumen in the oil sands in general ranges from 0-16% by weight.⁵ The ore with bitumen content above 10% is usually considered high-grade oil sands ore.⁵ Bitumen is an extremely viscous and high molar mass unconventional oil. As a result, bitumen does not flow easily to the production wells under gravity and existing reservoir conditions.⁵ Crude bitumen extraction from the oil sands ore is usually achieved either by in-situ extraction method such as steam-assisted gravity drainage (SAGD), vapor

extraction process (VAPEX), etc. or by the traditional open-pit surface mining extraction process, depending on the depth of the oil sands deposits.^{5,64,65} In-situ bitumen extraction is usually used for oil sands deposits that are buried deep underground (> 200 meters) that cannot be economically accessed by open-pit mining.⁶⁴

The most common open-pit mining method in the extraction of crude bitumen from the oil sands ore is the Hot Water-based Extraction (HWE) process.⁵ In this extraction process, the oil sands ore is mined and crushed, followed by the addition of water, heat and other additive solvents to prepare oil sands slurry. Then, the prepared slurry is pumped into a hydrotransport slurry pipeline to help liberate bitumen from the bitumen-rich oil sands. During this mechanical shear process, air is usually injected into the hydrotransport slurry pipeline, in which the bitumen droplets are permitted to attach to the air bubbles. The aerated slurry is then pumped into the gravity separation vessels to recover the bitumen as bitumen froth as shown in Figure 2.1. At this stage the slurry is separated into primary bitumen froth, middlings and tailings.

The bitumen froths generated from the separation vessels and flotation cells, are complex mixtures of bitumen-continuous and water-continuous phases.⁵ The froth from these two steps contains approximately 60% bitumen, 30% water and 10% solids by weight, and is highly viscous. Consequently, hydrocarbon solvent is usually added to bitumen froth to lower the viscosity and density, which facilitates further water and solids separation from the bitumen froth.⁵

The main purpose of the froth treatment is to remove the aqueous phase and solids present in the bitumen froth for a clean bitumen product. Most of the hydrocarbon solvent is recovered from the diluted bitumen and reused in the operations. In general, even after extensive froth treatment, the solvent-diluted bitumen product still contains micron size water droplets in the form of water-in-oil emulsions and colloidal mineral particles ($\sim 0.5\%$).⁵

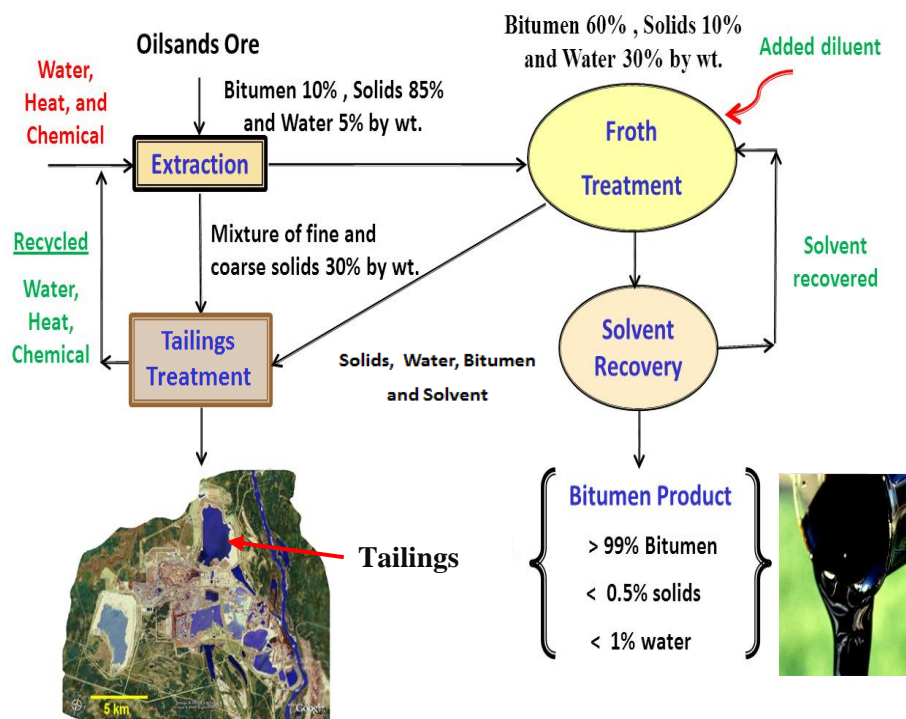


Figure 2.1. Simplified schematics of bitumen production process from oil sands ore by Hot Water-based Extraction (HWE) process. The Google view satellite map of the oil sands extraction and tailings pond site was taken from reference [66] and the diluted bitumen crude oil image was taken from reference [67].

A number of studies have shown that after the use of multiple stage centrifugation centrifuges and several stages of gravity settling, some emulsified

water droplets remain within the diluted bitumen.^{5,42,43,68-70} Generally, it has been reported in the literature that the final recovered diluted bitumen product contains 1-2% water, which is present as 1-5 μm diameter water droplets in the form of stable water-in-oil emulsion.^{42,43,68-70} There are two major technologies used in the oil sands operations to-date for froth treatment. These are naphtha-based and paraffin based froth treatment techniques.

Naphtha-based froth treatment (NFT) is a common technique employed by Suncor, Syncrude and CNRL. In this conventional technique, the solvent naphtha is usually added as a diluent at a reasonably low solvent to bitumen ratio to lower the bitumen froth viscosity and density. It has been reported that, in the naphtha-based froth treatment, no major heavy organic compounds such as asphaltenes are precipitated out throughout the treatment processes. Although the naphtha-based froth treatment easily removes the majority of the water and solids present in the froth product, a fairly high amount of water about 1% by weight and solids are still present in the final diluted bitumen product, regardless of the use of more settling area and demulsifiers.⁵

The second froth treatment method is the paraffinic solvent-based method. With the paraffinic solvent-based method, the collected froth is diluted with the paraffinic diluent such as *n*-heptane or hexane to a desired solvent to bitumen ratio. Although, the water and solid content of the final bitumen product decreases sharply as compared to the NFT, the method still suffers from a number of detriments.⁵ The addition of the paraffinic solvent always leads to the precipitation of the heavy organic components of the crude oil.⁵ Therefore,

monitoring the precipitation onset of the heavy organic compounds is an important factor in this froth treatment process.^{5,71,72}

Masliyah *et al* (2009)⁵ noted, the following two most common shortcomings of this method: (i) the settled layer of water, solids and precipitated heavy organic compounds in the waste tailings needs to be further handled to isolate each of the by-products, and (ii) during the froth treatment process some of the heavy organic compounds are removed from the diluted bitumen in which it negatively affects the overall bitumen upgrading strategies currently used in the oil sands sector. Despite the above mentioned drawbacks, however, the paraffinic froth treatment process is still a better method in treating emulsified water droplets than the conventional NFT method. The main reason is that it eliminates most of the water contaminants and fine solids from the bitumen froth. The removal of solid fines, in particular, is very important since it impacts greatly the bitumen upgrading process. Solid fines in the diluted bitumen always cause damage by reactor plugging and increasing the rate of coke formation.⁵

2.2 Crude Bitumen Analysis

SARA (saturated, aromatics, resins and asphaltenes) fractionation method as shown in Figure 2.2 is the most commonly used and standard method for separation of crude bitumen into various crude oil fractions. However, the details of the SARA fractionation and their characterization technique vary from one laboratory to another. It is therefore important to follow the same technical procedures when studying bitumen components.⁹ Based on this fractionation method, asphaltenes are first removed by precipitation from the crude oil using a

paraffinic solvent (i.e., n-heptane or pentane). The remaining maltenes or deasphalted oil is then further separated using different polar solvents into saturates (e.g., using hexane solvent), aromatics (e.g., using toluene solvent) and resins (e.g., using methanol solvent) by chromatographic column. Each fraction of the crude oil has different polarity, molecular weight, aromaticity and heteroatom contents.

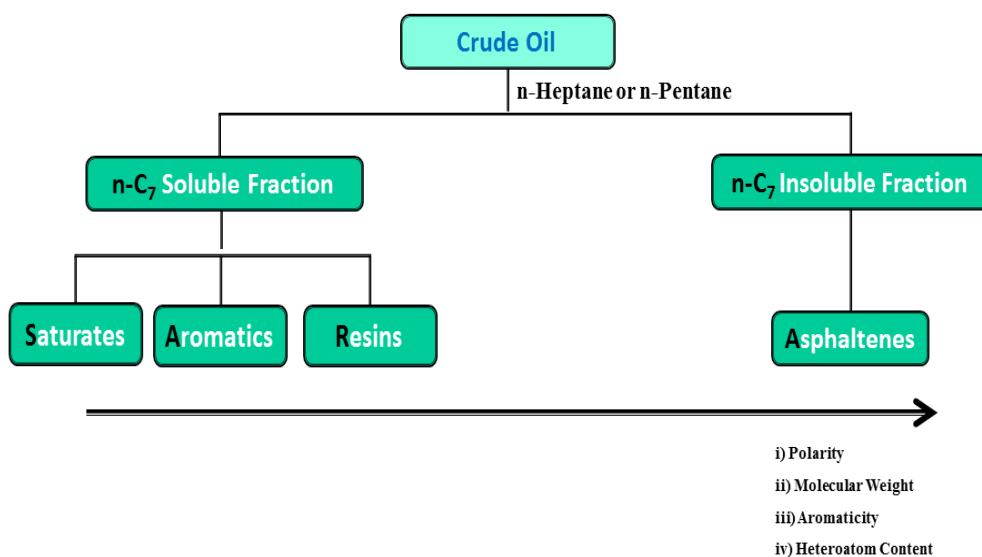


Figure 2.2. A typical schematic diagram of SARA fractionation method which is used for the fractionation of crude bitumen components based on solubility behaviour.

The saturate fraction of the crude oil generally contains aliphatic compounds, while the aromatic fraction of the crude oil mostly consists of an aromatic group with a very short aliphatic side chains attached. Resins are defined as the non-volatile and polar fraction of the crude oil that is soluble in the liquids that precipitate asphaltenes.^{5,45} Resins are commonly isolated or extracted from the crude

bitumen by adsorption onto a polar surface such as the hydrophilic silica particles. Resins possess lower molar mass, slightly higher hydrogen to carbon ratio, and lower heteroatom contents than asphaltenes.^{5,45,69}

2.2.1 Asphaltene Molecular Composition

Speight *et al.* (2004)⁴⁷ noted that the characteristics and amount of asphaltenes in a crude oil depend to a large extent on the source of the crude bitumen. Asphaltenes contain a wide range of functional groups. These functional groups include carboxylic, thiophenic, sulfide, hydroxy, pyridinic, pyrrolic, and a variety of other basic groups.^{5,47} As a result of this complex molecular composition and varying functional groups, the actual molecular weight and structure of the asphaltene compounds remain unknown.

One of the challenges in understanding asphaltenes is the difficulty associated with measuring the average molecular weight or their molecular weight distributions.^{12,73} This is mainly because asphaltenes tend to associate and form nanoaggregates even at an extremely low concentration. However, despite their molecular complexity and controversies on their molecular weight and chemical structure, their importance in petroleum processing, particularly their fouling propensity owing to aggregation and precipitation, is commonly acknowledged.

Klein and co-workers⁷⁸, in recent years, studied extensively molecular composition of bulk asphaltenes using ESI FT-ICR MS technique. Interestingly, they found over 6000 chemically distinct peaks, which in turn suggests that the composition of the precipitated asphaltenes are indeed a mixture of many distinct

compounds with different structures. Figure 2.3 shows the reported bulk asphaltene ESI FT-ICR MS result observed by Klein *et al.*⁷⁸

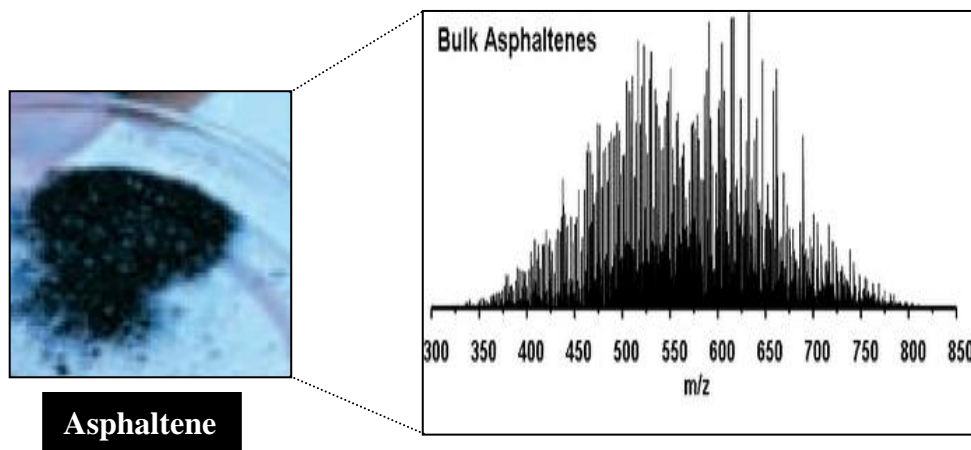


Figure 2.3. Analyses of bulk asphaltenes by ESI FT-ICR MS. The presence of over 6000 chemically distinct peaks indicates that asphaltenes are indeed a complex mixture of different compounds with different functional groups. The spectrum of Electrospray Ionization Fourier Transform Ion Cyclotron Resonance Mass Spectrometry (ESI FT-ICR MS) of the bulk asphaltene was obtained from the Klein research group at the Christopher Newport University: Petroleomics and Asphaltenes. Reproduced from [78].

2.2.2 Asphaltene Molar Mass and Elemental Composition

The most notable feature of asphaltenes in crude oil is their tendency to self-associate even at a very low concentration. Measuring the correct molecular weight and proper molecular structures of asphaltenes is difficult and usually leads to controversy among numerous scientists and engineers in the area of petrochemistry.^{74-77,79} Conversely, the extent of their aggregation in polar solvents

such as toluene is rather limited, terminating at the nanoaggregation level. It is equally important to emphasize that, not only the controversy revolves around its molecular weight, contentions also exist regarding the real cause of the molecular associations at extremely low concentrations. This is mainly due to the fact that the molecular functional group arrangements and structure of asphaltenes are not well defined.⁷⁴⁻⁷⁷ Nevertheless, it is widely believed that the van der Waals attraction between the large flat molecular area of the aromatic molecules is responsible for the onset of asphaltene nanoaggregations.^{34-38,79}

Over the years, various experimental techniques have been employed to derive the molecular weight of asphaltenes. The most widely used techniques are the vapor pressure osmometry (VPO), gel permeation chromatography, optics techniques, fluorescence depolarization, mass spectroscopy, etc.^{12,13,74-77,80-83} Although significant disparities on the measured “molecular weight” were observed from these experiments, the general consensus for asphaltene molar mass among scientists and engineers is started to settle with the mean values in the range between 700-800 g/mol.⁷⁵

Akbarzadeh *et al.* (2005),^{5,15,84} also reveals that with the exception of the Indonesian heavy oil, almost all of the n-pentane precipitated asphaltenes exhibit a density range between 1181-1193 kg/m³.^{5,84} It is also reported that the solubility parameter of C₇ asphaltenes ranges between 19 and 24 MPa^{0.5} at room temperature.^{77,85} As mentioned earlier, almost all asphaltenes irrespective of their source, contain heteroatoms such as oxygen, nitrogen, and sulfur. The elemental composition (in wt. %) of asphaltenes precipitated with n-heptane ranges ~ 78-

90% Carbon; 6.1-10.3% Hydrogen; 1.9-10.8% Sulfur; 0.7-6.6% Oxygen; 0.5-3.0% Nitrogen; and 0-1200 (ppm) Vanadium.⁴⁵

2.3 Asphaltenes at the Oil-Water Interface

Emulsion is a system containing a thermodynamically unstable dispersion of two immiscible liquid phases or mixtures in which one of them disperses as droplets or some sort of globules in the other.^{45-46,49,86-88} Emulsions are stable when the droplets of disperse phase do not coalesce or flocculate.⁷⁷ In general, the liquid which breaks up into droplets is termed as a dispersed phase, whilst the liquid surrounding the droplets as a continuous phase.^{45-47,49} It is reported in the literature that the stability of water-in-oil emulsions is steric in origin.^{5,45-47} Steric repulsion commonly referred to as the resistance of the adsorbed interfacially active species at droplet interfaces to interact with the adsorbed species on other droplets.⁵⁴ Figure 2.4 shows the nature of the steric interaction between two water droplets covered by the interfacially active species.

As mentioned above, emulsifying agents or interfacially active species are always required for the formation of emulsions during bitumen extraction and transportation processes. It is believed that asphaltenes and solid particles form a steric interfacial film covering the water drops, thereby, providing stabilization against water drop coalescence.^{45,49,54-58} Some of the emulsifying agents commonly found in crude bitumen are asphaltenes, resins, naphthenic acids and other materials such as iron, zinc and aluminum sulfates, calcium carbonate, silica, and iron sulfide.^{5,45-47,49}

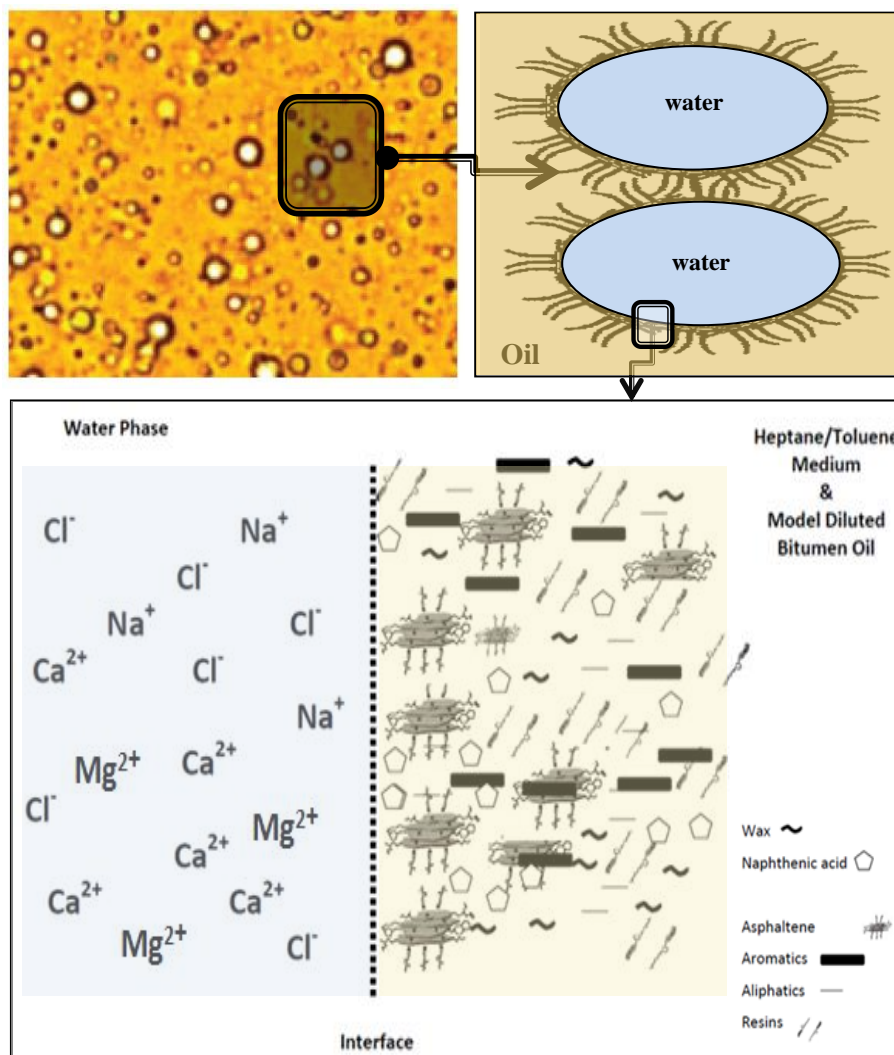


Figure 2.4. Crude oil interfacial active species adsorbed at the oil-water interface. The diagram also shows the nature of the steric interaction between two water droplets covered by the interfacially active species. Micrograph of water in diluted bitumen emulsions. Naphtha/Bitumen = 0.65, 5wt% water. Reproduced and modified from [5, 44, 54].

The interfacial film formed is composed of asphaltene aggregates that interact through donor-acceptor interactions.⁵ It has been reported in the literature that a low concentration of asphaltene in the crude oils is sufficient to form a

stable emulsion.^{5,45,34,35} Consequently, the interfacially active asphaltenes play a crucial role in emulsion formation and stabilization.

McLean *et al.* (1997)⁶⁹ stated that resins are non-volatile and polar fraction of the crude oil that are soluble in the liquids that precipitate asphaltenes. They often act as peptizing agents for asphaltenes in crude oils. It is well documented that resins do not participate in the formation of stable emulsions.^{43,44,69} However, the addition of resin to a constant asphaltene concentration increases the resin-asphaltene ratio (R:A), and hence decreasing the emulsion stability.^{69,43,44} This is achieved by making asphaltenes less surface active through strong solvation and formation of resin-solvated asphaltenic aggregates. Furthermore, McLean and co-workers pointed out that resin-solvated asphaltenic aggregates may lower their free energy by shedding the solvating resins on one side to form partially-solvated aggregates, which are interfacially-active and adsorb at the water-oil interface.^{43,44,69} It is important to note that, the extent to which the asphaltenes are solvated by resins is one of the most important factors controlling asphaltene aggregation at the oil-water interface.

Another important crude oil fraction, which affects emulsion stabilization is waxes. Waxes cannot act as emulsifying agents by themselves, but in conjunction with asphaltene and resin they can alter emulsion stability.^{49,89-94} Elsharkawy *et al.* (2009)⁹³ pointed out that, when the hydrophobic side of asphaltene aggregates adsorb on wax surface, its wettability will change from a total oil wet to biwetable. These solvated wax particles with the adsorbed asphaltene aggregates would then migrate to the oil water interface, contributing

to the stability of emulsions. Therefore the ratio of wax to asphaltene plays an important role in the formation of emulsions.^{54,67,93}

Oil aromaticity has also significant effect on the stability of emulsion. Several studies⁹⁴⁻⁹⁶ have shown that emulsion stability changes with the aromatic character of oil phase in a water-oil system. Førdedal *et al.* (1996)⁹⁶ observed that the aromatic nature of the oil phase has a greater impact on the stability of emulsion. They found that when the oil phase is a pure aromatic phase such as toluene, emulsions cease to exist. However, with pure aliphatic solvent as an oil phase, an emulsion of high stability was observed.^{95,96} The addition of the aromatic solvent creates an environment that is more conducive to the nature of the condensed polyaromatic asphaltenes (i.e., it neutralizes the surface-active nature of asphaltenes). Similar conclusion was also reached by McLean *et al.* (1997),⁶⁹ Li *et al.* (2002),⁹⁷ and Elsharkawy *et al.* (2008)⁹⁵. It is evident that the aromaticity of the oil phase plays a crucial role in emulsion formation and stability.

Sjöblom *et al.* (2002)⁹⁸ reported, in recent years, crude oils of higher than normal amounts of naphthenic acids in several oil field industries. As a result, some of the problems associated with emulsion issues during crude oil production are believed to be associated with the presence of enriched naphthenic acids in the crudes.⁹⁸⁻¹⁰⁰ Naphthenic acids are among the naturally occurring components in crude bitumen.⁹⁸⁻¹⁰⁰ These molecules adsorb at the oil-water interface in such a way that the polar groups are incorporated into the water phase while the hydrocarbon part of the molecules is oriented away from the water.⁹⁸ This phenomenon leads to the formation of surfactant film around the droplets that facilitates the process of emulsification. In

fact, it is believed that naphthenic acids compete with surface-active asphaltenes during crude oil production in the formation of emulsions.

Finally, the stability of emulsion is greatly affected by the salt concentration and pH of the aqueous phase. For example, at high pH of aqueous phase, the polar sites of the asphaltenes are subjected to complete ionization, leading to accumulation of charges on the interfacial film. This in turn destroys the skin surrounding the water droplets, and eventually breaking the emulsion. Increasing the salinity of the aqueous phase can also affect emulsion formation and stability by drastically reducing the Debye length in the double layer. Therefore, the concentration of the anionic and cationic species, and the pH of the aqueous phase play a crucial role in emulsion formation and stabilization.^{101,102}

2.4 Asphaltene Aggregation and Flocculation

The active sites on the surfaces of asphaltenes come together via different interaction mechanisms to irreversibly aggregate, flocculate and finally deposited in the system.⁵¹ As mentioned earlier, asphaltenes contain a wide range of functional groups such as carboxylic, thiophenic, sulfide, hydroxy, pyridinic, and pyrrolic with their mean molecular weight values in the range between 700-800 g/mol and density range between 1181-1193 kg/m³.

It is also reported that asphaltenes contain 4–10 number of fused aromatic rings per polycyclic aromatic hydrocarbon in asphaltene. The critical nanoaggregate concentration of asphaltenes is reported between 50–150 mg liter⁻¹.^{5,84,102} Based on the above information and other extensive experimental studies the conceptual framework of Yen-Mullins model was developed.^{16,60,76,102}

The modified Yen model (or the Yen-Mullins model), which conceptualizes the process of asphaltene aggregation and clustering mechanisms, is shown in Figure 2.5.^{16,60,76,102} The Yen-Mullins model was used as a guide in this research, particularly for our bulk phase study.

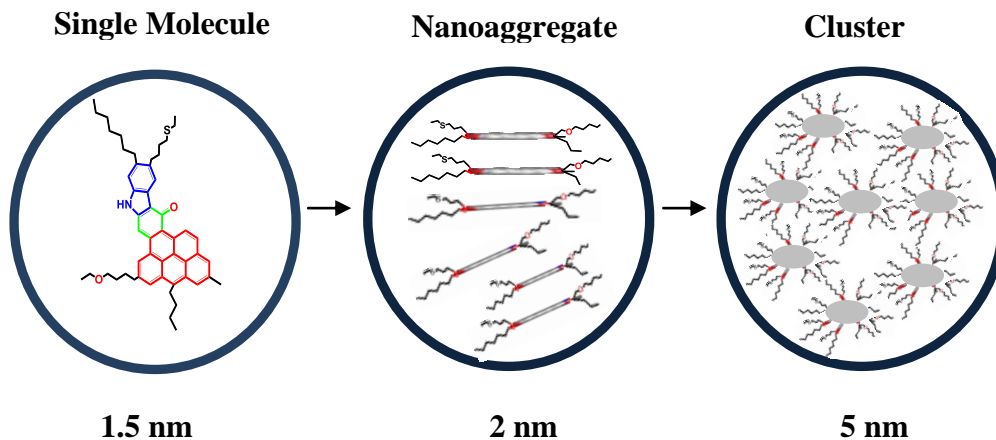


Figure 2.5. Yen-Mullins model. The model proposed by Yen and Mullins shows that the dominant molecular and colloidal structures for asphaltenes in laboratory solvents. Based on this model asphaltene molecules form nanoaggregates and then clusters with increasing concentration. Re-drawn from references [16, 60, 76, 102].

A better understanding of the chemical composition and structural features is vital in order to predict the aggregation onset of asphaltene molecules in their medium.

2.5 Proposed Asphaltene Structures

There still exists strong controversy regarding the “exact structure” of asphaltenes. Over the last decade, two equally competing models have been proposed to describe the anticipated chemical structure of asphaltenes based on

the experimental findings and consensus among the researchers in this area.^{34,35,102} These model structures are based on how the various functional groups or the aromatic cores of asphaltenes are arranged in the anticipated “real structure” of asphaltenes.^{34,35,102} These two competing models are known as “archipelago” and “continental” model as shown in Figure 2.6. The different functional groups are arranged at different active sites of asphaltenes in addition to the controversy of the aromatic core arrangements.^{34,35,102} The archipelago model describes asphaltenes as many aromatic cores interconnected by an aliphatic chain with different functional groups, while the continental model defines asphaltenes as a single aromatic core with aliphatic side chains of various functional groups.^{34,35}

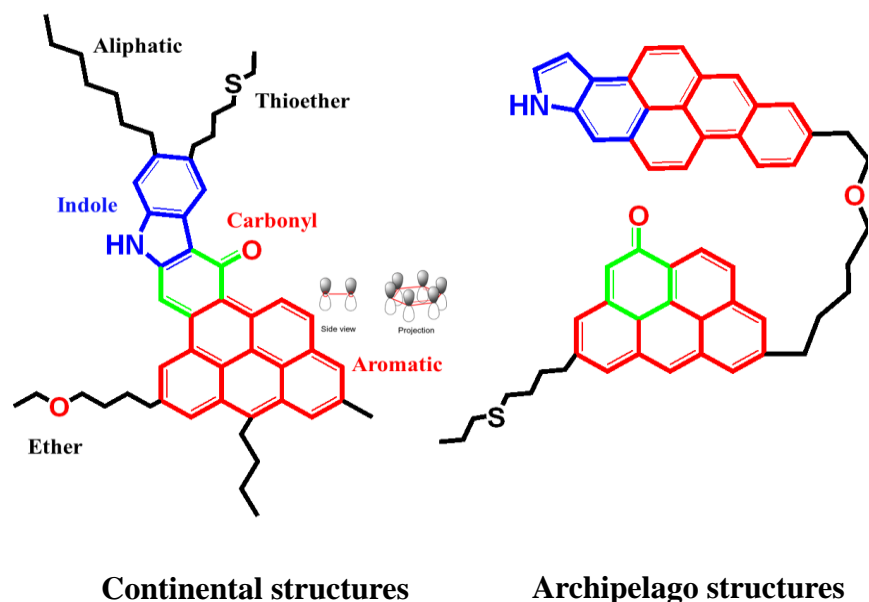


Figure 2.6. The two proposed and equally competing models for the “exact structure” of asphaltenes molecules. Re-drawn from references [34, 35].

The current research on asphaltenes using model compounds both experimentally or computationally revolves around these conceptual models of asphaltene structures. Although these two types of models have been proposed, the exact chemical identity of asphaltene remains unknown. They are equally valid and serve as a platform for designing model compounds in studying asphaltene physico-chemical behaviours. It is important to emphasise at this stage that the tendency of these asphaltene molecules to self-associate and form large aggregates or clusters is related to the structural arrangements of the functional groups.^{34,35}

2.5.1 Asphaltenes Model Compounds

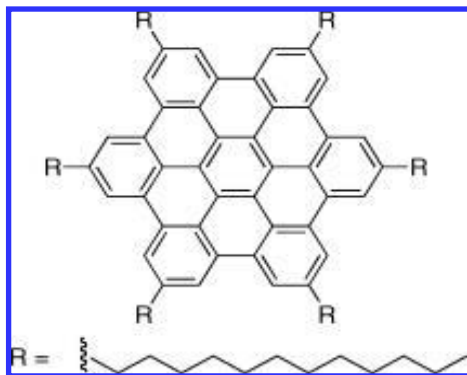
Many researchers have developed or used a number of asphaltene model compounds to study the structural stability and property of asphaltenes in various solution environments conditions.³³⁻³⁸ Some of the model compounds used to study asphaltenes are alkylated hexabenzocoronenes,³⁹ violanthrone-78 (VO-78),⁴¹ perylene bisimides (PBI),¹⁰³⁻¹⁰⁵ polycyclic aromatic hydrocarbons (PAHs), etc⁴⁰. Figure 2.7 shows some of the structures of asphaltene model compounds.

Sabbah *et al.* (2011)¹⁰⁶ studied extensively two competing model structures of asphaltenes (archipelago and continental) using a family of 23 model compounds and 2 petroleum asphaltene samples, and laser desorption laser ionization mass spectrometry. They found that all model compounds that resemble the archipelago nature of asphaltenes show little to no similarity to the observed behaviors for the two asphaltene samples, whereas the continental featured model compounds mimic the behavior of the real asphaltene molecules.

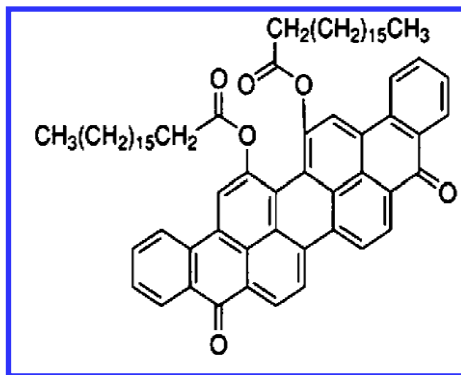
From their findings, they concluded that the dominant structural character of asphaltenes is island-like.¹⁰⁶ Their conclusion is based on the fact that asphaltenes and continental model compounds do not undergo fragmentation even under extremely severe fragmentation conditions, while the archipelago model compounds simply fragment with lesser power increase.¹⁰⁶ Moreover, their investigation was further supported by the recent experimental findings using scanning tunneling microscopy.^{102,107}

González *et al.* (2007)⁴¹ also observed that the adsorption of C₇-asphaltene from Athabasca bitumen and some model asphaltene molecules (amine modified Xylenol Orange, Violanthrone-78, and Violanthrone-79) on macroporous kaolin is independent of their molecular size. However, the molecular specificities such as structure and heteroatom content and type play a great role in the adsorption mechanism. They suggested that the continental type model compounds saturate the surface at a similar molecular extent as the sample asphaltenes, in contrast to the archipelago type, which saturates the surface plentifully.⁴¹ Although their study highlights the importance of different functional groups, how individually each functional group affects the adsorption process was not addressed in detail.

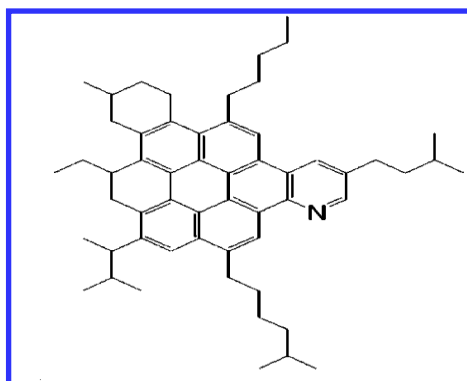
Rakotondradany *et al.* (2006)³⁹ reported an extensive study on polyaromatic model compounds (Alkyl hexabenzocoronene, HBC). Their study focuses on the self-association and aggregation behaviour of asphaltenes under typical extraction and upgrading conditions (e.g., over a range of temperatures).³⁹



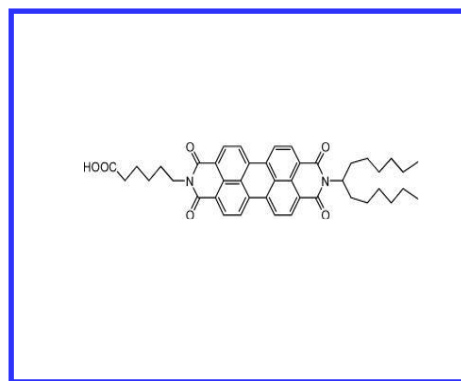
Rakotondradany *et al.* (2006)³⁹



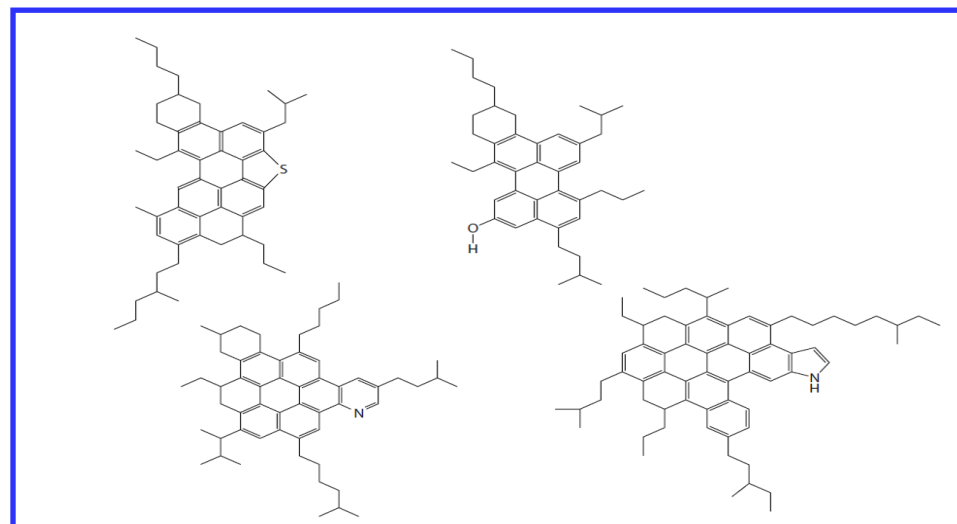
Gonzalez *et al.* (2007)⁴¹



Andrews *et al.* (2011)⁴⁰



Nordgård *et al.* (2008)¹⁰³



Mullins *et al.* (2011)¹⁰²

Figure 2.7. Typical asphaltene model compounds used to represent asphaltene molecules. Reproduced from references [39, 40, 41, 102, 103]

In their study, various experimental techniques were employed such as the vapor pressure osmometry (VPO), nuclear magnetic resonance (NMR), optical and electron microscopy, X-ray and small-angle neutron scattering, calorimetry (DSC/TGA) and high end computational simulation methods. The data from their study indicate that C₆HBC tends to form dimers at an extremely dilute solution and at temperatures as high as 400 °C, which is similar to the self-associate behaviour of asphaltenes even at an extremely low concentration and high temperature. They inferred that the self-association behaviour of the HBC model molecules is controlled by the interplay of alkyl-alkyl and π - π stacking interactions.³⁹

Headen *et al.* (2009)³⁷ for instance, presented a great work on modeling the dynamics of asphaltene aggregation using molecular dynamics simulations. They reported that nanoaggregation occurs in both toluene and heptane solvent. The aggregates persist for longer durations in heptane than in toluene. From their work, they concluded that the free energy of dimer formation for asphaltene molecules in both toluene and heptane ranges from -6.6 to -12.1 kJ mol⁻¹. This suggests the reason behind the formation of dense nanoaggregates in both solvents as observed by Small-angle X-ray scattering and small-angle neutron scattering (~5-10 nm).^{37,108-110}

Kuznicki *et al.* (2008)³⁴ reported extensive studies on the aggregation and partitioning of asphaltene-like model compounds with similar molecular weights in toluene, heptane and water.^{34,35} The most important contribution of their work is that, interfacial activity of these model compounds depends more on their

terminal groups rather than on their polyaromatic ring regions. Similar conclusions were reached regarding the importance of terminal functional groups by González *et al.*⁴¹ Follow-up work on these model molecules (Kuznicki *et al.* 2009)³⁵ revealed that all model asphaltene compounds partitioned completely into the toluene phase in the binary systems of toluene and water, indicating a strong affinity to partition completely into the oil phase rather than the water phase. Another important findings from their work is that while the ionized asphaltene model compounds (-COO⁻) remained cemented to the toluene-water interface, the uncharged asphaltene molecules (-COOH) prefer to aggregate in the bulk toluene phase, further demonstrating the importance of charge or pH in the system.^{34,35}

Pacheco-Sánchez *et al.* (2003)¹¹¹ conducted classical molecular dynamics simulations on 96 hypothetical asphaltene model molecules at different temperature ranges. Results from their study suggested that aggregation of different structures has different interactions, and the average number of asphaltene molecules in aggregates decreases with increasing temperature. Moreover, in their simulation work they also calculated the minimum of the potential energy well, which is in the range of 3.5 - 4.0 Å. Their work was mostly based on the gas phase, and the environmental factors such as the solvent effects were ignored. However, they were among the first to report on the minimum of the potential energy well using molecular dynamics simulation methods and correlated their results with the Yen model. Follow-up work (Pacheco-Sánchez *et al.* 2004)¹¹² was performed on various asphaltene model compounds in an attempt to understand the morphology of the aggregated asphaltene model molecules

using molecular dynamics simulations. Based on their results, it was concluded that face-to-face stacking is one possible scenario in asphaltene aggregates. Various other stackings such as π -offset and T-shaped stacking geometries were other possible ensemble structures that exist in the system.¹¹²

Murray *et al.* (2011)¹¹³ recently proposed a new approach in the way we perceive asphaltenes in crude oil. They claimed that the various components of the asphaltene molecules such as the carboxylic, thiophenic, sulfide, hydroxy, pyridinic, pyrrolic, and the aromatic core exhibit complex bridged structural organization of asphaltenes aggregating be it in a diluted bitumen or toluene solvent over a range of concentration and temperatures.

Consequently, they suggested that an asphaltene architecture dominated only by an aromatic stacking does not fully capture the essence of real asphaltene aggregation in a real system. Based on their extensive literature survey on the chemistry of asphaltenes and existing experimental and computational data, they proposed an alternative molecular association paradigm based on the concept of supramolecular assembly of molecules by incorporating different interaction phenomena such as Brønsted acid-base interactions, metal coordination complexation, hydrogen bonding, aromatic π - π stacking, interaction of alkyl groups that form hydrophobic pockets, etc. Finally, they suggested that model compounds based on elucidating different types of supramolecular association is a good approach in mimicking the complex architecture of asphaltenes.

2.5.2 Perylene Bisimide Derivatives (PBI)

Perylene based model compounds to represent asphaltenes have become a unique idea in the last few years since the aromatic core of these molecules can be easily altered through simple synthetic routes. Perylene bisimide derivatives, shown in Figure 2.8, are a class of distinct organic compounds with abundant applications.¹¹⁴⁻¹²³ They are unique compounds for their optical and electronic properties, chemical robustness, thermal stability, extended quadrupolar π system and high fluorescence quantum yields.¹¹⁴⁻¹²³ As a result of these distinct characteristics, they have found widespread and promising applications in many areas including thin film transistors, photovoltaic and fluorescence sensors, liquid crystals and the construction of self-assembling nanostructures, pigment and laser dyes, organic solar cells, etc.¹¹⁴⁻¹²³

The most fascinating aspect of these compounds is the dynamic control over the supramolecular interactions or assembly of the molecules you have by incorporating a photoswitchable unit at the side chain of the aromatic core.¹²⁴ For example, Wang *et al.* (2010)¹²⁴ demonstrated that the optoelectronic and aggregate properties of the perylene backbone can be tuning by pH. The results from their work showed a clear reversible aggregation or stacking modes by changing the pH of the system (using pH as assembly control mode). This intrinsic switchable property of these molecules makes them good candidates as asphaltene model compounds since pH is a key factor in the extraction of bitumen from the oil sands.

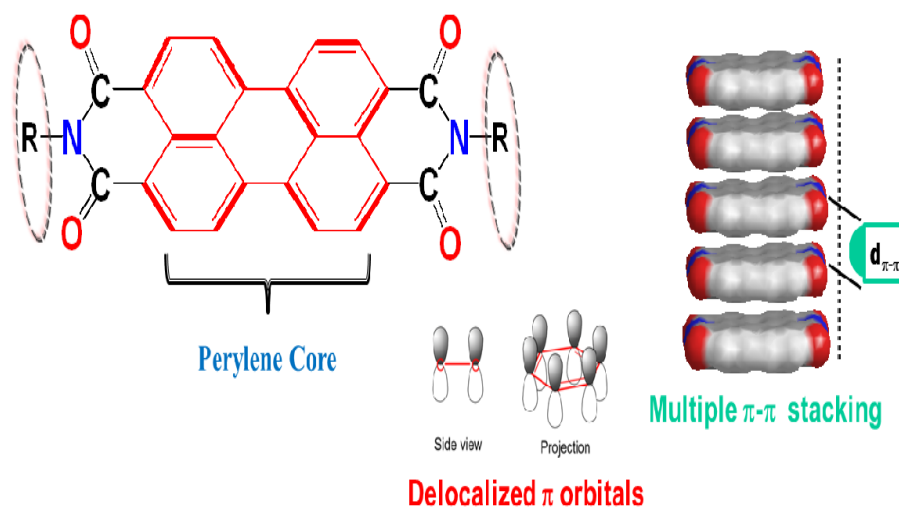
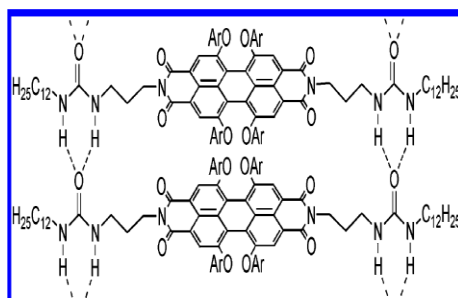
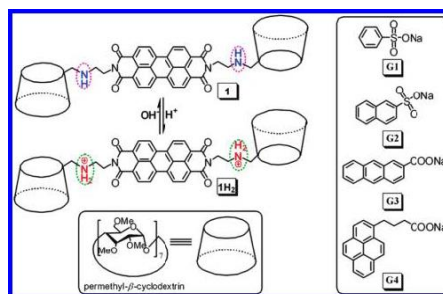


Figure 2.8. Perylene bisimide (PBI). The aromatic core of the molecule is perylene.

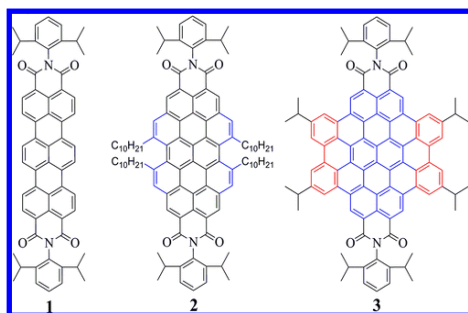
Ghosh *et al.* (2008),¹²⁵ also performed a series of experimental studies using UV-visible and CD spectroscopic, gelation tests and AFM to investigate the influence of peripheral alkyl side chains on the self-assembly and gelation properties of various structurally similar perylene bisimide derivatives. Results from their study reveal that depending on the nature of the alkyl substituents, different stacking phenomena were observed. Moreover, they indicated that the self-assembly mode of the system is largely dictated by the steric effect at the peripheral side chains of the aromatic core. They further revealed that the nature of the side chain (branched or linear alkyl groups) also has a tremendous impact on the self-aggregation mode of the stacking. With the aim of expanding the molecular optoelectronics applications of perylene bisimide derivatives numerous moieties or units were incorporated to perylene bisimide derivatives.



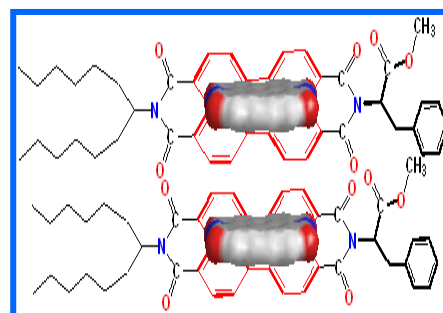
Würthner *et al.* (2005)¹²⁷



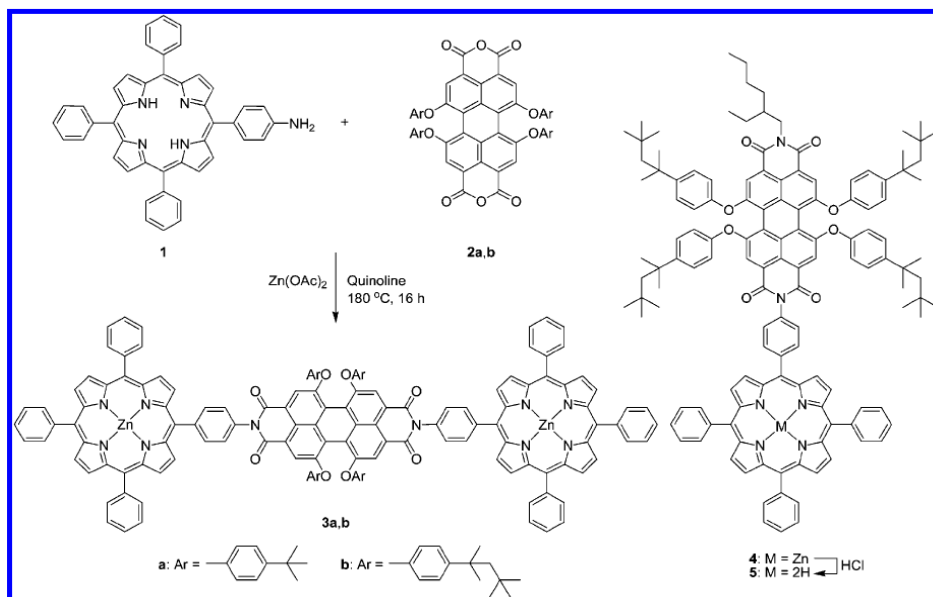
Wang *et al.* (2010)¹²⁴



Yongjun *et al.* (2011)¹²⁸



Nordgård *et al.* (2010)¹⁰⁵



Würthner *et al.* (2004)¹²⁹

Figure 2.9. Typical examples of perylene bisimide (PBI) derivatives. Reproduced from references [105, 124, 127, 128, 129]

For instance, Wasielewski *et al.* (2005)¹²⁶ were among the first who linked perylene bisimide with porphyrin moieties in the design of light-intensity dependent molecular biphotonics. In their study they synthesized two porphyrin donors rigidly attached to a perylene bisimide moiety.

Würthner *et al.* (2005)¹³⁰ recently developed perylene bisimide incorporated with zinc porphyrins. Their characterization showed a self-assembled oligomeric zigzag assembly. Therefore, the further functionalization of the PBI molecules by incorporating porphyrins in their building blocks is a special property that resembles certain constituents of the crude oil.⁴⁵

2.6 Summary

From the above literature review, it may be concluded that most of the existing modeling and simulation studies on asphaltene aggregation and adsorption were based on hypothetical model compounds in varying system conditions. Although most of the model compounds employed in these studies have proved useful in providing valuable information regarding crude oil behaviour, most of these molecules are not real molecules, and hence, these studies do not allow experimental validation of any of the simulation results. In addition, none of these hypothetical model compounds were designed with strategic structural and functional groups, such that one can easily alter and study diverse components of the crude oil separately while keeping the core feature of the crude oil behaviour intact. Thus, a synthetic and easily functionalized model compound, which mimics the actual crude oil behaviour under extraction and upgrading conditions, will be used in this thesis to explore the physico-chemical

properties of the crude oil components using MD simulations coupled with experimental techniques such as dynamic light scattering and nuclear magnetic resonance.

Chapter 3

MD Simulation and Experimental Methods

3.1 MD Simulation

Advances in both simulation speed and force field accuracy recently enabled us to simulate complex multi-phase fluid applications involving interfacial dynamics, macromolecular systems and biological systems.²²⁻³² However, the need to optimize the algorithm or find better simulation models that can work in an efficient way with the limited resource we have is also crucial. The fundamental and basic idea of MD simulation is to study the property of the molecules at an atomic level so that the macroscopic properties of the system can be predicted.²⁵ This is due to the fact that the collective behaviors of the many atoms that exist at the microscopic level determine the macroscopic dynamics of the system.

MD simulation was first introduced by Alder and Wainwright in the late 1950s¹³¹⁻¹³⁵ to study the condensed phase systems using a hard-sphere model. In this section, we describe the equations of motion, force field and the algorithm for integrating the equations of motion in greater detail.

3.1.1 Equation of Motion

For a system of N atoms treated at the classical mechanics level, the time evolution of a set of interacting atoms in the system is followed by the solution of the Newton's equation of motion^{18,19, 136,137} During the time evolution of the system, each atom is treated as a single point with a mass of m_i and charge of q_i . Thus, the Newton's equation of motion for all interacting atoms in the system is given by the following equation:

$$F_i(t) = m_i a_i(t) = m_i \frac{dv_i(t)}{dt} = m_i \frac{d^2 r_i(t)}{dt^2} \quad (3.1)$$

where $r_i(t) = (x_i(t), y_i(t), z_i(t))$ is the position vector of i^{th} atom in the system with F_i force acting upon it at time t . $v_i(t)$ and $a_i(t)$ describe the velocity and acceleration of i^{th} atom in the system, respectively. The atomic accelerations are computed from the forces and the masses. However, that Newton's equation of motion is simply stated that if the force acting on i^{th} atom is determined or predicted, one can easily determine the position of the i^{th} atom as a function of time by simply integrating the equation twice.^{18,19, 136,137} Conversely, the force exerted on the i^{th} atom can also be expressed as the gradient of the potential energy as shown in equation 3.2.^{18,19, 136,137} Combining equations 3.1 and 3.2 results in equation 3.3.

$$F_i(t) = -\nabla_i U(r) \quad (3.2)$$

$$-\nabla_i U(r) = m_i \frac{d^2(r)_i(t)}{dt^2} \quad (3.3)$$

The equations and the associated parameters that are used to determine the potential energy on the i^{th} atom in the system are collectively called the force fields. Over the last few years, a number of force fields have been developed for different molecular types. For example, CHARM¹³⁸ is used for biomolecules and organics; Chem-X¹³⁹ for organics; MM3¹⁴⁰ for organics and biomolecules; DREIDING¹⁴¹ for main-group organic and inorganic compounds; GROMOS¹⁴² for biomolecules; MMFF¹⁴³⁻¹⁴⁶ for organics and biomolecules; SYBYL¹⁴⁷ for organics and proteins; AMBER¹⁴⁸ for biomolecules and so on.

In order to effectively utilize the power of MD, the appropriate choice and selection of the experimentally validated force field is vital, in particular for the system of interest. Since we are dealing with a large complex organic molecule in organic solvents, we opted for GROMOS96 in all our simulations. GROMACS provides the Gromos96 force fields.^{142,149}

3.1.2 GROMOS96 Force Field

GROMOS is an abbreviation for GRONingen MOlecular Simulation software package. It was first developed at the University of Groningen, The Netherlands for modeling biological systems such as proteins, peptides and phospholipids.¹⁴⁹⁻¹⁵² In GROMOS, the chemical bond of the molecules are usually treated as springs, the hardness of which depends on the type of elements attached to it.^{151,152} Additionally, different types of springs are also used to model the changes in bond angles, proper and improper dihedral angles, etc.^{151,152} GROMOS96 treats molecules as bonded atoms, which have been distorted by the

non-bonded interactions such as van der Waals and Columbic interactions from their ideal geometry.^{136,151,152}

The simplified mathematical framework of the GROMOS96 force field used in this study is shown in Figure 3.1.

$$\begin{aligned}
 U(r) = & \sum_{n=1}^{N_b} \frac{1}{2} k_{bond} (r - r_0)^2 && \text{Bond Stretching} \\
 & + \sum_{n=1}^{N_\theta} \frac{1}{2} k_\theta (\theta - \theta_0)^2 && \text{Harmonic Angle Bending} \\
 & + \sum_{n=1}^{N_\xi} \frac{1}{2} k_\xi (\xi - \xi_0)^2 + \sum_{n=1}^N k [1 + \cos(n\phi - \phi_0)] && \text{Improper and Proper Dihedrals} \\
 & + \sum_{i < j}^{N_{at}} \left(4\epsilon_{ij} \left[\left(\frac{\sigma_{ij}}{r_{ij}} \right)^{12} - \left(\frac{\sigma_{ij}}{r_{ij}} \right)^6 \right] + \frac{q_i q_j}{4\pi\epsilon_0 r_{ij}} \right) && \text{van der Waals (Lennard-Jones) and Coulomb}
 \end{aligned}$$

Figure 3.1. Simplified mathematical framework of GROMOS96 force field, where $U(r)$ is the potential energy of the system, r , θ and ξ represent the bond distance, bond angle and improper dihedral respectively, whereas the terms r_0 , θ_0 and ξ_0 are defined as the ideal equilibrium values for the bond length, bond angle and improper dihedral, respectively; K_{bond} , K_θ and K_ξ refer to the stretch, bend and improper dihedral force constants, respectively; K and n refer to the amplitude and periodicity of the proper torsion angle, respectively; ϕ is the phase shift along the rotation angle axis; σ_{ij} refer to the degree of attraction and repulsion, and q is the charge.

It is important at this stage to mention that, the sensitivity and applicability of GROMOS96 force field to targeted molecules such as polyaromatic molecules^{34,35} was first tested and shown to be useful and valuable in exploring the conformational and structural dynamics of polyaromatic molecules in different solvents.

3.1.3 Integration of the Equations of Motion

In MD simulation, the numerical solution to the time evolution of the system takes place along discrete or finite time step, termed δt .¹³¹⁻¹³⁵ The main purpose of integrating the Newton's equation of motion is to locate the position of an atom at time $t + \delta t$ in terms of the previous position of the atom at time t . The new atomic position trajectory in the system was expressed using Taylor series mathematical expansion shown in Figure 3.2. Due to its simplistic nature, the Verlet algorithm is often deployed in most classical MD simulations. The idea behind this algorithm is to derive the position of the atom ($r(t + \delta t)$) from Taylor expansions and the velocity of the atoms is calculated from their positions.

It is noted that, in order to determine the exact trajectories of the atoms, it is vital to use an infinitesimally small integration time step. The value for the term δt is usually determined by the fast vibrational bond motion of the atoms in the system. As a result, one femtosecond is usually used as an integration time step to account for the fast bond vibrations in the MD simulations. However, constraining all bond lengths using LINCS or SHAKE algorithms allow us to use larger time-steps (e.g., 2 fs) without significantly affecting the equilibrium properties of the system.¹⁵²

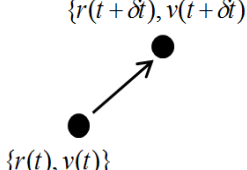
$r(t + \delta t) = r(t) + \delta t v(t) + \frac{1}{2} \delta t^2 a(t) + \frac{1}{6} \delta t^3 b(t) + \dots$	
$v(t + \delta t) = v(t) + \delta t a(t) + \frac{1}{2} \delta t^2 b(t) + \dots$	
$a(t + \delta t) = a(t) + \delta t b(t) + \dots$ Taylor Series	
$r(t + \delta t) = r(t) + \delta t v(t) + \frac{1}{2} \delta t^2 a(t) + \dots$	
$r(t - \delta t) = r(t) - \delta t v(t) + \frac{1}{2} \delta t^2 a(t) + \dots$ Reverse time	
$r(t + \delta t) = 2r(t) - r(t - \delta t) + \delta t^2 a(t) + \dots$ Position	
$v(t) = \frac{[r(t + \delta t) - r(t - \delta t)]}{2\delta t}$ Velocity	

Figure 3.2. The mathematical framework of Verlet algorithm

The main problem with Verlet algorithm is that the velocities are not calculated directly instead they are calculated from the position of the atom. However, despite the oversimplified nature of the algorithm, this method is computationally less expensive, yet still gives some very helpful qualitative predictions of the structural and dynamics of the system in dilute situations.¹³⁶ However, with the rapid advances of powerful computer hardware a number of modifications to the Verlet algorithms was proposed such as the so-called “leap-frog” algorithm, velocity Verlet algorithm etc. GROMACS MD program utilizes the so-called “leap-frog” algorithm for the integration of the equations of motion.

The general GROMACS MD algorithm follows these steps to perform simulation:

- i) Ensure that particles do not overlap at initial positions and then followed by Maxwell velocity distribution.

ii) Move and integrate (“leapfrog” method).

- 
1. Solve for a_i at t using: $-\frac{dU(r)}{dr_i} = f_i = m_i a_i(t)$
 2. Update v_i at $t + \frac{\delta t}{2}$ using: $v_i\left(t + \frac{\delta t}{2}\right) = v_i\left(t - \frac{\delta t}{2}\right) + a_i(t)\delta t$
 3. Update r_i at $t + \delta t$ using: $r_i(t + \delta t) = r_i(t) + v_i\left(t + \frac{\delta t}{2}\right)\delta t$

Although there is no distinct point of termination but usually the system will reach equilibrium if it runs for a long time, and that depends also on your system of interest. The advantage of using GROMACS software is that it is very fast and computationally inexpensive. Therefore, this technique is well suited for studying large molecules such as polyaromatic surfactants, proteins and peptides.

3.1.4 MD Simulation Parameters

When running MD simulations, a number of algorithms were used to control the simulation system under a specific thermodynamic ensemble. The most common algorithms deployed when performing an MD simulation are the thermostats, barostats, periodic boundary condition, particle Mesh Ewald summation methods, etc. The thermostats and barostats methods are used to control and keep constant temperature and pressure of the simulating systems. The periodic boundary condition (PBC) and Particle Mesh Ewald (PME) methods are on the other hand used to avoid problems with boundary effects caused by the finite size, and to efficiently compute long-range electrostatic force terms of the

system. When MD simulations are performed for a given system, GROMACS program will load those algorithms and execute accordingly.

3.1.4.1 Thermostats

Thermostats are frequently introduced during the MD simulations to ensure the system attaining a desirable temperature value. Depending on the computational cost and complexity of the algorithm, a number of thermostat methods are available in GROMACS.^{153-155,157-160} Some of the most popular thermostats widely used in the simulation of biomolecules are the Berendsen thermostat and Nosé-Hoover thermostat.

Berendsen *et al.* (1984)¹⁵³ introduced the framework for controlling the temperature of the system based on the concept of velocity scaling approach. In Berendsen's method, the system temperature ($T(t)$) is maintained by coupling weakly to an external bath with a desirable fixed temperature T_o . Hence, the external heat bath is used to balance out any temperature fluctuations by supplying or removing heat from the given system whenever appropriate.^{153,157} In general, the velocities are scaled at each time step so that a mean kinetic energy proportional with the desired bath temperature is achieved.¹⁵³ In other words, the rate of change in temperature is proportional to the difference in temperature between the system and external bath, and is given by Equation 3.4. The rescaling of the velocity is done by factor λ , which is given by Equation 3.5.

$$dT(t) = \frac{1}{\tau} (T_o - T(t)) \quad (3.4)$$

$$\lambda^2 = 1 + \frac{\delta t}{\tau} \left\{ \frac{T_o}{T(t - \frac{\delta t}{2})} - 1 \right\} \quad (3.5)$$

where τ and δt are the coupling parameter between the bath and the simulating systems, and the time step, respectively. The main drawback of this algorithm is that it suffers from inaccurate energy predictions. Nevertheless, it is a suitable technique for rapid relaxing of a system to a desirable temperature.¹⁵⁸⁻¹⁶⁰

The Nosé–Hoover thermostat is another mathematical model available in GROMACS used to control the temperature of the system around an average. The thermostat was originally developed by Nosé and further modified by Hoover in 1985.^{154,155} In this model, an additional degree of freedom is added into the equations of motion, as described in Equation 3.6, in which Q is some sort of fictional heat bath mass and includes the coupling time constant, and $\xi(t)$ is the scaling factor variable.

The main problem with this method is that the temperature can display large oscillations for small time constants and become unstable relative to simple velocity rescaling methods such as the Berendsen thermostat. However, this method usually reproduces reasonable well the energy of the system.¹⁵²

$$\frac{d^2 r_i}{dt^2} = \frac{F_i}{m_i} - \xi(t) \frac{dr_i}{dt}, \quad \frac{d\xi(t)}{dt} = \frac{1}{Q} (T(t) - T_o), \quad Q = T_o \tau^2 \quad (3.6)$$

3.1.4.2 Barostat

Most practical experiments are done at constant pressure and temperature, instead of constant volume and temperature. Therefore rescaling the volume of the system is vital in order to set the system pressure towards a desired value.^{157,158-160} This is usually achieved by changing the dimensions of the simulation box vectors (or volume fluctuation) at each time step of the simulation period. Unlike temperature control via the thermostats which is directly related to rescaling of the velocities, pressure rescaling is not directly related to the volume of the system but to the inner virial tensor.¹⁵⁸⁻¹⁶⁰ The most common algorithms for pressure control in GROMACS are the Berendsen and Parrinello-rahman methods.¹⁵⁸⁻¹⁶⁰ Similar to Berendsen thermostat, correcting pressure is achieved by weakly coupling the system to an external bath. The scaling factor for each dimension is given by Equation 3.7.

$$\mu = \left[1 - \frac{\beta \delta t}{\tau_p} (P_o - P(t))^{1/3} \right] \quad (3.7)$$

where τ_p , δt and β are the coupling time constant, time step and the isothermal compressibility of the system, respectively. It is important to emphasize that the rescaling of the coordinates is done for all components of the atom positions and the dimensions.

Lastly, we discuss the most often used Barostat called the Parrinello-Rahman method.¹⁵⁶ This method is similar to the mathematical framework proposed by Nosé-Hoover thermostat method, in which an extra degree of

freedom is added to the equation of motion. The Hamiltonian in Parrinello-Rahman method is further extended and altered to treat the cell shape and volume as fluctuating variables in the system rather than the instantaneous change of atom positions. The Nosé-Hoover thermostat and Parrinello-Rahman barostat are usually recommended for a realistic representational fluctuation of the temperature and pressure in a given system dynamics.

3.1.4.3 Periodic Boundary Condition

Periodic boundary condition (PBC) allows us to compute and estimate quite reasonably the macroscopic properties of the system directly from a very few molecules in an MD simulation system, thus mimicking the real experimental situations.^{152,160} In practice, the numbers of molecules treated or the concentration of the solute investigated is usually huge, larger than a system concentration that can be effectively modeled. Even with the advent of powerful computer hardware, the number of molecules that can be studied using MD simulation is very limited due to the influence of system boundaries. PBC was employed to minimize the boundary effect in the system.^{152,160} Figure 3.3 shows the schematic representation of PBC in a given simulating system, where the box at the center represents the original simulating box with N molecules while the others are images of the real simulating box. It is important to note that, when employing PBC, each particle interacts with all other particles in the box and in the images. This reduces the boundary effect and the self-interaction problem in the system.^{152,160} In the systems under periodic boundary conditions, combinations of short-range and long-range electrostatic methods are usually deployed. The coulombs cutoff

method is usually used for short-range interactions, while beyond the cutoff radius the particle-mesh Ewald method (PME) is used to account for the long-range electrostatic interactions in the system.

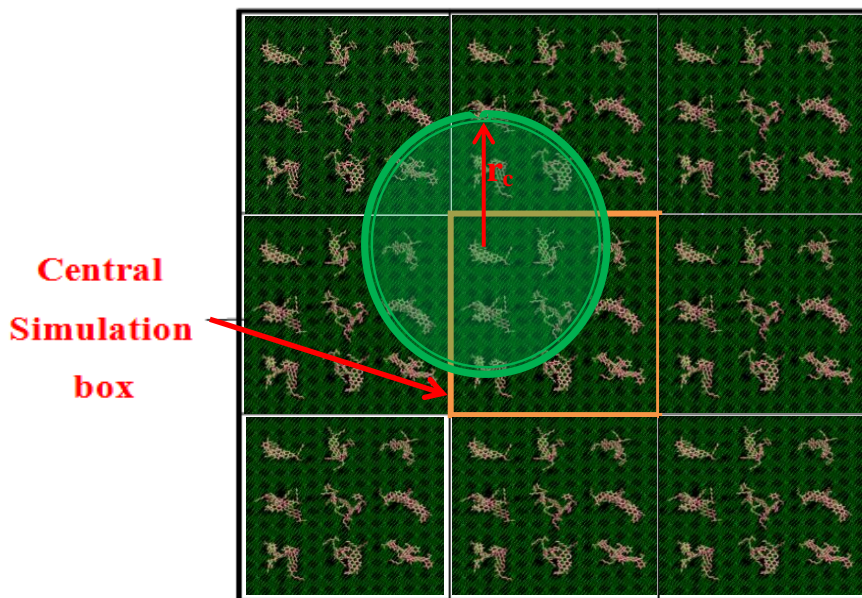


Figure 3.3. Schematic diagram of the periodic boundary conditions, where r_c denotes the distance cutoff for molecular interactions, usually for short-range interactions between molecules.

3.2 Experimental Techniques

Experiments are usually used in conjunction with MD simulations to supplement the data obtained from the MD and to extend and deepen our understanding of the observed phenomenon at microscopic and macroscopic levels. In this thesis, two main experimental techniques were employed, the dynamic light scattering (DLS) and nuclear magnetic resonance (NMR) methods to supplement the MD results. Both qualitative and quantitative approaches were

used to compare the experimental results with the MD simulation. DLS technique was employed to qualitatively compare the influence of various polar and non-polar side chain functional groups on the first steps of molecular association in the bulk, while NMR was used to validate MD dynamic variables and to measure the self-diffusivity of PA molecule in the bulk oil phase. These experimental techniques were used or coupled to supplement the entire molecular dynamic simulation studies beside an extensive literature review on the validation of the MD work.

3.2.1 Dynamic Light Scattering (DLS)

Dynamic light scattering is a useful technique for the measurement of the motion of a molecule, size distribution, protein folding, and conformational preference of a polymer or protein as a function of various sample preparations such as solvent environments, temperature, time etc.¹⁶¹⁻¹⁶⁴ In this technique, a coherent laser beam of monochromatic light is radiated upon a solution and the fluctuation of intensity of scattered light is recorded and analyzed. The time-dependent fluctuations observed in the scattered light are due to the random motion of the molecules under the influence of the Brownian motion. These fluctuations observed and detected are directly related to the rate of diffusion of the molecules in the prepared solution. In DLS experiments, the intensity-intensity time correlation function $G^{(2)}(\tau, q)$ was measured, where τ is the delay time of time interval and q is scattering vector. The normalized intensity-intensity time correlation function $g^{(2)}(\tau, q)$ is given by Equation 3.8.¹⁶²⁻¹⁶⁴

$$g^{(2)}(\tau, q) = \frac{\langle I(0, q)I(\tau, q) \rangle}{\langle I(q) \rangle^2} \quad (3.8)$$

where

$$q = \left(\frac{4\pi n}{\lambda_o}\right) \sin(\theta/2) \quad (3.9)$$

where n , θ , λ_o and I represent the refractive index of the solution, scattering angle, wavelength of the laser and scattered light intensity at given time, respectively. $g^{(2)}(\tau, q)$ is related to the normalized first-order electric field-time correlation function $|g^{(1)}(\tau, q)|$ via Siegert relation given by:

$$g^{(2)}(\tau, q) = 1 + \beta |g^{(1)}(\tau, q)|^2 \quad (3.10)$$

and

$$G^{(2)}(\tau, q) = A[1 + B |g^{(1)}(\tau, q)|^2] \quad (3.11)$$

where $\beta = B/A$ is the spatial coherence factor of scattering volume, A is baseline of the autocorrelation curve and B intercept of the autocorrelation function. For a polydisperse system of particles in suspension, $|g^{(1)}(\tau, q)|$ is related to characteristic relaxation distribution $G(\Gamma)$ by the following Equation 3.12.¹⁶³⁻¹⁶⁴

$$g^{(1)}(\tau, q) \equiv \frac{\langle E_s^*(0, q)E_s(\tau, q) \rangle}{\langle I(q) \rangle} = \int_0^\infty G(\Gamma)e^{-\Gamma\tau} d\Gamma \quad (3.12)$$

Note that the scattered field E_s is a complex quantity (the* denotes the complex conjugate) and Γ is the decay rate. Therefore, the rate of decay Γ can be determined directly from the Laplace transformation of the measured intensity-

intensity time correlation function $G^{(2)}(t, q)$. The translational diffusion coefficient (D) can then be obtained by $\Gamma = Dq^2$. The hydrodynamic radius distribution (R_h) is then determined by the Stokes-Einstein equation. The CONTIN program supplied with the correlator is often used to calculate $G(\Gamma)$ and R_h .

3.2.2 Nuclear Magnetic Resonance

Nuclear magnetic resonance (NMR) is one of the most effective techniques used to investigate and determine the three-dimensional (3D) molecular organizations or aggregation, the environment of the constituent system, diffusion coefficients, and kinetic parameters of biomolecules in a solution.¹⁶⁵⁻¹⁶⁷ This is done generally by manipulating the individual atomic nuclei (to be specific the spin of the nuclei) of the molecules in the solution. The basic principles and concepts of NMR spectroscopy technique are well-established¹⁶⁵⁻¹⁶⁷ and will not be discussed further in this thesis. For the characterization of self and aggregate molecular state of the polyaromatic molecules, the 2D NOESY (Nuclear Overhauser Effect SpectroscopY) technique was used as shown in the next section. This method is based on the exchange of magnetisation during cross-relaxation of the spins through the dipole-dipole coupling.¹⁶⁶

3.3 Validation of the Simulation Parameters

To examine the sensitivity and applicability of the united atom force field and simulation parameters, we have compared the experimental bulk properties of the solvent and TP molecules against our MD simulation. In this work, we

simulated the polyaromatic molecule shown in Figure 3.4 in different organic solvents. The simulations were performed in an isothermal-isobaric (NPT) ensemble, at a temperature of 298 K and pressure 1 bar. Periodic boundary condition and Particle-Mesh Ewald summation methods were used in this simulation. A cutoff of 1.4 nm was used for the van der Waals interactions. Finally, GROMOS96 force field with a parameter set of 53a6 was used in all our simulations.

The average value of the density obtained for the simulated bulk heptane and toluene at ambient temperature is $686.4 \pm 2.1 \text{ kg/m}^3$ and $873.2 \pm 0.9 \text{ kg/m}^3$, respectively. These values are in reasonable agreement with the published experimental results of 684 kg/m^3 and 867 kg/m^3 , respectively.¹⁶⁸

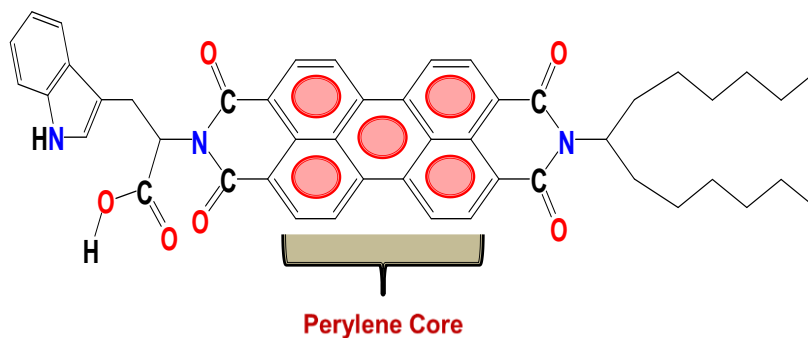


Figure 3.4. The structure of N-(1-hexylheptyl)-N'-(2-indol-3-yl-propanoic acid)-perylene-3,4,9,10-tetracarboxylicbisimide polyaromatic surfactant molecules (TP). TP has a chemical formula of $\text{C}_{48}\text{H}_{47}\text{N}_3\text{O}_6$ and molecular weight 762 (g/mol).

The self-diffusion coefficient of toluene and heptane was calculated by linear fitting the mean square displacement (MSD) over a fixed time interval of

the simulation (6-8 ns). From the slope of the mean square displacement, the self-diffusion coefficients (D) of heptane and toluene were calculated using the Einstein relation:

$$D_{MSD} = \frac{1}{6} \lim_{t \rightarrow \infty} \frac{d}{dt} \left\langle \left| \vec{r}(t) - \vec{r}(0) \right|^2 \right\rangle \quad (3.13)$$

where $\left\langle \left| \vec{r}(t) - \vec{r}(0) \right|^2 \right\rangle$ is the long-time limit of the mean square displacement of the molecules in x , y and z directions, t is the time and $\vec{r}(t)$ is the position of the molecules at time t . The simulation predicts the bulk self-diffusivity of heptane and toluene molecules as $(3.82 \pm 0.05) \times 10^{-9} \text{ m}^2\text{s}^{-1}$ and $(2.26 \pm 0.02) \times 10^{-9} \text{ m}^2\text{s}^{-1}$, respectively. These calculated results are in reasonable agreement with the reported literature values of $4.02 \times 10^{-9} \text{ m}^2\text{s}^{-1}$ and $2.26 \times 10^{-9} \text{ m}^2\text{s}^{-1}$, respectively, as shown in Figure 3.5 (a-b).^{34,35,169-171} The slope of the $\log(t)$ vs. $\log(\text{MSD})$ for heptane and toluene, as shown in Figure 3.5 (c-d), is equal to one and thus diffusion regime is reached. Therefore, the value obtained is definitely representative of the actual behavior of the system. The computed enthalpy of evaporation of heptane and toluene were also in good agreement with the reported experimental values, shown in Table 3.1.

It is also important to mention that the Berendsen and Nosé-Hoover thermostat algorithms produce similar density and radial distribution function, indicating that both methods can be used simultaneously for our systems. Similar observations were also obtained for the pressure values using the Berendsen and Parrinello-Rahman methods.

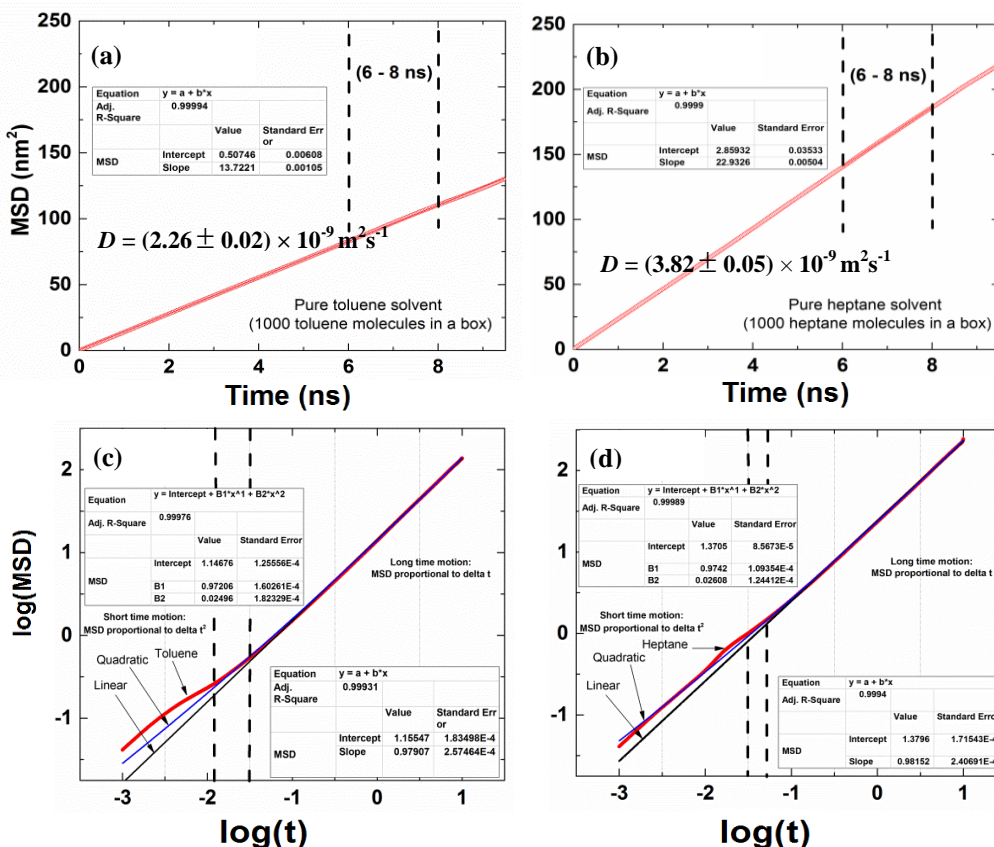


Figure 3.5. (a) t vs. MSD for toluene; (b) t vs. MSD for heptane; (c) $\log(t)$ vs. $\log(\text{MSD})$ for toluene; (d) $\log(t)$ vs. $\log(\text{MSD})$ for heptane.

We have also performed a 2D-NOESY NMR experiments on TP molecules at different concentrations to investigate the self and aggregate diffusivity of the molecule in chloroform solvent. Figure 3.6 shows the diffusion coefficient of TP molecules as a function of concentration in chloroform. It is interesting to observe from the results two distinct regions as the concentration of the TP molecule changes. The lower concentration region shows the range of the self-diffusivity of TP molecules, while the higher concentration region reflects its aggregate diffusivity.

Table 3.1. Density, Self-diffusivity and Enthalpy of Vaporization of Toluene and Heptane at 298 K and 1 bar, in Comparison with reported data (Refs 168–172)

Solvent	D _{MSD} (x10 ⁻⁹) (m ² s ⁻¹)	D _{EXP} (x10 ⁻⁹) (m ² s ⁻¹)	Heat of vaporization MD KJ/mol	Heat of vaporization EXP KJ/mol	Density MD Kg/m ³	Density EXP Kg/m ³
Heptane	3.82 ± 0.01	4.02 ^c , 4.0 ^d and 3.12 ^e	38.2	36.57 ^a	686.4 ± 2.1	684 ^a
Toluene	2.29 ± 0.01	2.26 ^b	38.8	38.1 ^a	873.2 ± 0.9	867 ^a

^a Ref 168. ^b Ref 169. ^c Ref 170. ^d Ref 171. ^e Ref 172.

Thus, the experimental self-diffusivity of TP molecules in chloroform was estimate to be in the range of $(0.75 - 0.8) \times 10^{-9} \text{ m}^2\text{s}^{-1}$. To compare the experimental value with the simulated data, we performed an additional simulation of a single TP molecule in chloroform. The result obtained for the self-diffusivity is $(0.78 \pm 0.05) \times 10^{-9} \text{ m}^2\text{s}^{-1}$. The result is in reasonable agreement with the experimental value derived from NMR measurement. Therefore, we are convinced that the molecular simulation and force field used in this study reproduces reasonably the experimental physical properties of the solvents and polyaromatic molecules. The results show that given a sufficiently long simulation time ($\sim 10\text{--}20 \text{ ns}$), our simulation reproduces reasonably the density, enthalpy of evaporation and self-diffusivity of the solvent and polyaromatic molecules at the specified temperature and pressure.

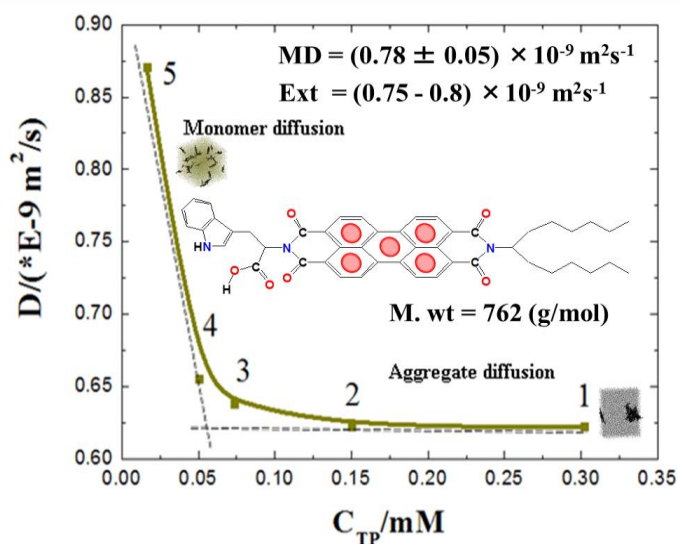


Figure 3.6. The diffusion coefficient as a function of concentration for TP molecules in chloroform at 298 K. The 2D-NOESY NMR experiments were used to measure the diffusion coefficient of the molecules using deuterated chloroform (CDCl_3) as a solvent. At low and high concentrations it reflects self and aggregate diffusivity of TP surfactant molecules, respectively.

3.4 Summary

In this chapter, we have discussed about the mathematical formulation of classical mechanics theory and how large-scale classical molecular dynamics (MD) simulation program can be applied to describe aggregation and interfacial behaviours of PA molecules in different solvents such as toluene, heptane and water. We have also performed a series of 2D-NOESY NMR experiments to validate the applicability of GROMOS96 force field to polyaromatic molecules. The use of MD technique to predict the long range structural behaviour of PA molecules may be of limited importance due to the system evolves through extremely slow dynamics. However, MD simulations can certainly provide some

valuable information regarding the initial molecular association and adsorption of polyaromatic molecules in different organic solvents. In the following chapters, we focus on the exploration and investigation of the early stages of molecular association and adsorption mechanism of the PA molecules in an organic medium and at the oil-water interface.

Chapter 4

Probing Structure-Nanoaggregation Relations of Polyaromatic Molecules: A Molecular Dynamics Simulation Study*

4.1 Introduction

“Structure dictates function” is a fundamental scientific tenet in materials, proteomics, biochemistry and pharmaceuticals, that utilizes structural information of macromolecules or nanoscale materials to understand its function.¹⁷²⁻¹⁷⁷ What is common for this diverse multidisciplinary approach is to understand and detect the influence of molecular fingerprint on the first steps of molecular association into nanoaggregates, where these aggregates represent the first level of molecular clusters or building blocks in three-dimensional structures with immense importance in advanced three-dimensional (3-D) materials, drug carriers, and so on.

In the past few years, constructing supramolecular nanomaterials from stacked polyaromatic building blocks has become a new phenomenon in the design of novel functional materials.¹⁷⁸⁻¹⁸¹ In polyaromatic stacking multiple π - π interactions are involved.¹⁸²⁻¹⁸⁴

* Published paper: Robel, B. Teklebrhan.; Ge, L.; Bhattacharjee, S.; Xu, Z.; Sjöblom, J. *J. Phys. Chem. B* **2012**, 116, 5907-5918.

To investigate π - π stacking and the influence of different functional groups, individually or in combination, on π - π stacking and hence molecular assembly in organic media, perylene bisimide with various attached hydrophilic/hydrophobic side chains has been used as a versatile polyaromatic building block.

Perylene bisimide (PBI) is unique for its optoelectronic properties, thermal stability, multiple π - π interactions, and high fluorescence quantum yields.¹⁸⁵⁻¹⁸⁸ Perylene bisimide analogues have found widespread applications in many areas including organic thin film (or field-effect) transistors (OFETs),¹¹⁴ organic (opto)electronic devices and sensors,^{115,116} light harvesting arrays,¹¹⁷ liquid crystals,¹¹⁸ pigment and laser dyes,^{119,120} and organic solar cells,¹²¹ etc. Furthermore, polyaromatic-based functional arrays such as PBI analogues display a distinct electroactive and photoactive property due to their three-dimensional molecular assemblies.^{122,123} The non-covalent nature of the molecular association by polyaromatic stacking in turn brings about adaptivity and allows recycling of the functional materials.¹⁸⁹

Although the construction of supramolecular nanostructures from polyaromatic building blocks in aqueous solutions are well-established,¹⁹⁰⁻¹⁹³ little attention has been given to understanding the molecular association of polyaromatic building blocks in organic media despite its great importance in for example the petroleum industry.^{9-13,75-77} It is well-known that polyaromatic associations in crude oil lead to precipitation and deposition of the condensed polyaromatic fraction of the crude oil during transportation and production, which results in blocking of reservoir rocks and transport pipes.⁹⁻¹³ Furthermore, the

polyaromatic association phenomena in crude oil strongly influence solubility, viscosity, density, and other physical properties of the crude oil.^{9-13,75-77}

In this chapter, five well-defined polyaromatic molecules (PA) based on perylene bisimide moieties were used as building blocks to probe structure-nanoaggregation relationship in organic media. All of these five molecules contain the same pronged aliphatic double chains on one side of the PBI. However, the other side of the PBI incorporates structural facets of different types of amino acids or aliphatic alkyl groups such as β -alanine, phenylalanine and tryptophan, making these molecules surface active.⁸⁰⁻⁸²

Herein, we investigate the molecular association, nanoaggregate formation, and dynamics of the polyaromatic molecules in a bulk nonaqueous solution using molecular dynamics simulation (MD) with the objective to gain molecular insight into the hierarchy of interactions in molecular nanoaggregation.

4.2 Simulation Method

All of the classical MD simulations were carried out using GROMACS 3.3.3¹⁵⁸⁻¹⁶⁰ software package on a multiprocessor computing cluster. The GROMOS96 force field¹⁵⁸⁻¹⁵⁹ with the 53a6 parameter set was used in all calculations. This force field is a united atom force field primarily parameterized for biological macromolecules, in particular for proteins and peptides, DNA and phospholipids. The applicability of GROMOS96 force field to polyaromatic molecules^{34,35} was first tested and shown to be useful and valuable in exploring the dynamics of polyaromatic nanoaggregate formation.

4.2.1 Molecular Models

Five PA molecules shown in Table 4.1 are used in this study. These compounds are specially designed and synthesized in-house except for the last entry, *N*-(1-hexylheptyl)-*N'*-(methyl 2-phenylpropanoate)-perylene-3,4,9,10-tetracarboxylicbisimide (PCH). The PCH is a hypothetical compound and included in this study to investigate and probe the effect of a carboxylate group instead of a carboxylic acid group in polyaromatic on its nanoaggregation.

PCH is a variation of *N*-(1-hexylheptyl)-*N'*-(2-phenylpropanoic acid)-perylene-3,4,9,10-tetracarboxylicbisimide (PAP) in which the hydrogen atom of the hydroxyl group (–OH) is replaced by an alkyl group (–CH₃). As compared with PAP molecules, this change of functionality from carboxylic acid (–COOH) to ester (–COOCH₃) features a lower polarity of PCH molecules and weaker intermolecular hydrogen bonding. Including this compound in our study allows us to investigate the effect of the hydrogen bond network and polarity of the side chains on nanoaggregation of PA molecules. The synthesis and characterization of the other four PA molecules have been reported recently.¹⁰³⁻¹⁰⁵ The initial molecular geometries (PDB coordinates) of these PA molecules were obtained using Chem 3D ultra 10.0 software.¹⁹⁴ The coordinates of these PA surfactant molecules were then transferred, as an input file, to the PRODRG 2.5¹⁹⁵ server to generate the necessary molecular topology and GROMACS structure files. All the double bonds and aromatic rings were modeled with *sp*² hybridized carbons.

Table 4. 1. Compounds, Molecular Weights, and Structures of PA Molecules^a

Compound (Abbr.)	Mol. wt. (g/mol)	Molecular structure
<i>N,N'</i> - (1-hexylheptyl)- perylene-3,4,9,10- tetracar-boxylicbisimide (BisA)	755 C ₅₀ H ₆₄ N ₂ O ₄	
<i>N</i> -(1-hexylheptyl)- <i>N'</i> - (2- phenylpropanoic acid)-perylene-3,4,9,10- tetracar-boxylicbisimide (PAP)	723 C ₄₆ H ₄₆ N ₂ O ₆	
<i>N</i> -(1-hexylheptyl)- <i>N'</i> - (5- carboxylicpentyl)- perylene-3,4,9,10- tetracar-boxylicbisimide (C5 Pe)	689 C ₄₇ H ₄₈ N ₂ O ₆	
<i>N</i> -(1-hexylheptyl)- <i>N'</i> - (2-indol-3-yl-propanoic acid)-perylene-3,4,9,10- tetracar-boxylicbisimide (TP)	762 C ₄₈ H ₄₇ N ₃ O ₆	
<i>N</i> -(1-hexylheptyl)- <i>N'</i> - (methyl 2- phenylpropanoate)- perylene-3,4,9,10- tetracarboxylicbisimide (PCH)	721 C ₄₇ H ₄₈ N ₂ O ₅	

^a The synthesis and characterization of these PA molecules were reported elsewhere.¹⁰³⁻¹⁰⁵ The molecular design of the PA molecules incorporates a polyaromatic perylene core with two alkyl chains attached to one end and a different functional group (polar or nonpolar) attached to the other end of the molecules.

Furthermore, the polar and aromatic hydrogen atoms were modeled explicitly while aliphatic hydrogens were treated as unified interaction sites (hence, united-atom models). In our simulations, toluene and heptane were used as solvents of two extreme polarities or solvent qualities. The topology of toluene was generated from phenylalanine amino acid fraction through the *pdb2gmx* routine in GROMACS. Lipid aliphatic chain was used for heptane. Heptane is a nonpolar molecule, its atomic charge was therefore set to zero for all interaction sites.

4.2.2 Simulation Setup and Conditions

Molecular dynamics simulation of five well-defined PA molecules in toluene and heptane was performed over the time range of 20 ns. Initially, the dimensions of the simulation boxes were set at 12 nm × 12 nm × 12 nm. A total of ten simulation boxes were constructed with each box containing 24 molecules of a single type of PA molecules in an ordered placement, as shown in Figure 4.1. It is important to note that for all simulation systems the same initial molecular configuration was assumed.

The systems were solvated with either toluene or heptane molecules. After setting up the initial configurations, the system energy was minimized using the steepest descent and conjugate gradient methods as implemented in GROMACS 3.3.¹⁵⁷⁻¹⁶⁰ A cutoff of 1.2 nm was used for both Coulomb and van der Waals interactions during energy minimization. The hydrogen-bond interaction is considered as a form of electrostatic interactions in molecular modeling.

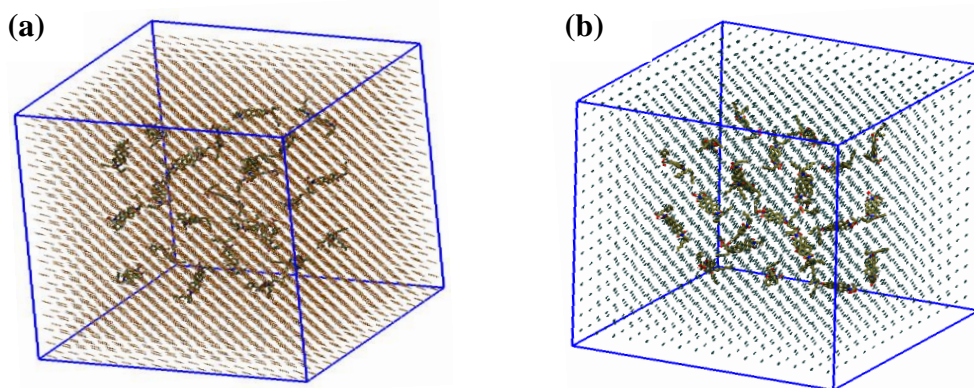


Figure 4.1. Initial molecular arrangement of PAP molecules in toluene (a) and heptane (b).

The system maximum force was converged to less than $200 \text{ KJ mol}^{-1} \text{ nm}^{-1}$ threshold set to generate a stable system for the simulations. The detailed information on the simulated systems is listed in Table 4.2. All simulations were carried out under the NPT ensemble at 298 K and 1 bar pressure. For the first 3 ns, the Berendsen thermostat and barostat¹⁵³ were used to quickly relax the system to a constant pressure and temperature. After 3 ns, all the simulations were performed using Nosé-Hoover thermostat^{154,155} and Parrinello-Rahman pressure coupling algorithm.¹⁵⁶ The pressure and temperature coupling constants of $\tau_p = 3 \text{ ps}$ and $\tau_T = 0.3 \text{ ps}$, respectively, were used throughout the simulations.

In all simulations, an isothermal compressibility of $1.47 \times 10^{-4} \text{ bar}^{-1}$ and $9.08 \times 10^{-5} \text{ bar}^{-1}$ were applied for heptane and toluene, respectively.¹⁶⁸ Periodic boundary condition (PBC)¹⁵² was applied in the x, y and z directions, and a leap-frog Verlet algorithm^{152,196-197} with a time step of 2 femtosecond (fs) was used for integration of the trajectories. The electrostatic interaction was computed using

the Particle-Mesh Ewald summation (PME)¹⁹⁸ method with a fast Fourier transform (FFT) grid spacing of 0.16 nm to account for long-range electrostatic interactions of the system. A cutoff of 1.4 nm was used for the van der Waals interactions and is consistent with GROMOS96 parameterization.

Table 4.2. Composition of Simulation Systems

simulation A: 24 PA molecules in toluene				
system	PA molecules	time (ns)	N_{toluene}	final volume size (nm ³)
BT3	BisA	20	5571	$9.96 \times 9.96 \times 9.96$
PT1	PAP	20	5601	$9.99 \times 9.99 \times 9.99$
CT2	C5 Pe	20	5601	$9.98 \times 9.98 \times 9.98$
TT4	TP	20	5591	$9.97 \times 9.97 \times 9.97$
PT5	PCH	20	5598	$9.97 \times 9.97 \times 9.97$
simulation B: 24 PA molecules in heptane				
system	PA molecules	time (ns)	N_{heptane}	final volume size (nm ³)
BH8	BisA	20	4660	$10.44 \times 10.44 \times 10.44^*$
PH6	PAP	20	3898	$9.89 \times 9.89 \times 9.89$
CH7	C5 Pe	20	3911	$9.86 \times 9.86 \times 9.86$
TH9	TP	20	3905	$9.87 \times 9.87 \times 9.87$
PH10	PCH	20	3907	$9.90 \times 9.90 \times 9.90$

* The initial simulation box size was set at 12.5 nm \times 12.5 nm \times 12.5 nm.

All bond lengths in our system were constrained using LINCS algorithm.¹⁹⁹ A neighbour list with a cutoff of 1.2 nm was updated every 5 steps. The initial atomic velocities of the system were set using the Maxwell-Boltzmann distribution employed in GROMACS at the specified temperature of 298 K. After simulations for 20 ns, the structure and dynamic properties of the system were analyzed using the GROMACS built-in analytical tools. The time evolutions of the structure of the system were also visualized using visual molecular dynamics (VMD).²⁰⁰

4.3 Experimental Methods

4.3.1 Materials and Solution Preparations

Synthesis and structural characterization of the PA molecules were performed at the Ugelstad Laboratory (NTNU, Trondheim, Norway). The PA molecules passed an extra purification step with flash chromatography as described elsewhere.¹⁰³⁻¹⁰⁵ Pertinent information regarding these compounds is provided in Table 4.1. The compounds were dissolved in toluene (Fisher Scientific, optima grade) under sonication. For dynamic light scattering experiments, the solutions prepared were filtered through 0.45 μm PTFE filters (Millipore) directly into dust-free light scattering cells, which were sealed immediately. After filtration, the solutions were thermostated at 25 $^{\circ}\text{C}$ overnight without disturbance before measurement.

4.3.2 Dynamic Light Scattering (DLS)

DLS measurements were carried out with an ALV 5022 laser light-scattering (LLS) instrument equipped with a cylindrical He-Ne laser (model 1145p-3083; output power = 22 mW at $\lambda = 632.8$ nm) in combination with an ALV SP-86 digital correlator of a sampling time range from 25 ns to 40 ms. Since our objective is to qualitatively compare the aggregation tendency of PA molecules as a function of concentration in toluene, only scattering angle of 90° were used in this study. The LLS cell was held in an index matching vat filled with high purity, dust-free toluene. The temperature of the experiments was controlled at 298 K within ± 0.02 °C by a thermostat. The DLS experiments were completed in 10 min and repeated at least twice.

4.4 Results and Discussion

4.4.1 Nanoaggregate Formation and Growth

Figure 4.2 shows snapshots of the simulation box at $t = 20$ ns for each of the PA molecules in the two solvents. From these snapshots we can directly observe that all PA molecules form nanoaggregates to varying degrees of association. For example, BisA and PAP show smaller, less structured aggregates while C5 Pe and TP form larger aggregates in both solvents. Furthermore, BisA and PAP in toluene show the least aggregation amongst all the simulations performed in this study. However, loosely packed and fairly large aggregates of C5 Pe and TP are noticeable in both toluene and heptane.

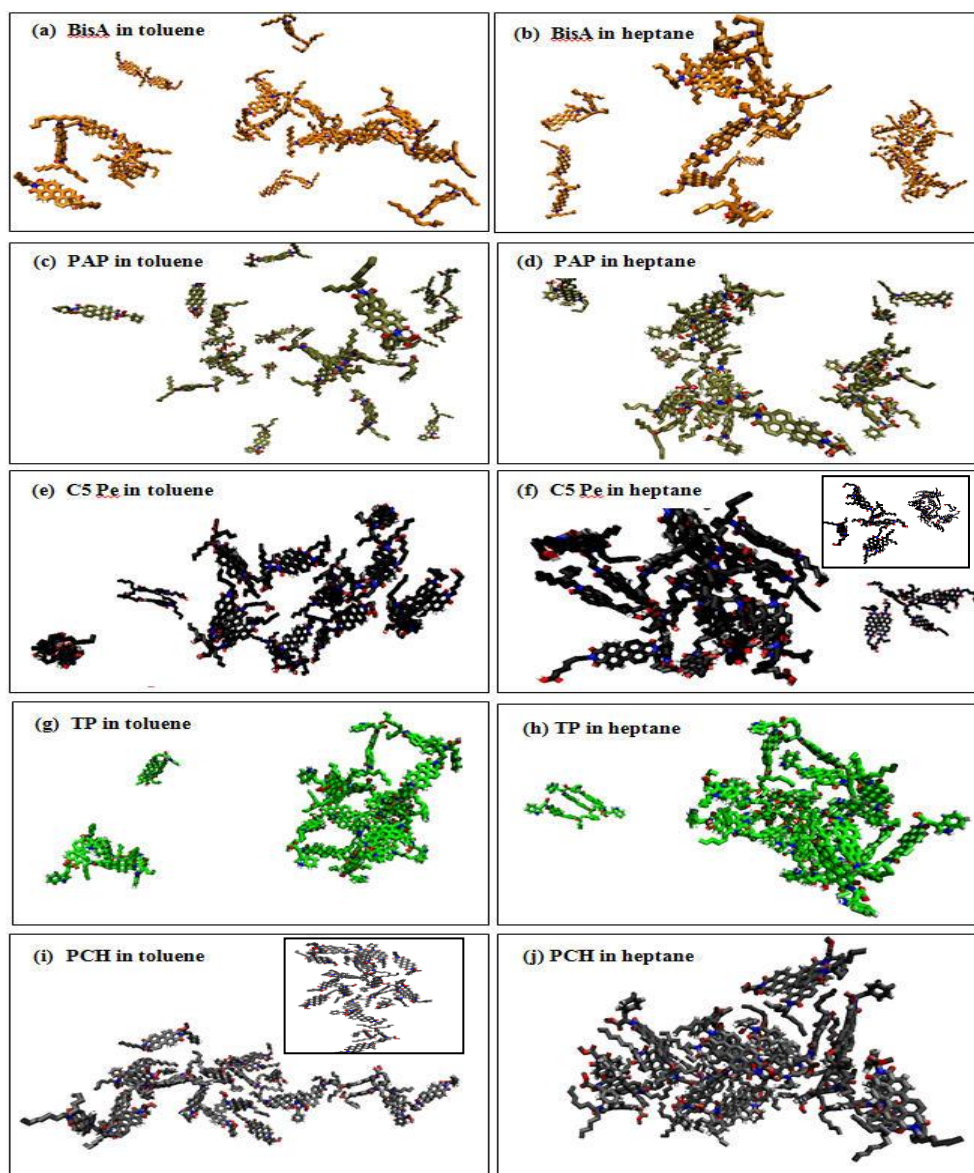


Figure 4.2. Snapshots of molecular configurations of the five PA surfactant molecules in heptane and toluene, taken at the end of 20 ns simulation time. PAP and BisA compounds show a weak aggregate in both solvents. Each molecule is presented by a different color to distinguish one from the other: BisA in orange, PAP in tan, C5 Pe in black, TP in green and PCH in gray. In all structures oxygen, nitrogen and hydrogen atoms are presented by red, blue and white, respectively. All the snapshots are along the z-direction (2D side view). Top view snapshots of PCH in toluene (i) and C5 Pe in heptane (f) are shown as insets.

Thus, the MD snapshots qualitatively indicate that C5 Pe and TP tend to form aggregates in both solvents, and their tendency to aggregate in heptane is far greater than in toluene. Previous experimental and computational studies have shown significant aggregation of PA moieties in both heptane and toluene. However, the extent of their aggregation and association in toluene is rather limited, and they terminate at the nanoaggregation level.^{9-13,33-38,75-77,82,83} Visual inspection of molecular trajectories reveals that BisA molecules prefer T-association or tail-to-tail arrangements with minimum π - π stacking due to strong steric hindrance associated with the branched side chains. In contrast, PAP and PCH show a much different aggregation behavior despite their similar structural features. Figure 4.3 shows the PA-PA radial distribution functions (RDFs) calculated from the PA center of mass in both toluene and heptane, $g(r)$.

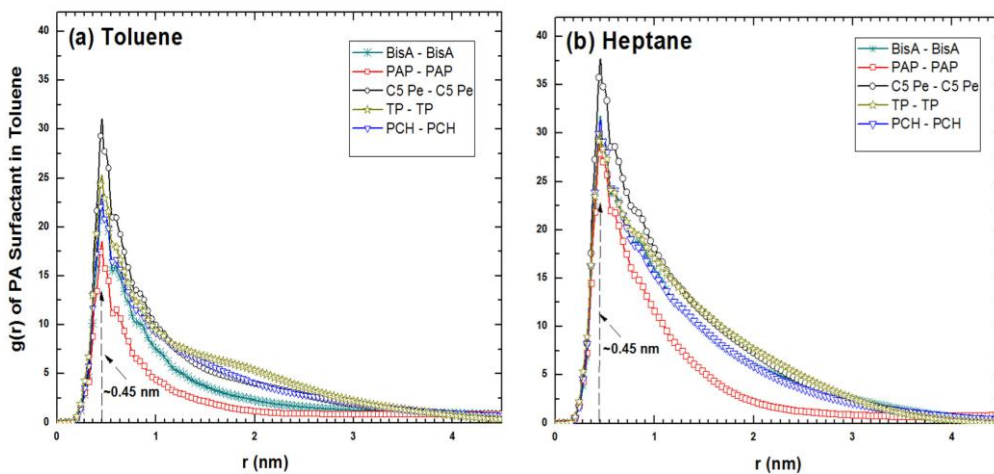


Figure 4.3. Radial distribution functions calculated from the PA center of mass averaged over the last 2 ns of the simulation time (18 ns - 20 ns) of PA molecules in toluene (a) and heptane (b) at 298 K.

These RDFs are the average over the last 2 ns of the simulations (18 ns - 20 ns) for all the PA molecules in toluene and heptane. It is interesting to note the similar peak positions and shapes of the RDFs among these PA molecules in both toluene and heptane. In both solvents a strong peak at 0.45 nm is seen, indicating strong short-range association of PA molecules in the system. Interestingly, irrespective of the nature of the solvent, the positions of these three peaks remain almost identical for all the PA molecules. Similar observation was noticed in our previous work on putative model compounds in toluene and heptane.^{34,35} In heptane, these PA surfactant molecules tend to show a slightly broader peak, mainly due to an extended nanoaggregate formation and growth. In contrast, a relatively sharper peak of the $g(r)$ in toluene indicates toluene is a better solvent than in heptane.

To investigate the role of different functional groups in the nanoaggregate formation and growth, we monitored the radial distribution peak heights of PA molecules as a function of time in both solvents (for example, see Fig. 4.4a-b for PAP molecules). A close examination of the time evolution of the pair correlation function reveals that the nanoaggregates were fully developed and become stable over a shorter simulation time of less than 6 ns in toluene than in heptane. In heptane, the growth of larger aggregates was visible even beyond 10 ns. Interestingly, although C5 Pe, TP and PAP molecules all have a polar $-\text{COOH}$ functional group in their side chains, the tendency for these molecules to aggregate in both solvents varies significantly. TP has a high tendency to

aggregate in both solvents. PAP, on the other hand shows a weak tendency to aggregate in toluene.

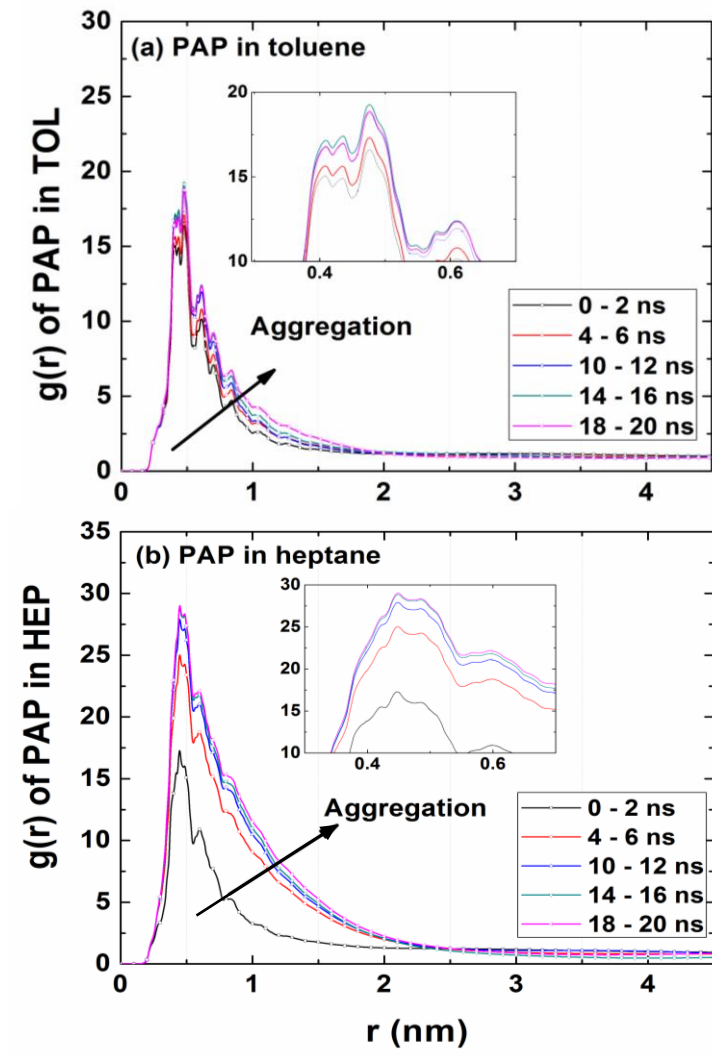


Figure 4.4. PAP-PAP radial distribution functions calculated from the PAP center of mass as a function of time in toluene (a) and heptane (b).

To determine more specifically the impact of $-\text{COOH}$ functional group on nanoaggregation, PCH and PAP molecules were closely studied in this work. Results indicate that these molecules in toluene exhibit little differences in the

aggregate formation and growth. PAP shows a lower peak height in toluene. Here, the change from $-\text{COOH}$ to $-\text{COOCH}_3$ functionality enhances nanoaggregate formation and growth in toluene. In heptane, both compounds show similar peak heights. The observed disparity in toluene is attributed to the polarity difference of the molecules and their effect on hydrogen bonding.

It is known that $-\text{COOCH}_3$ is less polar with limited opportunity for hydrogen bonding than $-\text{COOH}$. Therefore, the polarity and hydrogen bonding formation of the side chains in toluene contribute to some extent to altering the nanoaggregate formation and growth.

In Table 4.3 we report the radius of gyration (R_g) and the variation of the ratio between the solvent accessible surface area (SASA) and the total accessible volume (AV), and the number of molecules (N) in a large nanoaggregate cluster and the free PA molecule in the simulation system. The solvent accessible surface area was determined with a probe 1.4 Å in radius. The total accessible volume was computed by `g_sas` in GROMACS.

The criterion for determining the number of associated molecules per nanoaggregate is by the linkage algorithm in GROMACS with a cutoff distance of 0.5 nm, which is within the range of the π - π stacking. In both toluene and heptane, the single molecules for all PA molecules were found to have similar radius of gyration and SASA:AV. However, these PA molecules form nanoaggregates of different structures.

Table 4.3. The Radius of Gyration, SASA:AV Ratio and Number of Aggregated Molecules of the Large Nanoaggregate Cluster in the Simulated System

PA molecules in toluene					
PA surfactant	(SASA/AV) monomer (nm ⁻¹)	(SASA/AV) nanoaggregate (nm ⁻¹)	N _{molecules} nanoaggregate	R _g monomer (nm)	R _g nanoaggregate (nm)
BisA*	6.40 ± 0.10	---	---	0.65 ± 0.01	---
PAP*	6.30 ± 0.13	---	---	0.67 ± 0.02	---
C5 Pe	6.40 ± 0.10	4.90 ± 0.12	3	0.69 ± 0.01	0.76 ± 0.01
TP	6.30 ± 0.11	4.70 ± 0.01	8	0.68 ± 0.02	1.29 ± 0.20
PCH	6.20 ± 0.09	5.30 ± 0.13	3	0.65 ± 0.02	0.86 ± 0.05
PA molecules in heptane					
BisA	6.20 ± 0.14	4.90 ± 0.02	4	0.64 ± 0.01	0.96 ± 0.01
PAP	6.30 ± 0.09	4.70 ± 0.10	4	0.67 ± 0.02	0.93 ± 0.01
C5 Pe	6.40 ± 0.09	4.80 ± 0.02	7	0.69 ± 0.02	1.15 ± 0.10
TP	6.30 ± 0.07	4.10 ± 0.01	21	0.67 ± 0.01	2.62 ± 0.23
PCH	6.20 ± 0.05	3.70 ± 0.01	20	0.65 ± 0.01	1.82 ± 0.16

* BisA and PAP in toluene does not form nanoaggregate clusters (very weak association). The mean value was obtained over the last 1 ns of the simulations time.

This finding suggests that the concept of critical molecular packing parameter widely accepted for predicting geometry of molecular aggregates in aqueous solutions is inapplicable to predicting molecular aggregation of the PA molecules in an organic solvent.

The number of molecules, radius of gyration and SASA:AV ratio of the large nanoaggregate cluster of all the PA molecules show a significant variation from one another in both heptane and toluene. The nanoaggregates of C5 Pe, for example, show a larger SASA:AV ratio but a smaller N than the nanoaggregates formed from TP molecules in heptane. This higher SASA:AV ratio indicates that C5 Pe molecules in heptane exhibit less compact, rod-like nanoaggregate structures while TP compounds form a relatively compact and spherical in shape. In toluene, on the other hand, PCH and TP compounds show the highest and lowest SASA:AV ratio, respectively.

4.4.2 π - π Stacking with Side Chain Terminal Groups

Considering the complex nature of the interactions in PA molecules, it would be valuable to study the effect of side chains in PA molecules on π - π stacking and hence nanoaggregation of these type of PA molecules. The presence of side chains is anticipated to hinder the π - π stacking and hydrogen-bonding by steric hindrance, retarding molecular aggregation. To study such effect, RDF between the center six-membered rings of the polyaromatic cores (perylene core) was calculated. Figure 4.5 shows the RDF normalized with respect to the first peak height with the actual $g(r)$ being shown in the insets. Among all the RDFs, only C5 Pe in toluene shows a remarkably sharp first peak at around 0.45 nm, indicating a strong dimerization. All remaining simulations show variable structures of molecular association of these PA molecules in the two solvents, depending on the nature of side chains. The first peak at around 0.45 nm in both solvents corresponds to the formation of strong polyaromatic π - π stacking of the

PA molecules. These values are confirmed explicitly by calculating the mean distance among the polyaromatic cores (distance between the individual atoms of the center aromatic ring in the polyaromatic core) of these molecules as shown in Table 4.4. The results in Figure 4.5 show that the normalized RDF has a strong first peak at around 0.45 nm for all the compounds except for BisA.

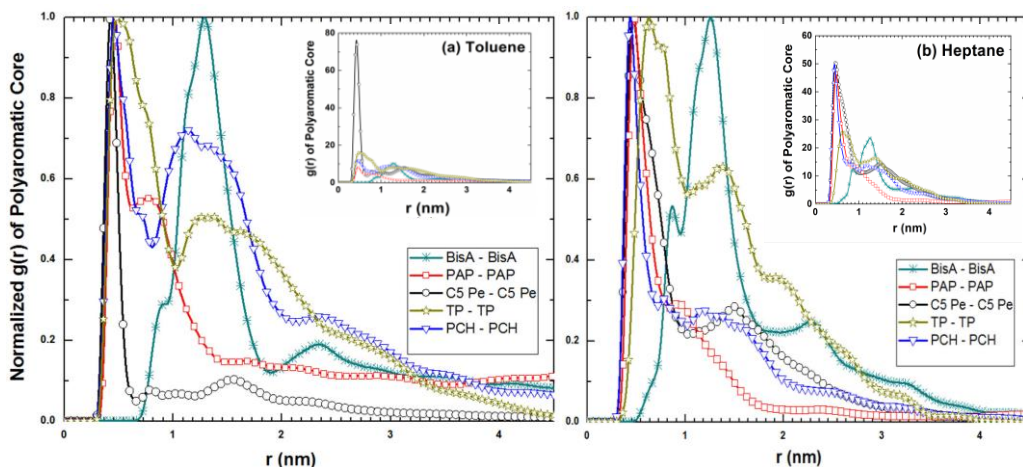


Figure 4.5. Normalized radial distribution functions, $g(r)/g(r)_{Maxpeak}$, of polyaromatic core (perylene core) averaged over the last 2 ns of the simulation time (18 ns - 20 ns) in toluene (a) and heptane (b) at 298 K. BisA does not form polyaromatic π - π stacking due to its strong steric hindrance in both solvents (Inset).

The width of the first peak correlates with the number of stacked monomers present in a nanoaggregate. In toluene, C5 Pe exhibits clearly the formation of stacked dimers, whereas PAP, PCH and TP show increasingly higher levels of stacking association between the polyaromatic cores. The presence of a second peak in the RDFs at around 1.16 nm (1.1 nm – 1.3 nm) indicates the formation of perpendicularly (T-shaped) associated structures. Note that BisA in

toluene shows weakly associating configuration at around 1.23 nm. The RDFs in Figure 4.5b show quite similar π - π stacking except that the association of C5 Pe, PAP and PCH becomes more comparable. These results reveal that BisA with an aliphatic functional group in both side chains, does prevent the formation of polyaromatic π - π stacking due to its strong steric hindrance in both solvents. For the other PA molecules, we observed varying degrees of stacking association. C5 Pe has a high tendency to dimerize in toluene (see the inset of Figure 4.5a), but these molecules do not form large stacking associations. The stacking arrangements of the PA molecules in heptane are depicted in Figure 4.6. Similar stacking behaviour in toluene was also observed.

Table 4.4. Mean Distance between two Polyaromatic Cores

compound	toluene (nm)	heptane (nm)
BisA	negligible stacking	negligible stacking
PAP	0.3975 ± 0.0217	0.3920 ± 0.0115
C5 Pe	0.3880 ± 0.0056	0.4040 ± 0.0100
TP	0.4110 ± 0.0085	0.4020 ± 0.0100
PCH	0.4150 ± 0.0038	0.3868 ± 0.0059

The preference for dimerization arises from its stronger steric hindrance due to the presence of long linear alkyl side chains in C5 Pe molecules as compared to PAP, TP, and PCH. For PAP, TP, and PCH in toluene, the aromatic

or heteroaromatic group such as benzene or indole as a side chain, tends to have lower steric hindrance towards the formation of larger associated structures.

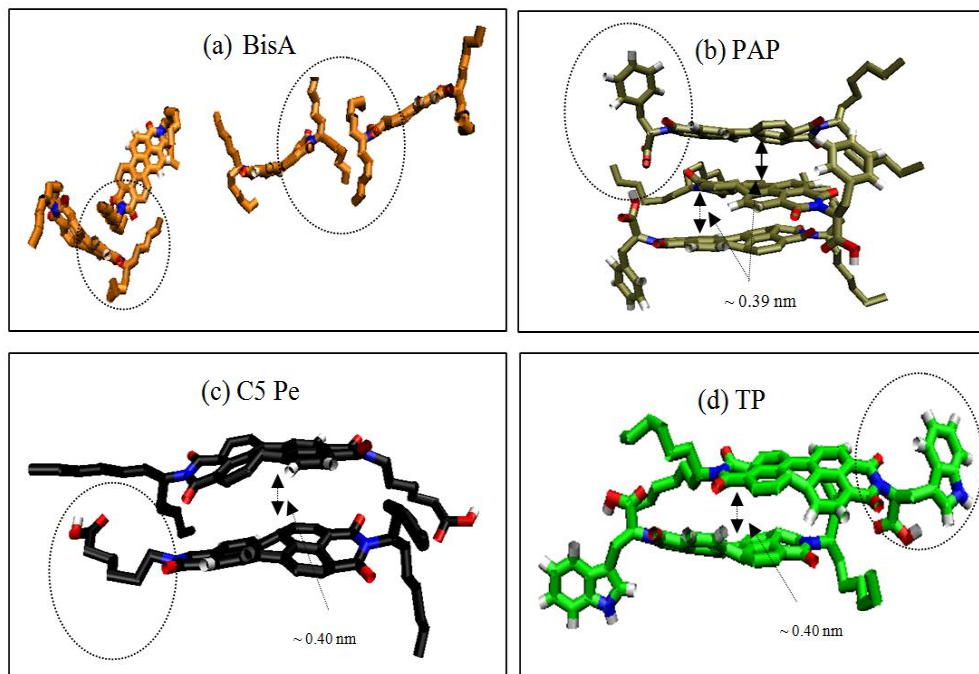


Figure 4.6. The configuration and steric hinderances (doted circles) of polyaromatic stacking between two PA surfactant molecules: (a) BisA - BisA T-shaped or tail-to-tail association, (b) PAP - PAP π - π polyaromatic stacking, (c) C5 Pe - C5 Pe π - π polyaromatic stacking, and (d) TP - TP π - π polyaromatic stacking. The snapshots were taken at the end of 20 ns simulation time. PCH and PAP show similar stacking arrangements, but the extent of their stacking is different.

This lower steric hinderance associated with these molecules in toluene results from the strong interactions between the toluene solvent molecules and the aromatic side chains. In heptane, all the PA surfactants studied except for TP and BisA show similar stacking distributions. TP, a nitrogen bearing compound, in

heptane also shows a weak polyaromatic π - π stacking. From the RDF obtained from the molecular dynamics simulation, we can conclude that the strong polyaromatic π - π stacking is the main driving force for molecular aggregation of PA surfactant in the bulk, which is greatly influenced by the steric hindrance and polarity of its side chains. The more steric barriers the compound possesses, the less likely they stack, in particular, in the presence of aliphatic or alkyl side chains in its good solvent environment.

4.4.3 Radial Distribution Function of Solvent Molecules near Polyaromatic Core

Figure 4.7 shows the RDF of solvent molecules around the polyaromatic core of the PA surfactant molecules. The RDF in Figure 4.7 shows how the solvent molecules associate with the polyaromatic cores.

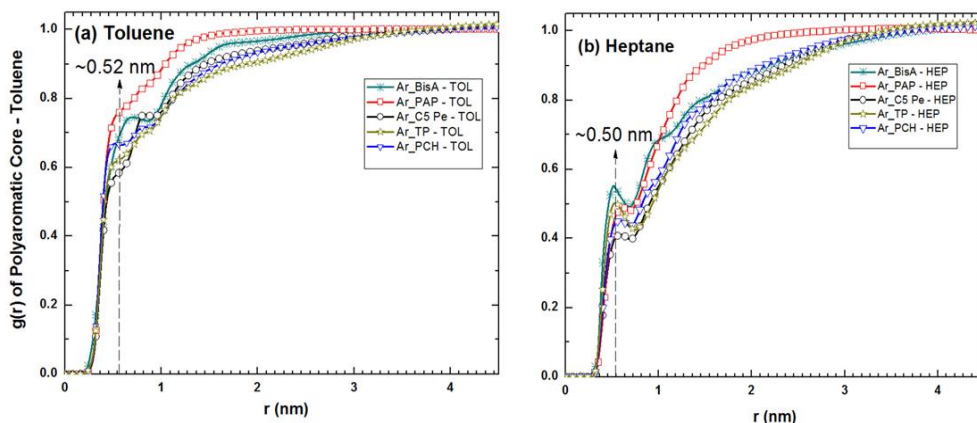


Figure 4.7. The RDFs of solvent molecules near a polyaromatic core of the PA molecules averaged over the last 2 ns of the simulation time (18 ns – 20 ns) in toluene (a) and heptane (b) at 298 K.

For toluene which readily solubilizes the PA molecules, there is no significant short-range structure of the solvent molecules. The first peak of the solvent distribution appears beyond 0.5 nm, suggesting that the solvent molecules are excluded from the interstices of the stacked polyaromatic cores (Table 4.4). Increased levels of dimerization lead to a reduction in solvent accessibility of the polyaromatic cores, which is evident by reduction in the first peak of the $g(r)$ curve for C5 Pe in toluene. With increased association between the polyaromatic cores in heptane, the solvent distribution around the polyaromatic rings in Figure 4.7b shows a much lower $g(r)$ as compared to toluene, but has a more prominent peak. The solvent accessible surface area (SASA) of the various model PA surfactant molecules in toluene and heptane is depicted in Figure 4.8 (a) and (b), respectively. One would expect a systematic decrease in SASA as the molecules associate.

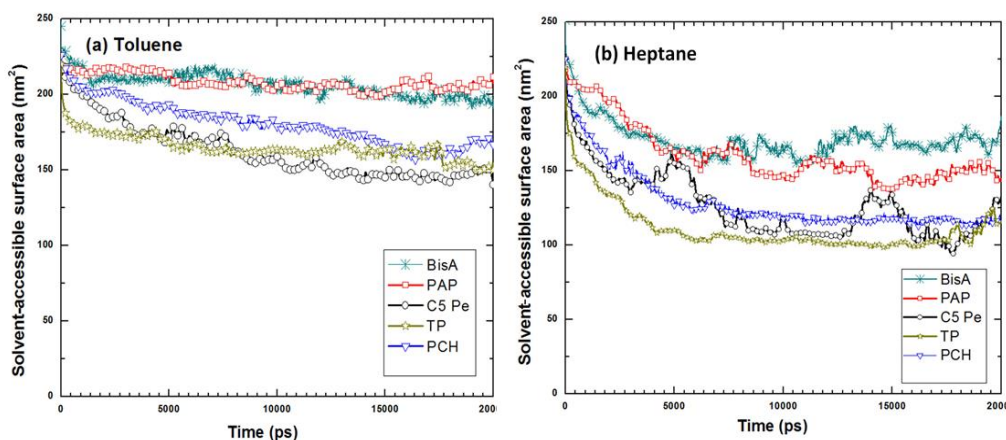


Figure 4.8. Solvent-accessible surface area of the PA surfactant molecules over the simulation time of 20 ns in toluene (a) and heptane (b) at 298 K.

The formation of T-stacks or imperfect association structures will not result in a significant decrease in the SASA. However, each π - π stack in a dimer will cause a 50% reduction in the SASA. Figure 4.8a shows how the SASA is related to the degree of association. For BisA and PAP, we see a negligible change in SASA, which correlates well with the lack of aggregation. For TP and C5 Pe, we observe the most significant reduction in SASA. In heptane, the association is more pronounced than in toluene, as shown in Figure 4.8b.

4.4.4 Effect of Intermolecular Interactions on Diffusion

To examine the effect of different side-chain substituents on the first steps of PA molecular association into nanoaggregates, where these aggregates represent the first level of molecular clusters, the diffusion coefficient of these PA molecules were also computed by linear fit of the mean square displacement (MSD) to the Einstein relation given in Equation 3.13 on log-log plot over a fixed time interval of the simulation (2 - 4 ns). From the slope of the fit, the diffusion coefficient (D) of the various PA molecules was computed. It is important to note that all the simulations were performed over the time span of 20 ns. The mean square displacement as a function of time for PA molecules in toluene and heptane is shown in Figure 4.9 (a-b).

In order to confirm the Brownian motion regime, and thus the validity of the linear relationship between MSD and time, the $\log(t)$ vs. $\log(\text{MSD})$ were plotted for all PA molecules in toluene and heptane. The results in Figures 4.10 and 4.11 indicate a good linear relationship over a long simulation time. The slope

of the $\log(t)$ vs. $\log(\text{MSD})$ for all PA molecules in heptane and toluene was found to be close to one.

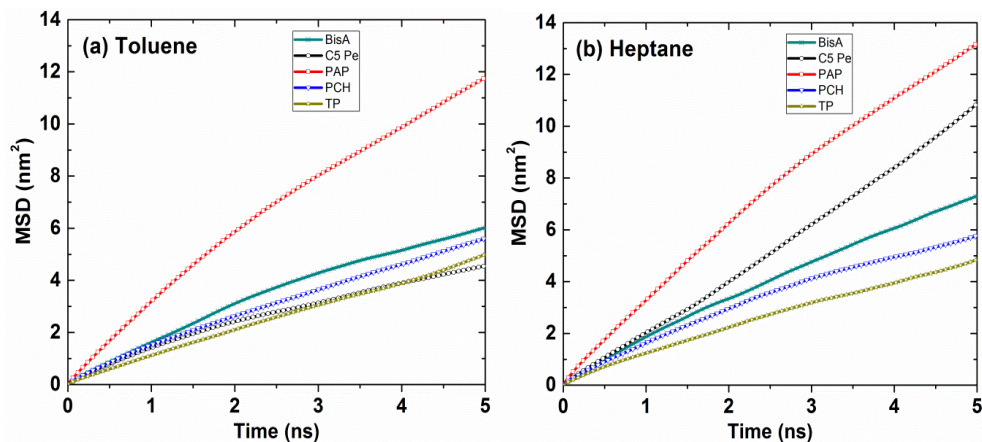


Figure 4.9. Mean square displacement as a function of time for PA molecules in toluene (a) and heptane (b) at 298 K.

It is important to note that unlike toluene and heptane solvent molecules (see Fig.3.5) where the slope of the $\log(t)$ vs. $\log(\text{MSD})$ is equal to one, the slope of the $\log(t)$ vs. $\log(\text{MSD})$ for all PA molecules in heptane and toluene is slightly lower than one (in the range of 0.8 to 0.9). Since polyaromatic association evolves through extremely slow process in both heptane and toluene, a very long simulation time (> 20 ns) is needed to reach the Brownian regime (slope close to 1). Due to computational limitations we were only able to simulate the system for 20 ns.

With this simulation time, the mean square displacement as a function of time shown in Figure 4.9 (a-b) exhibits a slope in the range of 0.8-0.9 towards the end of the simulation time. Hence, the values obtained from this calculation only serve as a qualitative measure actual diffusion coefficient of the PA molecules in

the system. Since our objective is to examine the degree of intermolecular interactions of the various PA molecules in toluene and heptane with time (the first steps of PA molecular association into nanoaggregates), we use this computed diffusion coefficient to infer the aggregation of PA molecular tendency in heptane and toluene (see Table 4.6).

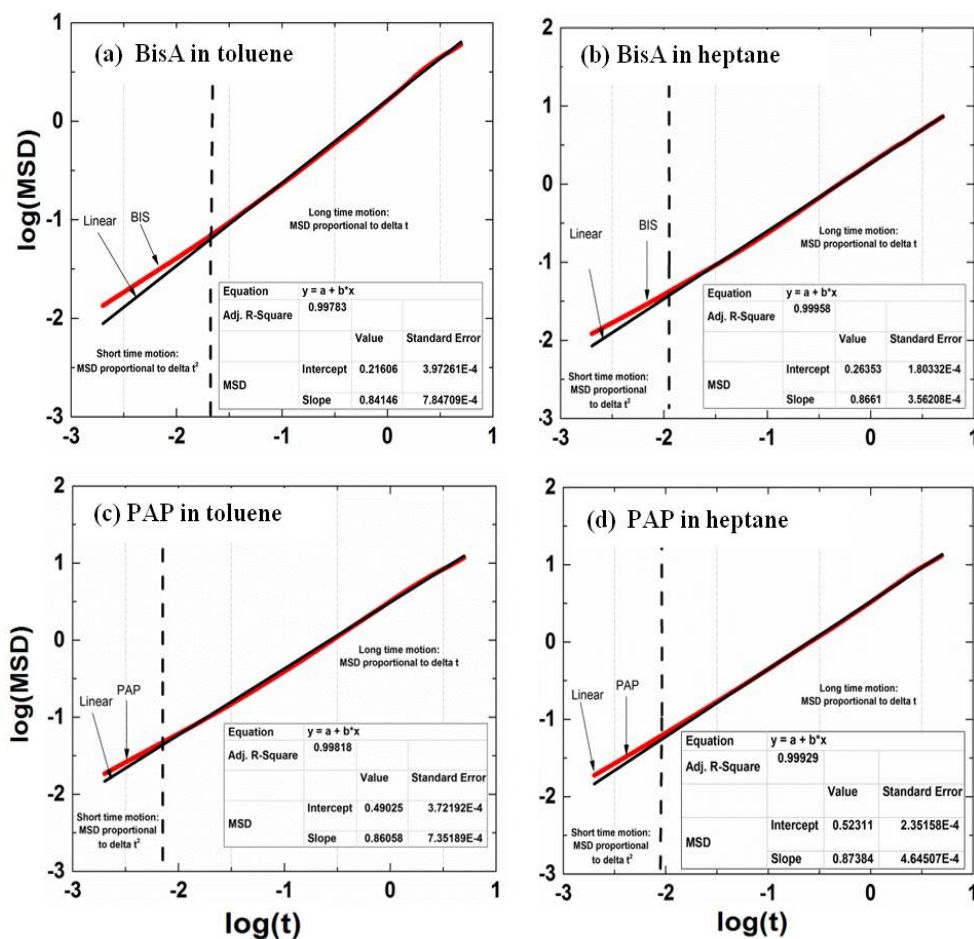


Figure 4.10. (a-b) $\log(t)$ vs. $\log(\text{MSD})$ for BisA in toluene and heptane; (c-d) $\log(t)$ vs. $\log(\text{MSD})$ for PAP in toluene and heptane.

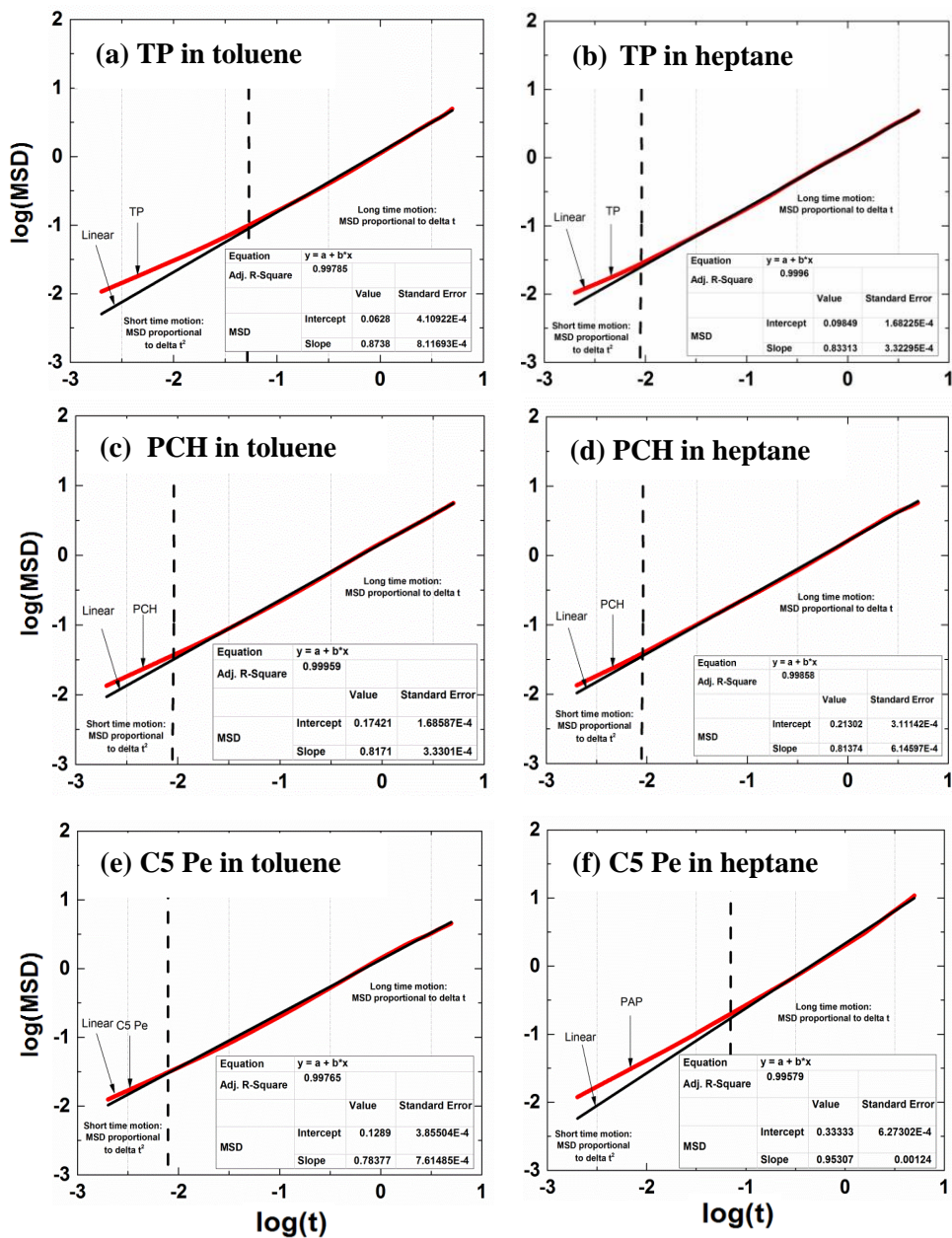


Figure 4.11. (a-b) $\log(t)$ vs. $\log(\text{MSD})$ for TP in toluene and heptane; (c-d) $\log(t)$ vs. $\log(\text{MSD})$ for PCH in toluene and heptane; (e-f) $\log(t)$ vs. $\log(\text{MSD})$ for C5 Pe in toluene and heptane.

In addition, the diffusion coefficient of a single PA molecule in the absence of any intermolecular interactions with other PA molecules in heptane and toluene is computed using the Stokes-Einstein equation:

$$D_{SE} = \frac{K_B T}{6\pi\eta(0.678\langle R^2 \rangle^{1/2})} \quad (4.1)$$

where K_B is the Boltzmann constant, T is the absolute temperature, η is the viscosity of the fluid, and $\langle R^2 \rangle^{1/2}$ is the average radius of gyration over a fixed time interval of the simulation (2 ns). Since equation 4.1 is applicable to molecules of spherical shape, the average radius of gyration of all the PA molecules in x, y, z directions was computed to qualitatively determine the shape of the PA molecules in both toluene and heptane solvent systems.

The results of radius of gyration in Table 4.5 suggest near-spherical shape of PA molecules in these solvents, validating the use of equation 4.1 for determination of diffusion coefficient of individual PA molecules in toluene and heptane.

The results in Table 4.6 show that the diffusion coefficient values of single PA molecules in both solvents obtained from MSD are much higher than that of PA molecules obtained by Stokes-Einstein equation, indicating the existence of strong intermolecular interactions among the various PA molecules. The highly variable (more than 200%) diffusion coefficients obtained from the MSD indicate that the intermolecular interaction among the various PA molecules depends on the side chain substituents.

Table 4.5. The radius of gyration of a single PA molecule in toluene and heptane

PA molecules in toluene			
PA molecules	R _x (nm)	R _y (nm)	R _z (nm)
BisA	0.47 ± 0.10	0.55 ± 0.05	0.50 ± 0.09
PAP	0.55 ± 0.08	0.52 ± 0.11	0.53 ± 0.10
C5 Pe	0.44 ± 0.09	0.60 ± 0.06	0.63 ± 0.05
TP	0.47 ± 0.09	0.64 ± 0.08	0.56 ± 0.07
PCH	0.42 ± 0.06	0.59 ± 0.04	0.58 ± 0.04
PA molecules in heptane			
PA molecules	R _x (nm)	R _y (nm)	R _z (nm)
BisA	0.45 ± 0.01	0.51 ± 0.09	0.55 ± 0.04
PAP	0.57 ± 0.07	0.41 ± 0.08	0.61 ± 0.05
C5 Pe	0.48 ± 0.08	0.54 ± 0.10	0.58 ± 0.07
TP	0.46 ± 0.09	0.62 ± 0.05	0.64 ± 0.06
PCH	0.49 ± 0.09	0.49 ± 0.10	0.59 ± 0.04

TP in heptane for example, shows very slow diffusion as compared to the other four PA molecules, demonstrating the existence of strong intermolecular interaction among TP molecules. The results further indicate that the presence of a bulky aromatic amino acid tryptophan residue in PA molecule enhances the intermolecular interaction among PA molecules, which results in the formation of larger nanoaggregates in the organic phase. In contrast, PAP shows the highest diffusion coefficient in heptane indicates the formation of weak and small nanoaggregates.

Table 4. 6. Diffusion Coefficient of PA Molecules in Heptane and Toluene

PA Molecule	heptane		toluene	
	$D_{\text{MSD}} (\times 10^{-9} \text{ m}^2\text{s}^{-1})$	$D_{\text{SE}} (\times 10^{-9} \text{ m}^2\text{s}^{-1})$	$D_{\text{MSD}} (\times 10^{-9} \text{ m}^2\text{s}^{-1})$	$D_{\text{SE}} (\times 10^{-9} \text{ m}^2\text{s}^{-1})$
BisA	0.232 ± 0.001	1.310 ± 0.014	0.172 ± 0.002	0.846 ± 0.012
PAP	0.397 ± 0.004	1.250 ± 0.017	0.330 ± 0.003	0.815 ± 0.020
C5 Pe	0.307 ± 0.001	1.210 ± 0.019	0.123 ± 0.001	0.798 ± 0.019
TP	0.141 ± 0.002	1.240 ± 0.009	0.147 ± 0.001	0.809 ± 0.019
PCH	0.164 ± 0.026	1.290 ± 0.013	0.167 ± 0.001	0.841 ± 0.015

Therefore, depending on the nature and type of the side chain attached to the PA molecules, the diffusion coefficient changes dramatically. In contrast, the variation in the diffusion coefficient of a single PA molecule in both heptane and toluene is insignificant, as anticipated. These findings indicate that a change in the side chain functional group of the PA molecules does not have a profound impact on the diffusion coefficient of a single PA molecule in both heptane and toluene. The direct comparison of the calculated diffusion coefficients from the SE method of the PA molecules in heptane and toluene reveals that PA molecules show a lower diffusivity in toluene than in heptane, indicating a weaker association in toluene than in heptane as confirmed in our previous simulations.^{34,35}

4.4.5 Aggregation Behavior of PA Molecules in Toluene Studied by Dynamic Light Scattering

Since the focus of our study is to use molecular dynamics modeling to investigate molecular aggregation of polyaromatic molecules in two different solvent, we only show in this thesis the experimental results from the dynamic

light scattering to qualitatively compare the trend of the molecular aggregation of PA molecules in toluene. The examination or inspection of the correlograms in the DLS technique can provide a wealth of information on the nature of the molecular aggregation of PA molecules in toluene.¹⁶¹⁻¹⁶⁴ For example, the correlation function takes a long time to decay for large aggregates, while small aggregates usually exhibit a rapid decay in their correlation function. Furthermore, qualitative information regarding the polydispersity of the aggregates in the system can also be obtained from the steepness of the curve.¹⁶¹⁻¹⁶⁴ A steep decay curve reflects monodisperse aggregates, while extended decay curve reflects polydisperse aggregates in the system. It should be noted, however, that the structural and dynamic properties of the polyaromatic molecules in toluene are concentration dependent. In fact, polyaromatic molecules have a greater tendency to associate and form nanoaggregates even at an extremely low concentration.^{5,16,60,76,84,102} It is, therefore, imperative to compare molecular aggregation at the same PA molecular concentrations.^{9-17,73} Since the MD simulation was conducted using a box dimension of 12 nm × 12 nm × 12 nm (~ 40 mmole/L) with a simulation time of 20 ns, a direct comparison of the measured and predicted aggregate sizes is difficult. Therefore, in this thesis we only qualitatively compare the trend of molecular aggregation of PA molecules in toluene determined by MD simulation and DLS measurements. Figure 4.12 shows the dynamic light scattering results of the PA molecules at different concentrations. Careful inspection of the scattering profiles, revealed a negligible decay in the correlation function for PAP and BisA, indicating a negligible

aggregation of PAP and BisA in toluene. On the other hand, TP shows two distinct features, depending on the concentration of TP in toluene. At low concentrations, no decay is observed, which indicates most of the compounds being dissolved as individual molecules. The correlation function starts to decay at higher concentrations, which suggests the aggregation of TP molecules at higher concentrations. The molecular aggregation pattern observed from the DLS experiment qualitatively explains the MD results described in section 4.4.1. Our MD simulation revealed that in toluene, PAP and BisA do not form large aggregates (negligible aggregates), as determined by DLS. As shown in Figure 4.13, the normalized scattering intensities of both PAP and BisA are very low at all the concentrations investigated, indicating that PAP and BisA exist as almost single molecules in toluene. In contrast, TP forms larger nanoaggregates due to increasingly higher levels of stacking between the polyaromatic cores, which is also seen in DLS experiments. C5 Pe, on the other hand, form very small molecular aggregates in the form of dimers. C5 Pe has a high tendency to dimerize in toluene (see the inset of Figure 4.5a), but these molecules do not form large stacking associations.

As a result, very low scattering intensity was observed as shown in Fig.4.13. The high level of TP molecular aggregation observed in the DLS experiment (see Fig. 4.13) is consistent with our prediction that TP form larger aggregates in comparison to other PA molecules in toluene.

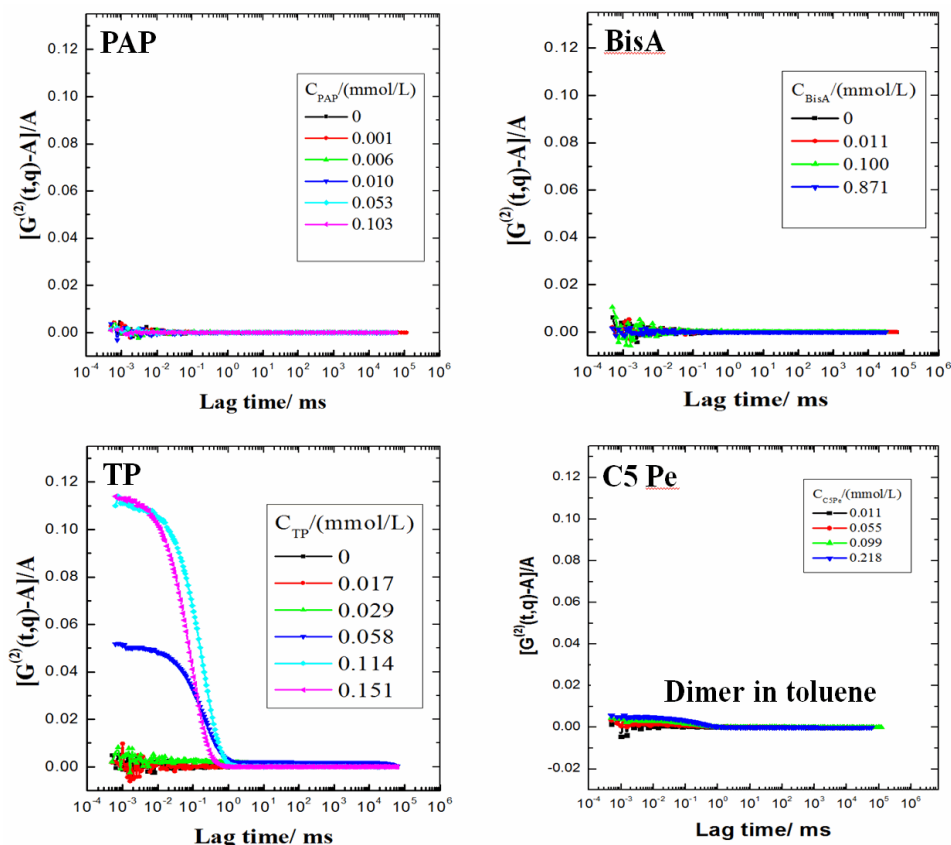


Figure 4.12. Intensity-intensity time correlation functions *vs.* PA molecules concentration in toluene. BisA and PAP show negligible molecular aggregation at both high and low concentrations, while TP shows strong aggregation at high concentrations. C5 Pe shows very small aggregates and it could be dimerization in toluene at all concentrations.

Although the results obtained from the DLS technique qualitatively describe the nature of the molecular aggregation pattern of PA molecules in toluene, a more detailed experimental studies of the molecular assembly of these compounds using high level experimental techniques such as UV-vis, atomic force microscopy, freeze-fracture TEM, etc. is needed to fully characterize and

understand the aggregation mechanism of these compounds in toluene and heptane. Finally, this work is considered as a stepping stone for further characterization and understanding of these compounds in different solvents at a greater depth experimentally.

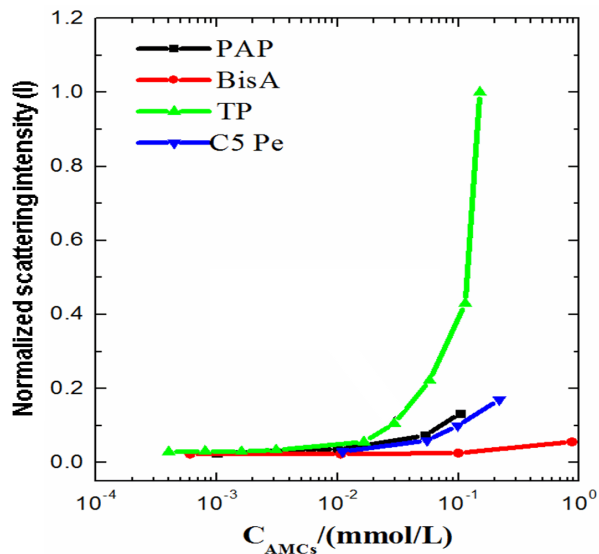


Figure 4.13. Normalized scattering intensities (I) as a function of PA molecules concentration in toluene. BisA, PAP and C5 Pe show very low scattering intensities while TP shows very high scattering intensities.

4.5 Conclusions

The molecular association and nanoaggregate formation dynamics of five polyaromatic molecules in heptane and toluene were studied using molecular dynamics simulation. Analysis of RDFs of the PA molecules show that a change in molecular structure and polarity of substituent side chain functional group has a

significant impact on molecular association, nanoaggregation dynamics, nanoaggregate structure and aggregate stability in both heptane and toluene.

The aggregates of PA molecules grow too much larger sizes in heptane than in toluene. In toluene, the substitution of tryptophan side chain in TP by phenylalanine in PAP makes PAP dissolve as individual molecules. The presence of a branched *n*-alkane side chain in BisA leads to the lowest aggregation and hence the highest SASA:AV ratio of BisA in heptane. In contrast, the presence of a nitrogen-bearing aromatic side chain in TP makes it aggregate strongly in heptane, leading to the lowest SASA:AV ratio due to its less compatible nature with heptane. Only C5 Pe in toluene exhibit a very sharp first peak at around 0.45 nm in the normalized RDFs of the polyaromatic cores, indicating a strong dimerization. All other PA surfactant molecules show variable structures of molecular association in both toluene and heptane, depending on the nature of side chains attached to the polyaromatic core. The peaks in the RDF at around 0.45 nm and 1.23 nm in both solvents correspond to the formation of polyaromatic π - π stacking and perpendicularly (T-shape) association of the PA molecules, respectively. In the extreme case, BisA with an aliphatic functional group in both side chains almost do not form polyaromatic π - π stacking in both solvents due to its strong steric hindrance. The RDFs of the solvent molecules near the polyaromatic core, on the other hand, show that the solvent molecules are excluded from the interstices of the stacked polyaromatic cores in nanoaggregates. The results from the MSD calculations indicate that the presence of a bulky aromatic amino acid tryptophan residue in PA molecule enhances the

intermolecular interaction among PA molecules, which results in the formation of larger nanoaggregates in the organic phase. In contrast, PAP shows the highest diffusion coefficient in heptane indicates the formation of weak and small nanoaggregates. In both toluene and heptane, the single molecules for all PA molecules were found to have similar radius of gyration and SASA:AV, while these PA molecules form nanoaggregates of a wide range structures. This finding suggests that the concept of critical molecular packing parameter widely accepted for predicting geometry of molecular aggregates in aqueous solutions is inapplicable to predicting molecular aggregation of the PA molecules in an organic solvent.

Chapter 5

Initial Partition and Aggregation of Protonated Polyaromatic Molecules at the Oil-Water Interface*

5.1 Introduction

Initial molecular adsorption and aggregation of polyaromatic molecules (PA) at the oil-water interface to form a viscoelastic interfacial film as a result of various intermolecular interactions, such as, dipole-dipole, H-bonding, $\pi\cdots\pi$, and Cation $\cdots\pi$, are of fundamental interest as they are relevant in a wide range of industrial processes, including oil recovery and oil-contaminated waste-water treatment.^{68-70,201-203}

PA molecules with ionized head groups are surface active molecules (SAM) in which, the hydrophilic head groups reside in water, whereas the hydrophobic nonpolar tails remain in the oil phase.²⁰⁴⁻²⁰⁶ The accumulation of these interfacially active PA molecules from the bulk oil phase to the oil-water interface promotes the formation of cross-linked viscoelastic interfacial films, which stabilize oil-water emulsions.²⁰⁴⁻²⁰⁶

* Published Paper: Robel, B. Teklebrhan.; Ge, L.; Bhattacharjee, S.; Xu, Z.; Sjöblom. *J. Phys. Chem. B* **2014**, 118, 1040–1051. (from page 86 to page114)

Several studies^{43,206} have shown that films created by the interfacially active PA molecules prevent the coalescence of dispersed water droplets in water-in-oil emulsions, thereby impeding oil-water phase separation. Once the interfacially active PA components or molecules are removed from the bulk oil phase, emulsions became unstable.^{42,43,70,207-209} Using both theoretical and experimental methods, significant progress has been made in the field of studying surfactant mediated emulsion formation and stability.^{11,34,35,43,47,209-212} Many synthetic and natural surfactants have been extensively studied, including anionic molecules^{213,214}, zwitterionic molecules^{215,216}, biomolecules²¹⁷, etc. It has been observed that protonated moieties show strong interfacial activity in oil-water systems.^{34,35} Accordingly, in simulation-based studies, interfacially active molecules are often assigned charges to the functional groups that protonate or deprotonate in water. In oil-water systems, such molecules are always drawn to the interface with the deprotonated functional groups of the molecules remaining strongly associated with the water phase until all the interfaces are occupied.^{34,35} There are two main shortcomings of these electrostatically dominant systems. First, the electrostatic forces overwhelmingly influence the partitioning process, masking other factors that render interfacial activity to these surfactants less visible. Second, surfactants are mostly protonated in the oil phase, and the charges are acquired only through protonation/deprotonation of the molecules when they come in contact with the water at the oil-water interface. Thus, the initial migration of an oil-dispersed surfactant from bulk oil to the oil-water interface is most likely dictated by other mechanisms, namely, polarity, $\pi \cdots \pi$, dipole-dipole

interactions, etc. in the absence of a charge on the surfactant molecules. A careful assessment of these other interactions is therefore crucial in evaluating the surface activity and initial molecular partitioning of oil-dispersed PA molecules at oil-water interfaces. It is also important to note that the initial migration process of PA molecules from the bulk phase to the oil-water interface is extremely difficult if not impossible to probe experimentally due to inadequate instrumentation. Computational approaches such as molecular dynamics simulation are particularly suitable for such kind of investigations.

Relatively speaking, few molecular level studies on PA molecules at the oil-water interface have been reported despite the evident importance of these molecules in oil recovery and oil-field water treatment.^{34,35} Lack of detailed molecular level knowledge on the structural and conformational arrangements, 3D intermolecular network formation and dynamics of the adsorbed PA molecules at the oil-water interface limits rational design of appropriate chemical demulsifiers under specific process conditions. When chemical demulsifiers are added to an emulsion system stabilized by PA molecules, they will adsorb at the oil-water interface and partly dislodge the PA molecules adsorbed at the interface, thereby forming a new interfacial film of lower mechanical strength or poor stability.²¹²

In Chapter 4, we explored the association of PA molecules into initial nanoaggregates in the bulk oil phase by molecular dynamics (MD) simulation.²¹⁸ In that study, we showed a significant impact of the molecular fingerprints on the first steps of molecular association into nanoaggregates in aliphatic and aromatic bulk solvents. Chemical and structural modification on the side-chain functional

groups (aliphatic, steric, polarity, aromaticity, etc.) of the PA molecules leads to significant variations in molecular association, dynamics of molecular nanoaggregation and structure of resultant nanoaggregates in these solvents. The aggregates of PA molecules are larger in aliphatic solvents than in aromatic solvents, as a result of weakened π - π stacking of the PA molecules by the penetration and association of aromatic solvent molecules.

In this chapter, we study adsorption and association of five protonated perylene bisimide based PA molecules at oil-water interface by molecular dynamics simulation. The role of competitive molecular interactions between the π - π stacking and hydrogen bonding between the hydrophilic groups of PA molecules and water molecules in molecular association and formation of viscoelastic films at an oil-water interface is investigated. The influence of various polar and non-polar side chain functional groups on the partition of PA molecules between the interfacial region and the bulk oil phase is shown. The effect of the solvent (oil) polarity is also considered. The molecular orientations and dynamics of the PA molecules at the oil-water interface are revealed. The results obtained in this study provide a rationalization of the interfacial activities of the protonated PA molecules at oil-water interfaces with respect to their molecular fingerprints.

5.2 Details on Molecular Models and Simulation

Molecular dynamics (MD) simulations were conducted using the GROMACS¹⁵⁸⁻¹⁶⁰ simulation software and GROMOS96-53a6 force field. This force field is primarily parameterized for biological macromolecules, in particular

for proteins, peptides and phospholipids. All the double bonds and aromatic rings were modeled by considering the sp^2 hybridization of carbons. The polar and aromatic hydrogen atoms in the molecule were modeled explicitly, while aliphatic methyl groups of the molecules were treated as unified interaction sites.^{152,153,158,159}

Our previous simulation results showed that GROMOS96-53a6 force field is capable of predicting the self-diffusivity and other physical property of the solvents reasonably. The general simulation methodologies employed in this study are reported elsewhere.^{34,35,218} However, a new version of PRODRG was used in this study to generate the initial molecular geometries and topology files of the PA and solvent molecules. The carboxylic functional groups, which are ionizable groups in the PA molecules, were set to either protonated (-COOH) or deprotonated (-COO⁻) states depending up on the system being studied. The box size, solvents added, simulation parameter and time remains the same for all the simulations. For the deprotonated PA molecules, a total of 24 sodium ions were included in the molecular topology to keep the systems electro-neutral. The detailed design and construction scheme of the cubic boxes, oil-water interface, molecular geometries and topology files of the PA molecules, toluene and heptane solvent molecules are the same with our previous chapters. For the easy reference, the different types of PA structures used in this study are summarized in Figure 5.1 (a–b).

For the water model, the simple point charge (SPC) model was used in our simulation as this model was able to provide a reasonable estimation of the

interfacial properties of the oil-water systems (see Appendix A, for a detailed water model comparisons). The simulation boxes were constructed by first packing 24 PA molecules in vacuum in a cubic box of 10 nm size. The boxes were then solvated with either heptane or toluene molecules followed by energy minimization. The concentration of PA molecules in our simulation box falls within the range of (27.4 – 30.4) g/L. The boxes were then extended in the z -direction by 5 nm and filled with water molecules. The system energy was then minimized using the steepest descent method. The detailed system setup is described in Table 5.1.

A total of 16 simulation boxes were designed in this manner (10 for protonated and 6 for deprotonated PA molecules). After equilibration, all the boxes contained an organic and an aqueous layer with well-defined flat interfaces. Simulations were performed in an NPT ensemble at 298 K and 1 bar pressure using Nosé-Hoover thermostat^{154,155} and Parrinello-Rahman pressure coupling algorithm.¹⁵⁶ Pressure and temperature coupling constants of $\tau_p = 3$ ps and $\tau_T = 0.3$ ps, respectively, were used throughout the simulations. The isothermal compressibility of water ($k(T) = 4.5 \times 10^{-5} \text{ bar}^{-1}$) was used in all the simulations.¹⁶⁸ Periodic boundary conditions¹⁵² were applied in all dimensions. Long-range electrostatic interactions were computed using the Particle-Mesh Ewald Summation (PME)¹⁹⁸ method with a grid spacing of 0.16 nm and cutoff distance of 1.2 nm. The van der Waals interactions were truncated with a cutoff distance of 1.2 nm. The van der Waals interactions were truncated with a cutoff distance of 1.4 nm.

The LINCS algorithm was used to constrain all the bond lengths in the simulation system.¹⁹⁹ A neighbour list with a cutoff distance of 1.2 nm was updated every 5 steps. The initial velocities of the moving atoms in the system were set using the Maxwell distribution at 298 K.¹⁵² Simulations were performed for 10 ns using a leap-frog Verlet algorithm^{152,196,197} with a time step of 2 femtosecond. Previous study showed that 10 ns simulation time is sufficient to see the adsorption of the PA molecules at the oil-water interface.^{34,35,218} All the analysis of the energies, structural and dynamic properties of the systems was performed using the GROMACS built-in analytical tools. The graphics of the molecular structure of the system were extracted using Visual Molecular Dynamics (VMD) program.²⁰⁰

Table 5. 1. System Composition and Simulation Setup

PA molecules	24 PA molecules in toluene-water system		24 PA molecules in heptane-water system	
	N_{toluene}	N_{water}	N_{heptane}	N_{water}
C5 Pe	3124	14868	2001	15622
PAP	3144	14868	2023	15613
TP	3159	14877	2025	15625
PCH	3136	14635	2019	15262
BisA	3123	14878	1987	15638

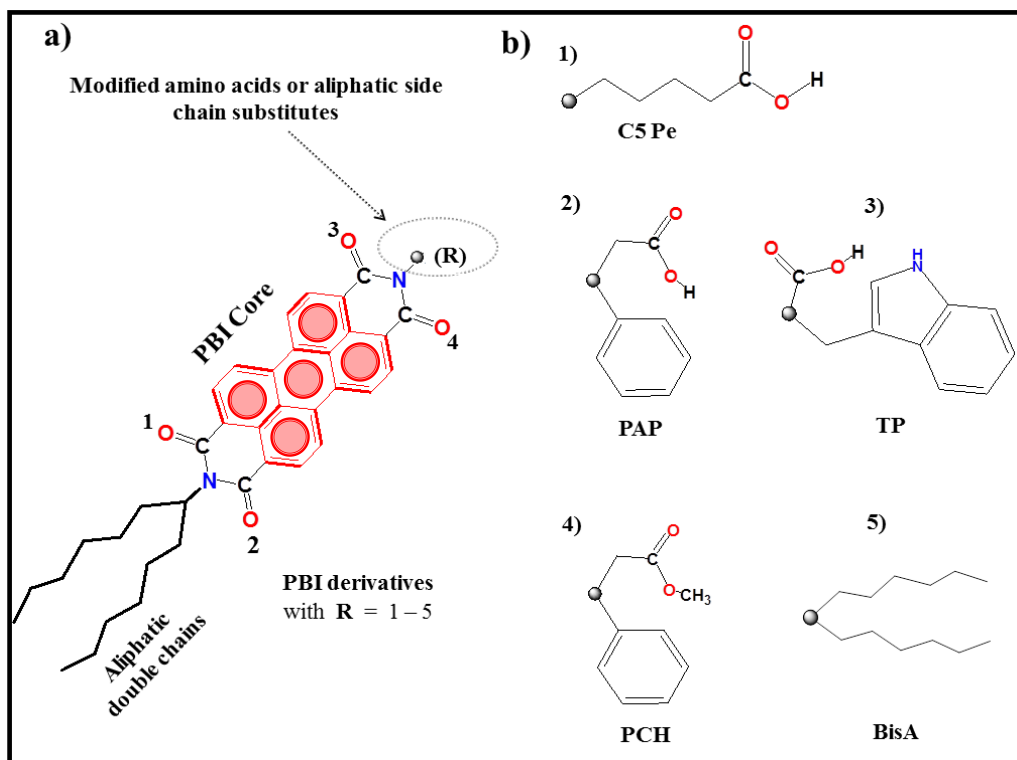


Figure 5.1. Two-dimensional schematic representation of the perylene bisimide-based polyaromatic (PA) molecules used in this study. All the PA molecules incorporate a polyaromatic perylene core with two alkyl chains attached to one end (a) and a different functional group attached to the other end of the molecules (b). This gives rise to asymmetric PA molecules with one portion of hydrophilic polar head group and the other hydrophobic nonpolar group. R is substituted by different types of amino acids or aliphatic alkyl groups such as β -alanine, phenylalanine, tryptophan and branched n-alkanes (R = 1-5, the black filled circle in (a) 2D structure refers to the linkage site for the various side-chain substitutes)^{103-105,219-221} The carboxylic functional groups were set to either protonated (-COOH) or deprotonated (-COO⁻) states.

5.3 Results and Discussion

5.3.1 Density Profiles of Protonated PA Molecules

Figure 5.2 shows the density profiles of the systems averaged over the last 2 ns of the simulation time. To compute the density distribution of the system, the simulation box was divided into 50 slabs of equal thickness along the z-direction, which is perpendicular to the oil-water interface, followed by calculating the density of various species in each slab. The oil (toluene or heptane) and water phases remain partitioned into two layers in all simulations. The oil-water interfaces in these density profiles were located at the location where the two (oil and water) lines intersect. The partition of the various protonated PA molecules at the oil-water interface was found to be highly sensitive to the variations of the side chain functional group and the polarity of oil phase. In toluene-water systems, most of the protonated PA molecules (except for C5 Pe) slightly prefer to stay in the bulk toluene phase (core-bound molecules). For most of these PA molecules, the tendency of forming small nanoaggregates in the bulk toluene phase was more predominant than the tendency to partition at the toluene-water interface.

The density distribution for the PA molecules exhibits small peaks at the two interfaces, but these peaks are generally comparable to the density peaks in the bulk. In contrast, PA molecules (except for TP) tend to predominantly concentrate or position near the heptane-water interface and form large nanoaggregates at the vicinity of the interface (interface-bound molecules).

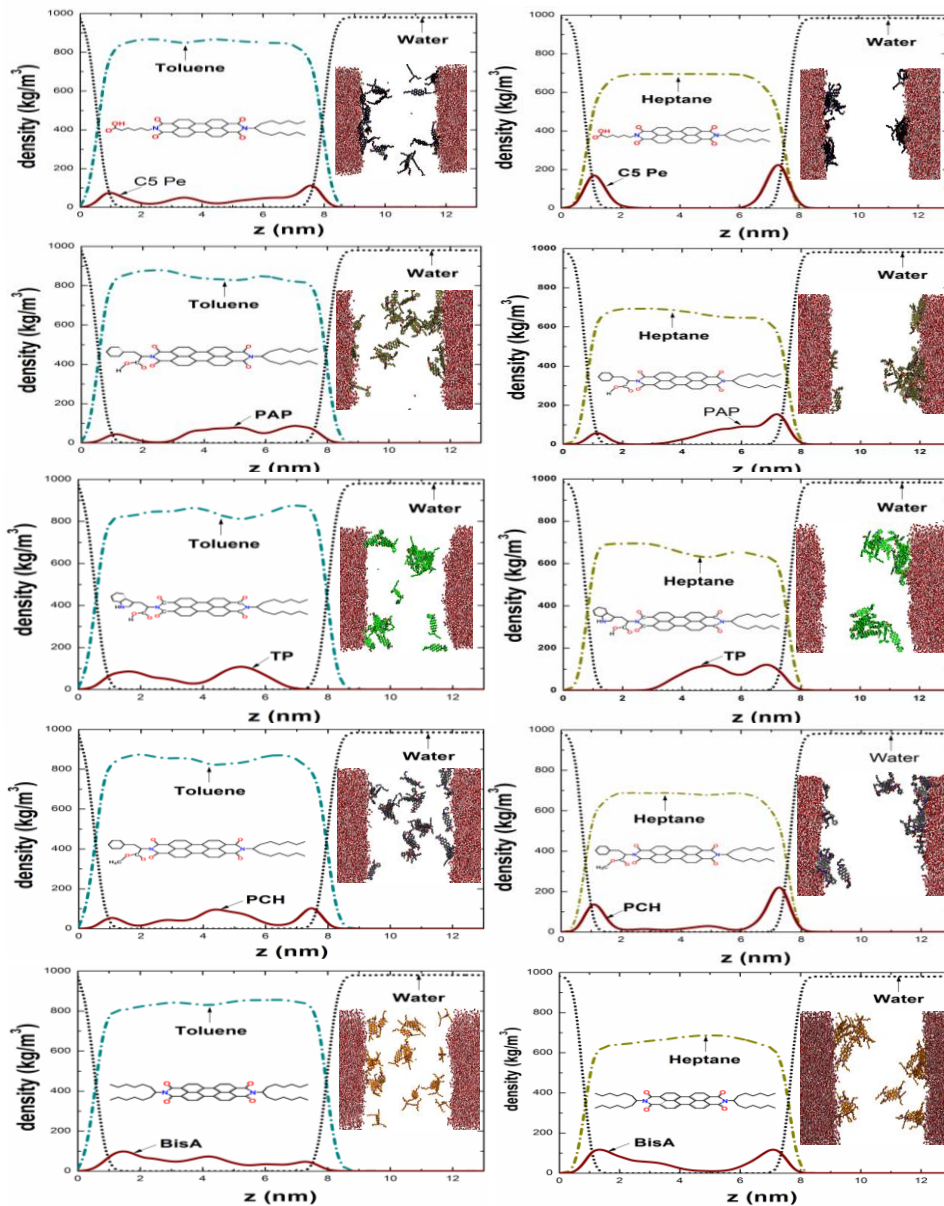


Figure 5.2. Density profiles of toluene-water and heptane-water systems containing various protonated PA molecules, averaged over the last 2 ns of the simulation time at 298 K. In all the simulations, the carboxylic acid group in the PA molecule is protonated. The snapshots of the PA molecules at the end of the simulation are also shown in the figure (Inset). The toluene and heptane molecules are not displayed for clarity.

These results indicate that the adsorption of the PA molecules to the oil-water interface is hindered when the oil phase consists of aromatic molecules (toluene). Figure 5.3 depicts pair correlation functions between the protonated PA molecules and between PA molecules and water. The results show a monotonic increase in pair correlation functions between the PA molecules and water in both solvents with increasing the separation distance between the aromatic core and water (Fig. 5.3 a and b). This finding implies that the centroids of all the PA molecules are most likely embedded in the organic phase. Among the PA molecules investigated in both oil-water systems, the $g(r)$ of C5 Pe shows the sharpest increase with increasing the distance from the aromatic core. In contrast, the $g(r)$ of TP in both oil-water systems exhibits the least increase with increasing the distance from aromatic core, indicating that TP is the least interfacially active and prefers the organic phase (core-bound molecule).

In order to investigate the impact of the water phase on the association of these molecules in the organic solvent, we have calculated the $g(r)$ of the PA molecules (Fig. 5.3 c and d). Comparing these results with our previous chapter results for the $g(r)$ in bulk toluene and heptane,²¹⁸ it is evident that while the presence of water phase does not dramatically alter the behavior of the $g(r)$ of these molecules, it does show some subtle differences in the self-association. For instance, in bulk heptane, C5 Pe had the highest peak²¹⁸, whereas in the presence of water, TP exhibits the highest peak (Fig. 5.3d). Thus, for deprotonated PA molecules, the self-association remains the dominant mode of interaction. For the three molecules containing carboxyl functionality (TP, C5 Pe, and PAP), the pair

correlation functions between the carboxyl groups and the water show substantial variations (Fig. 5.4 a and b).

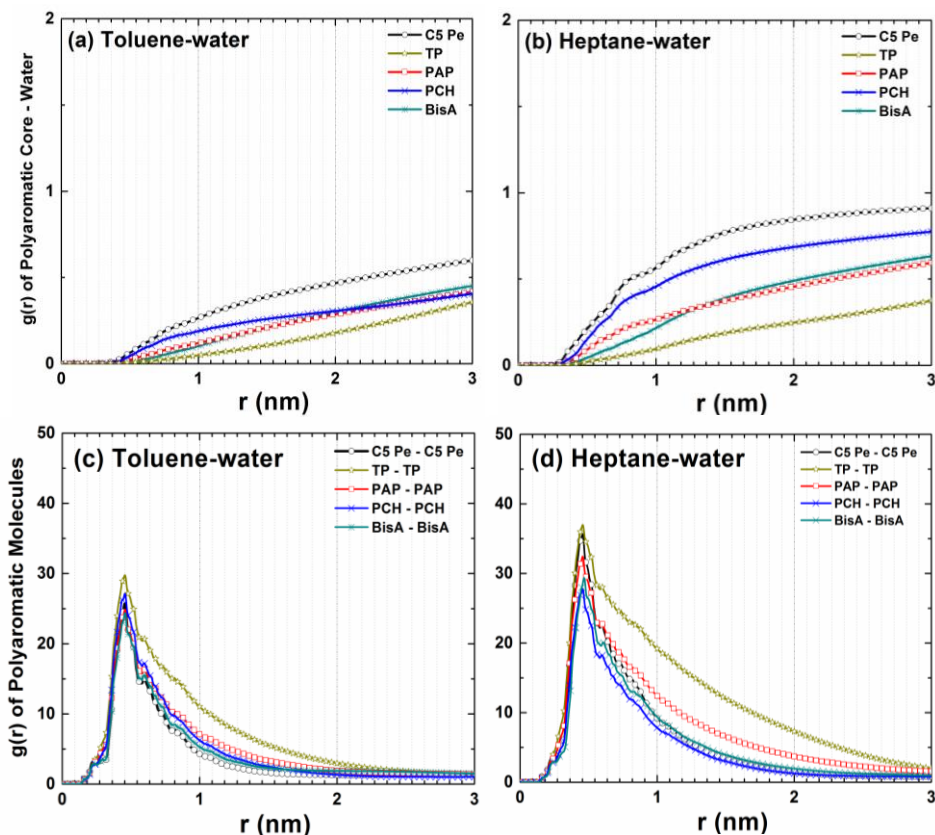


Figure 5.3. Radial distribution function calculated from the center of mass between the PA molecules and water (a-b), and among PA molecules in the bulk oil phase (c-d) averaged over the last 2 ns of the simulation time in toluene-water and heptane-water systems at 298 K. The presence of a hydrophobic aromatic residue at the side chain of the PA molecules such as tryptophan moiety decreases the interfacial activity and increases their propensity to form nanoaggregates in the bulk oil phase.

C5 Pe carboxyl groups were found to be most attracted to the oil-water interface among the three types of PA molecules. The tendency of the carboxyl groups of C5 Pe to be in the vicinity of the heptane-water interface is more pronounced than that of the toluene-water interface. However, as the -COOH groups in our simulations are protonated (uncharged), we do not find them embedded in the water layer. All the molecules remain within the organic phase, and do not partition into the water phase. Keeping the molecules protonated in these simulations allows us to remove the effect of charges on the partitioning (which is the strongest driving force for interfacial activity) and probe the influence of other types of interactions (such as π - π interactions, steric effects, dipole-dipole interactions and H-bonding) on the nanoaggregation and interfacial partition of these types of molecules. Furthermore, the pair correlation function between the side chains of TP, PAP and PCH molecules and the water molecules were computed to investigate the effect of side chains on partition of PA molecules at oil-water interfaces. In toluene-water systems, all PA molecules exhibit similar tendency of being concentrated near the interface, whereas in heptane-water systems, PCH exhibits a slightly higher tendency to be concentrated near the interface (Fig. 5.4 c and d).

In studying the role played by the side chain functional groups of PA molecules in their adsorption at the oil-water interface, the presence of an aromatic amino acid tryptophan residue in PA molecules (TP) was found to severely inhibit the migration of the PA molecule to the oil-water interface. Tryptophan residue prefers to remain buried in hydrophobic aromatic cores of PA

molecules, which results in the formation of larger nanoaggregates in the bulk organic phase. Thus the interfacial activity of this type of molecules is typically low. These results are consistent with our previous findings that TP molecules have a higher tendency to aggregate in both toluene and heptane (see Chapter 4).

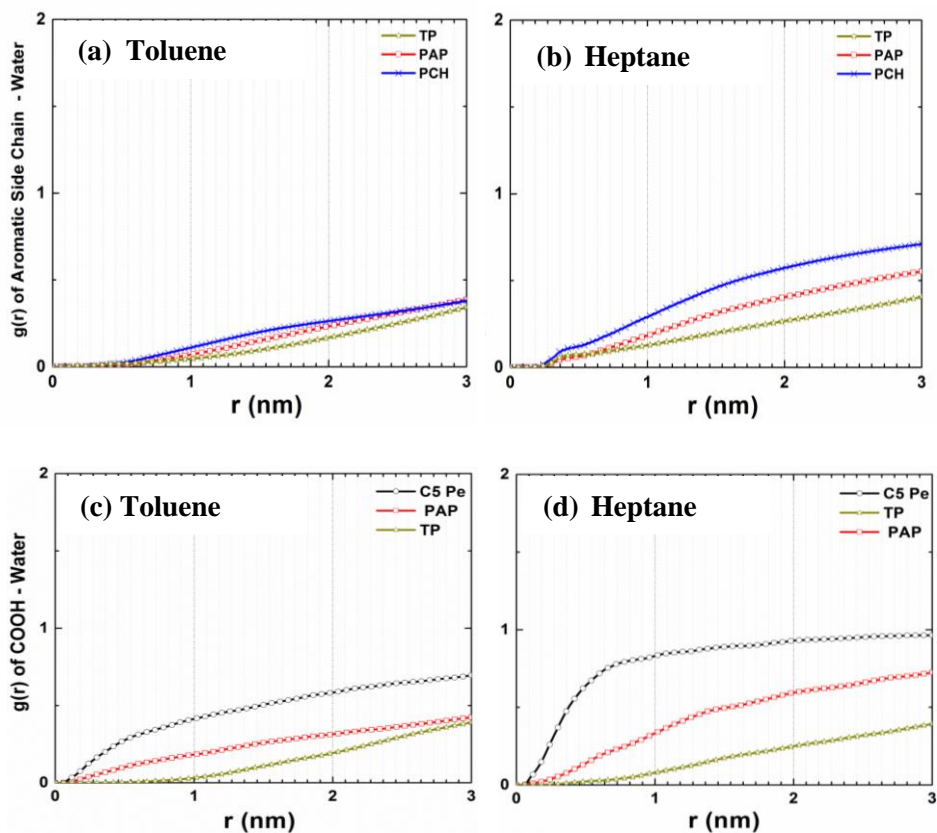


Figure 5.4. Radial distribution function calculated from the center of mass between the aromatic side chain and the water (a-b), and the carboxyl groups of PA molecules and the water (c-d) averaged over the last 2 ns of the simulation time in toluene-water and heptane-water systems at 298 K.

Variation in the size, number and heterocyclic nature of the hydrophobic aromatic rings at the side chains also alters the interfacial activity of the

protonated PA molecules. This is evident by comparing the results of TP and PAP. The larger, the size of the aromatic rings (for example phenyl ring \rightarrow indole ring), the lower the interfacial activity due to stronger π - π interactions in the bulk oil phase and reduced intermolecular hydrogen-bond interactions between the PA and water molecules.

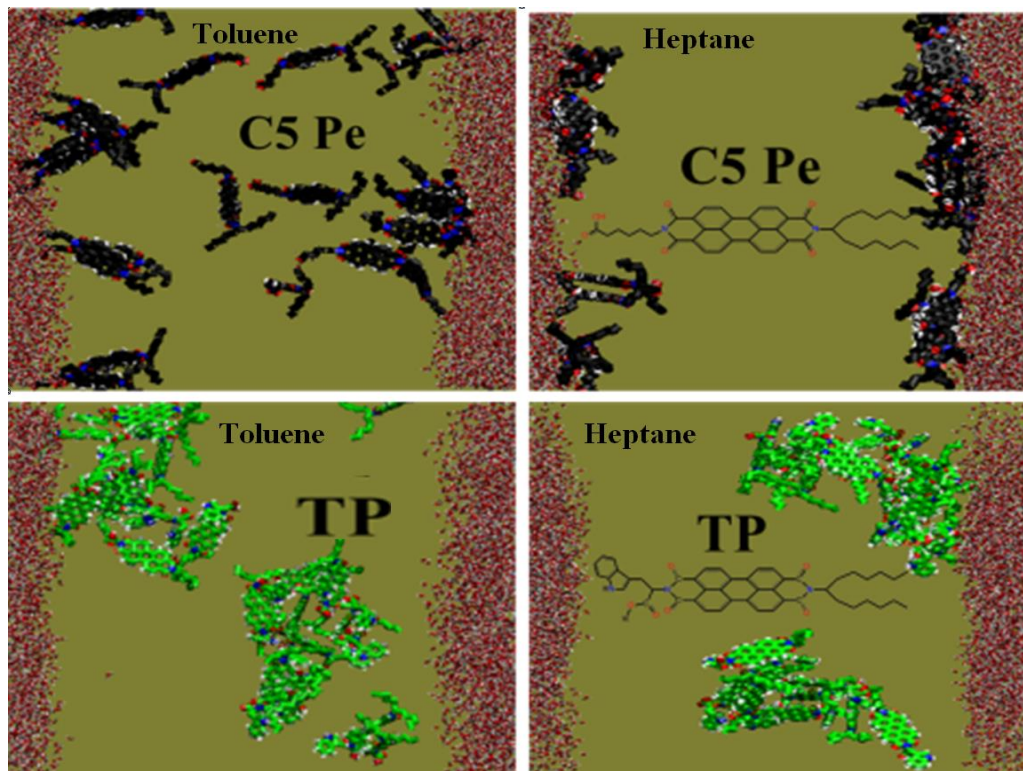


Figure 5.5. Snapshots of molecular configurations of C5 Pe and TP molecules at the end of the simulation time. Each molecule is presented by a different color to distinguish one from the other: C5 Pe in black, TP in green and water in red. All the snapshots are along the x-direction.

Our results further indicate that PA molecules with short-chain aliphatic acids (C5 Pe) tend to concentrate much more near the oil-water interface

(interface-bound molecules) than PA molecules of phenylalanine, tryptophan and/or aliphatic moieties in the side chains. These results indicate that making the side-chain substituents less hydrophobic and aromatic increases the interfacial activity of the PA molecule. It is also important to mention that phenylalanine and tryptophan side-chains contain a bulky aromatic head group, which could prevent or shield its carboxylic acid group from interacting with the water molecules via hydrogen bonding. Interestingly, none of the polyaromatic cores of the PA molecules are associated with the aqueous phase. They prefer to remain in the organic solvent (see Fig.5.5).

5.3.2 Partition and Aggregation of Protonated Polyaromatic Molecules at the Oil-Water Interface

The partition and aggregation of the protonated PA molecules at the oil-water interface have been investigated further in a quantitative manner in this section. In all simulations, the PA molecules are initially evenly dispersed in three layers on a regular lattice configuration within a cubic box of 10 nm edge filled with an organic solvent. Each layer contains 8 PA molecules in the organic solvent as shown in Figure 5.6a. The solvent box is then extended in the z-direction by 5 nm and filled with water. Noting that the system is periodic, the oil-water interface is closest to the uppermost and lowermost layer of the PA molecules, indicating that 16 of the PA molecules out of a total 24 reside (simulation 1) at a distance of approximately 2.5 nm from the oil-water interface. The PA molecules in the central layer are, however, positioned equidistant from the two oil-water interfaces with an average distance of approximately 5 nm. The

root mean square distance (RMSD) of all the PA molecules as a function of time from the nearest oil-water interface (along z) is calculated using the following equation:

$$RMSD = \sqrt{\frac{1}{N} \sum_{i=1}^N \delta_i^2} \quad (5.1)$$

where N is the total number of PA molecules in the system and δ_i is the difference between the actual distance of the i^{th} PA molecule from the oil-water interface and the average distance of all the PA molecules in the system from the oil-water interface.

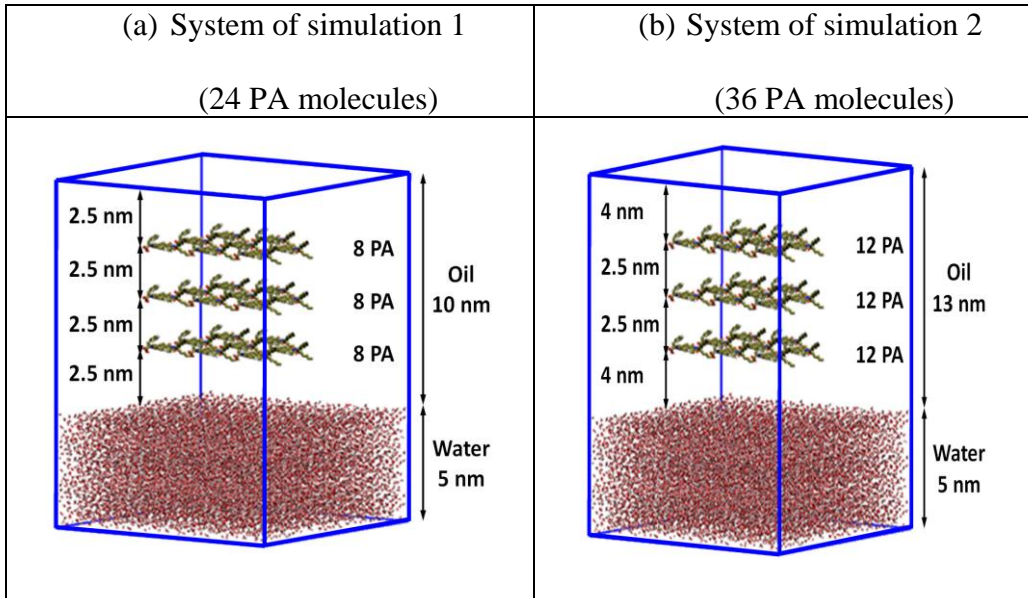


Figure 5.6. A schematic diagram showing the initial molecular arrangements of the PA molecules at the oil-water systems (a) 24 PA molecules, and (b) 36 PA molecules.

In order to validate the effect of the interface separation and box size on simulation results, we performed the following additional simulation by increasing the box size in all directions by 3 nm to 13 nm to check the convergence of simulations. The simulation box was constructed by first packing 36 C5 Pe (simulation 2) molecules in a cubic box of 13 nm size and then solvated with 3001 heptane molecules, followed by energy minimization. The concentration of C5 Pe molecules in this simulation box remained the same as in simulation 1. The box was then extended in the z-direction by 5 nm and filled with the water molecules.

In simulation 1, 16 PA molecules (upper and lower layer) are 2.5 nm away from the interface and the remaining 8 PA molecules are at a distance of 5 nm from the interface. The RMSD of this initial state is calculated to be $\text{SQRT} [((2.5 \text{ nm})^2 + (5 \text{ nm})^2 + (2.5 \text{ nm})^2)/3] = \sim 3.54 \text{ nm}$. In simulation 2 (Fig.5.6b), on the other hand, 24 PA molecules are 4.0 nm away from the interface and the remaining 12 PA molecules are at a distance of 6.5 nm. The RMSD of this initial state is calculated to be $\text{SQRT} [((4.0 \text{ nm})^2 + (6.5 \text{ nm})^2 + (4 \text{ nm})^2)/3] = \sim 4.97 \text{ nm}$.

It is evident that the difference in the initial RMSDs between the two for simulations 1 and 2 is $4.97 \text{ nm} - 3.54 \text{ nm} = \sim 1.43 \text{ nm}$. As shown in Figure 5.7, this difference caused the PA molecules in simulation 1 to reach the interface faster than the PA molecules in simulation 2 due to a shorter distance of PA molecules away from the interface in simulation 1 than in simulation 2. However they converged to the same state over a longer simulation period around 9.5 ns (in this particular case all the PA molecules reached the interface).

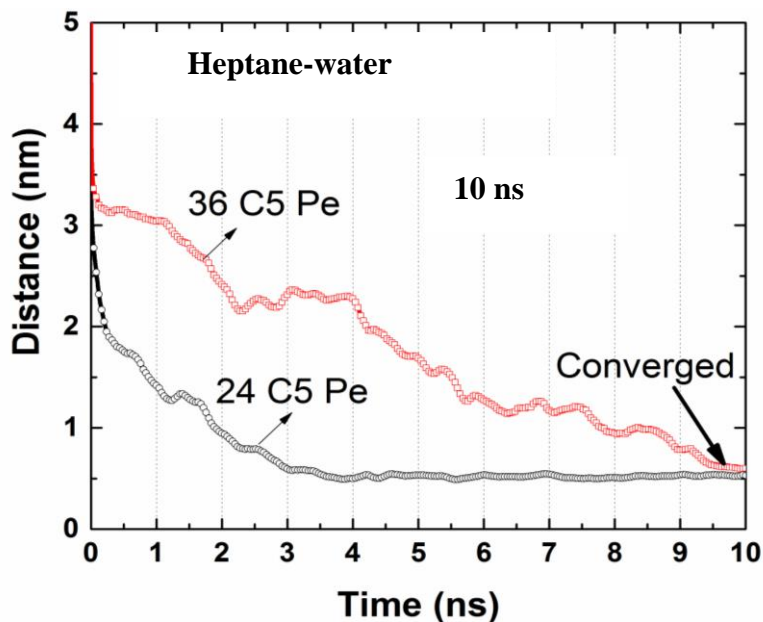


Figure 5.7. The root mean square distance of C5 Pe molecules as a function of time from the oil-water interface (along z) in heptane-water system at 298 K.

This finding indicates that the size of the simulation box does not change the dynamics and final state of C5 Pe adsorption but does change the time when the molecules reach the interface due to the differences in initial separation distances of C5 Pe molecules away from the interface. This additional simulation further confirms a minimal, if there is any, effect of box size on the adsorption of PA molecules to the oil-water interfaces.

In addition, to track the dynamics of these three layers of molecules, we first index the top, middle and bottom layers of molecules separately (simulation 1), followed by the calculation of their RMSD from the oil-water interface (along the z direction, which is normal to the oil-water interface). In Figures 5.8a and b, C5 Pe₈ represents C5 Pe molecules in the middle layer, while C5 Pe₁₆

represents C5 Pe molecules in the upper and lower layer since they are both equidistance from the oil-water interface.

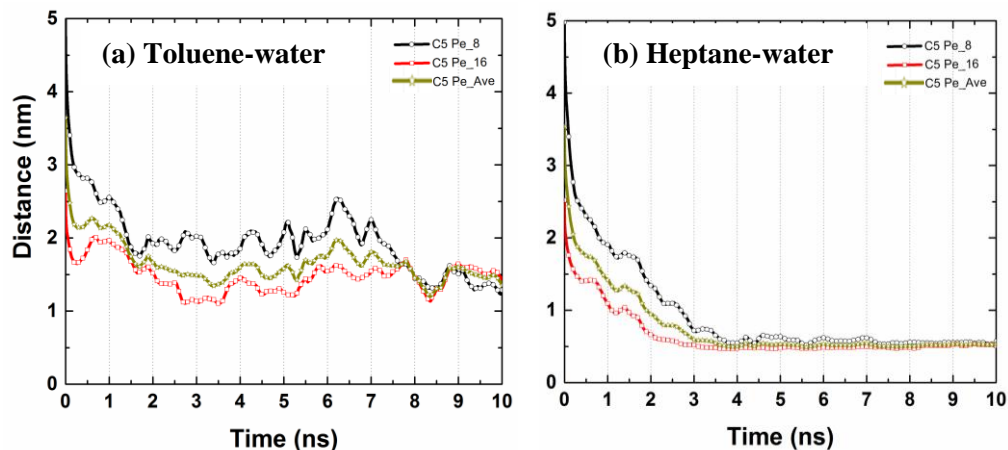


Figure 5.8. The root mean square distance of each layer of C5 Pe molecules as a function of time from the oil-water interface (along z) in heptane-water system at 298 K.

The results show that all the C5 Pe molecules, regardless of which layer they belong, migrated equally and consistently to the oil-water interface. This finding indicates the absence of initial bias in interactions of the PA molecules in three layers (top, middle and bottom) with the oil-water interface. C5 Pe_Ave represents the average of the three layers.

Figure 5.9 shows the root mean square distance (RMSD) between the PA and water molecules as a function of time. As shown in Figure 5.9a, all five PA molecules gave similar RMSD plots for toluene (weak tendency to go to the interface). The PA molecules prefer to partition to the organic-water interface when the organic phase is heptane. With the exception of TP molecules, the rate of approach of all PA molecules to the oil-water interface is faster in heptane than

toluene (Figure 5.9b), indicating a distinctly lower interfacial affinity of the PA molecules in toluene than in heptane.

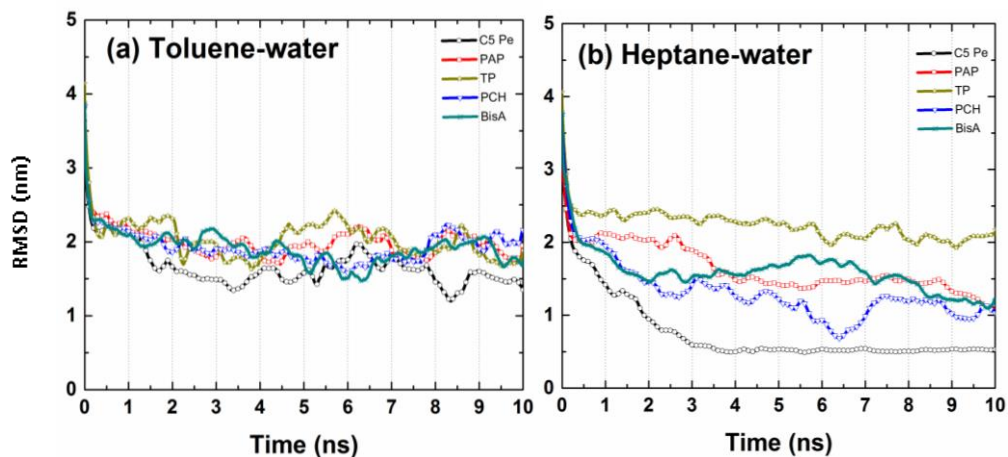


Figure 5.9. The root mean square distance of different PA molecules and oil-water interface as a function of time in toluene-water and heptane-water systems at 298 K.

The rate of different PA molecules approaching the heptane-water interface varied over a wider range than that approaching the toluene-water interface, depending on the side-chain substituents. For example, all C5 Pe molecules came to the heptane-water interface within the first 3 ns and equilibrated within 1 nm range from the interface. In contrast, TP molecules show poorer adsorption to the interface with an equilibrium distance of approximately 2.5 nm from the interface. In the first 3 ns, the rate of PA molecules approaching the heptane-water interface follows the order of C5 Pe > PCH > BisA > PAP > TP.

The partition ratio ($P_{I/T} = N_I / N_T$) and the total number of water molecules (N_{H_2O}) around the PA molecules were also calculated in this section. To calculate

the number of interface-bound molecules near the oil-water interface we use a cutoff distance of 1 nm from the oil-water interface to the bulk oil phase. All PA molecules within the 1 nm oil film from the oil-water interface are considered as interface-bound PA molecules. The remaining PA molecules in the system (core-bound molecules), however, associate to various degrees in the bulk organic phase to form nanoaggregates. Consequently, the partition ratio of each PA molecule, as well as the total number of water molecules around the PA molecules was calculated. The total number of water molecules around the PA molecules was calculated to examine the association of PA molecules with water in the system. All water molecules within 0.5 nm (radius) from the center of mass of the PA molecules were considered as water associated with the interface-bound PA molecules (molecules within the 1 nm of the oil film).

Figure 5.10 shows PA molecules containing aliphatic carboxylic acid functional groups exhibit the highest partition coefficient to the interface, whereas PA molecules containing the tryptophan residue show the lowest partition coefficient. The variation in partition coefficient observed in our simulation indicates that the adsorption of PA molecules to the interface decreases when bulk aromatic functional groups are incorporated as side-chain substituents, particularly when the oil phase is toluene.

For the hydration of the PA molecules, the PA molecules containing tryptophan residue have the lowest number of associated water molecules, as compared to the other PA molecules (see Table 5.2). In contrast, the PA molecules containing aliphatic carboxylic acid groups show the highest degree of association with water

molecules. This finding indicates that PA molecules containing aliphatic carboxylic acid in the side chain can lower the oil-water interfacial tension to a larger extent than PA molecules containing aromatic or aliphatic moieties in the side chains.

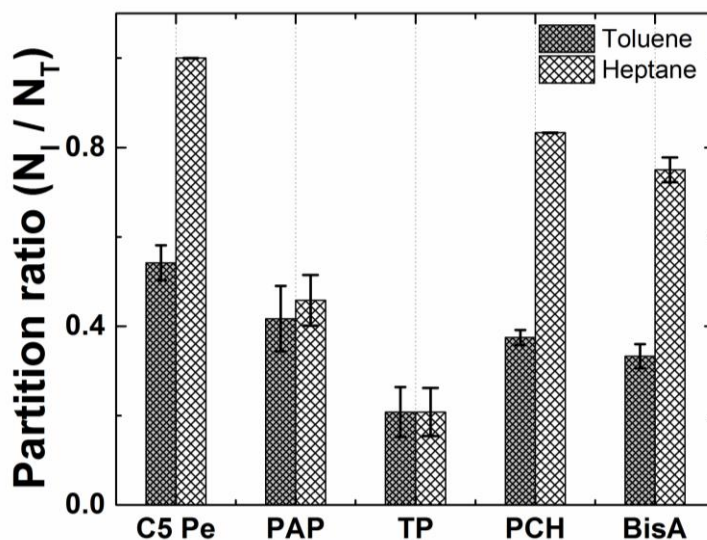


Figure 5.10. Partition ratio of the PA molecules in heptane-water and toluene-water systems averaged over the last 2 ns of the simulation time at 298 K.

The results obtained from these simulations indicate that C5 Pe has the highest tendency to migrate to the oil-water interface. Moreover, the presence of a carboxylic acid was found to be crucial for the interfacial activity. Therefore, even though the aromatic core of the PA molecules are identical and there are several polar C=O groups in the compound, which can form weak hydrogen bonds with the water molecules at the interface, the absence of the carboxylic group and the nature of the functional groups (such as indole) change the partitioning behavior of PA molecules dramatically.

Table 5. 2. The total number of water molecules around the interface-bound PA molecules (within the 1 nm oil film on the water) at the end of the simulation time

PA molecules	toluene-water system	heptane-water system
	N_{H_2O}	N_{H_2O}
C5 Pe	225	465
PAP	163	243
TP	30	39
PCH	137	339
BisA	28	271

5.3.3 Intermolecular Hydrogen Bonding of Protonated PA Molecules at the Oil-Water Interface

The hydrogen bonding between PA and water molecules has a significant effect on several physico-chemical properties of the oil-water interface.²²²⁻²²⁴ For example, PA molecules adsorbed at the oil-water interface through various intermolecular interactions (e.g., dipole-dipole, H-bonding, etc.) lower the interfacial tension by altering and disrupting the hydrogen bonding of the water molecules in the vicinity of the interface.^{225,226} In this section, the hydrogen bonds between PA and interfacial water molecules were determined. To calculate the hydrogen bonding in our systems, a geometric criterion of Donor – Acceptor distance $r_{DA} \leq 3.5 \text{ \AA}$ and Acceptor – Donor – Hydrogen (H) angle $\theta_{ADH} \leq 30^\circ$ was used, as implemented in GROMACS 3.3.3.

The calculated average number of intermolecular hydrogen bonds in our systems, normalized by the total number of PA molecules is shown in Table 5.3. The results in Table 5.3 indicate a large difference in the tendency of forming intermolecular hydrogen bonds between the PA and water molecules at the toluene-water and heptane-water interfaces. Interestingly, irrespective of the nature of the side chain functional groups attached to the PA molecule, fewer hydrogen bonds between the PA and water molecules were observed in toluene-water systems than in heptane-water systems.

Table 5. 3. The average number of intermolecular hydrogen bonds per PA molecule (N_{H-Bond}) at 298 K temperature and 1 bar over the last 2 ns simulation time

PA molecules	toluene-water system	heptane-water system
	N_{H-Bond}	N_{H-Bond}
C5 Pe	1.260 ± 0.074	2.570 ± 0.060
PAP	0.510 ± 0.116	1.100 ± 0.120
TP	0.204 ± 0.039	0.340 ± 0.093
PCH	0.780 ± 0.072	1.940 ± 0.044
BisA	0.310 ± 0.020	0.800 ± 0.050

The difference is attributed to the relatively more polar/aromatic nature of the toluene molecules, which retards the PA molecular adsorption to the interface. Among the PA molecules studied, C5 Pe molecule has a high tendency to form

hydrogen bonding with the water molecule in all systems. In contrast, TP and BisA show the least hydrogen bond in all systems. The results demonstrate that C5 Pe molecule has a high tendency to reduce the interfacial tension of the oil-water system than TP and BisA molecules. In toluene-water systems, PCH and PAP molecules exhibit comparable tendency of being concentrated near the interface, whereas in heptane-water systems, PCH exhibits a higher tendency to be concentrated near the interface. These results indicate that PCH in heptane-water system have a high tendency to form intermolecular hydrogen bond compared to PAP molecules.

5.3.4 The Preferential Orientation of Protonated PA Molecules at the Oil-Water Interface

The impact of aromatic and aliphatic substituents on preferred orientation of the PA molecules at the oil-water interface was investigated. In this calculation only molecules within the 1 nm oil film on the water were considered as interface-bound PA molecules. The remaining core-bound PA molecules in the bulk organic phase were entirely excluded from the quantitative analyses. Based on the results obtained from Figure 5.10 we chose PAP and C5 Pe molecules for the purpose of comparison due to their distinct constituents of diametrically opposite side chains and sufficient number of interface-bound molecules in both toluene-water and heptane-water interfaces.

Figure 5.11 (a-d) shows the distance of the individual interface-bound PA molecules from the oil-water interface as a function of time averaged over the last 2 ns of the simulations time. Each line represents a single interface-bound PA

molecule as a function of time. As one can see in Figure 5.11 (a-d), once the PA molecules enter the interfacial-bound region (< 1 nm from the oil-water interface) they will stay there for the rest of the simulation time (at least in most cases), indicating a strong stability of the PA molecules within this region.

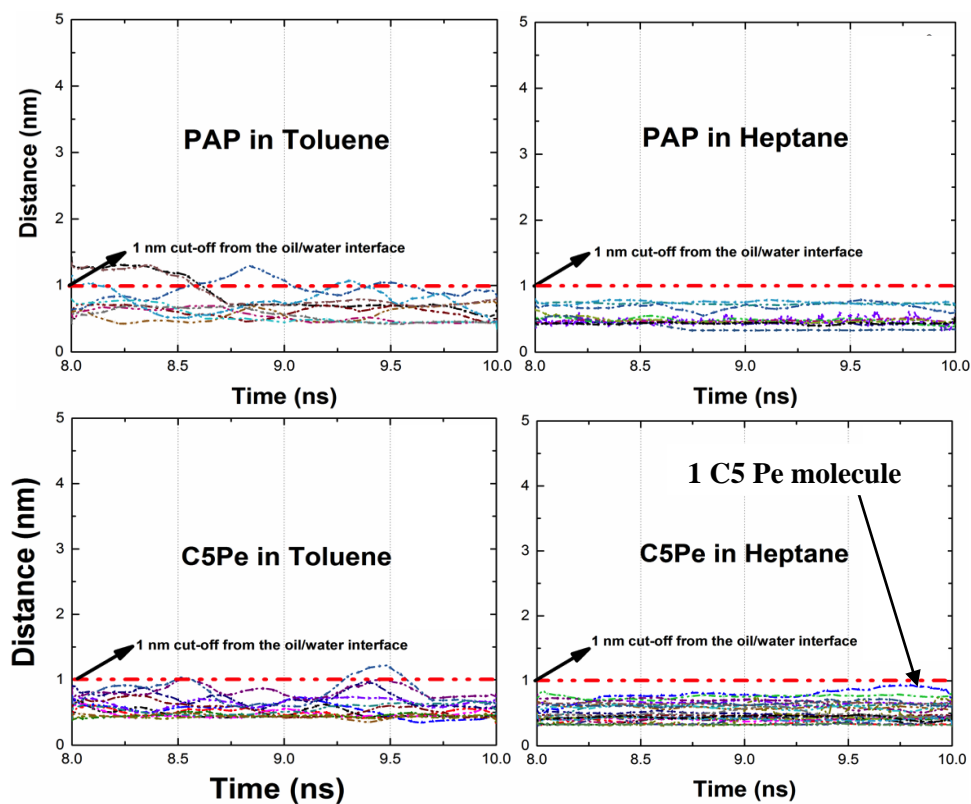


Figure 5.11 (a-d) The distance of the individual interface-bound PA molecules from the oil-water interface as a function of time averaged over the last 2 ns of the simulations time at 298 K.

A graphical illustration of the methodology used to calculate the preferential orientation of the adsorbed PAP and C5 Pe molecules with reference to the oil-water interface is shown in Figure 5.12. To obtain the angle distribution (θ) of the adsorbed molecules at the oil-water interface, we calculated the angle

between the vector \vec{n} , which is normal to the polyaromatic ring plane of the PA molecule and vector \vec{b} , which is perpendicular to the oil-water interface (Figure 5.12). The direction of vector \vec{b} is along the z-axis of the simulation box. The statistical averaging was performed over the last 2 ns of the simulation time. The $\langle\theta\rangle$ value ranges from 0° to 90° . We refer the adsorption as *flat-on* and *head-on* (or *side-on*) when $\langle\theta\rangle$ is $\leq 30^\circ$ and $\geq 60^\circ$, respectively.

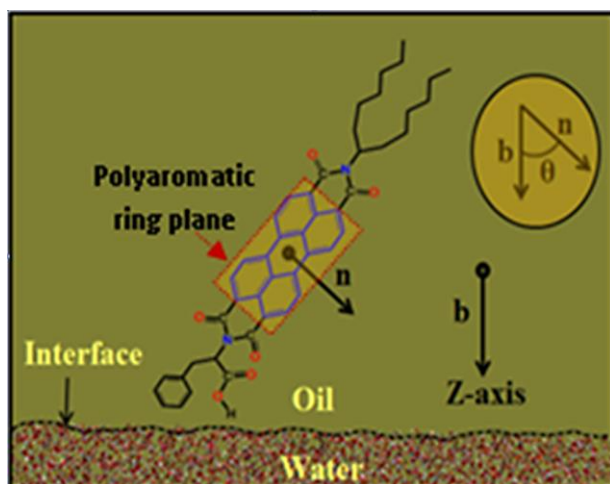


Figure 5.12. The schematic representation of the angle distribution (θ) of the polyaromatic ring plane of the PA molecules at the oil-water interface.

When $\langle\theta\rangle$ is $\leq 30^\circ$, the polyaromatic ring plane of the PA molecules is referred to as parallel to the oil-water interface. Conversely, when $\langle\theta\rangle$ is $\geq 60^\circ$, the polyaromatic ring plane of the PA molecules is considered as perpendicular to the oil-water interface. The angle ranges between the parallel and perpendicular are referred to as intermediate or inclined orientation of uncharged PA molecules adsorbed at the oil-water interface.

The angle distributions as a function of the number fraction of the adsorbed PA molecules of C5 Pe and PAP in toluene-water and heptane-water system are reported in Figure 5.13 (a-b). The statistics were collected for all the interface-bound molecules near the interface as reported earlier. The number fraction of the PAP and C5 Pe molecules over a given angle range (θ) was calculated by dividing the number each molecule spent over that angle range by the total data points collected over the last 2 ns of the simulation time ($N_f = N_i / N_{Total}$).

From the angle distribution results, it is evident that both C5 Pe and PAP, irrespective of the side-chain substituents and solvent property of the oil phase, tend to orient more *head-on (side-on)* configuration at the oil-water interface. However, various other minor angle distributions of the C5 Pe and PAP molecules at the interface were also observed. C5 Pe molecules, for example, partition into 12.8 % *flat-on*, 32.4 % intermediate, and 54.8 % *head-on* angles at the toluene-water interface. In contrast, in heptane-water interface, C5 Pe molecules exhibit a 29.4 % *flat-on*, 30.4 % intermediate, and 40.2 % *head-on* angle distribution. On the other hand, PAP molecules show a 9.4 % *flat-on*, 33.4 % intermediate and 57.2 % *head-on* angle distribution at the toluene-water interface, in contrast to 4.3 % *flat-on*, 23.9 % intermediate and 71.8 % *head-on* angle distribution at heptane-water interface. Figure 5.14 (a-d) shows the molecular configurations of C5 Pe and PAP at the end of the simulation time in toluene-water and heptane-water systems. The predominant conformational preference for *head-on or side-on* configuration of C5 Pe and PAP in both cases could be due to the influence of π - π stacking between the polyaromatic rings and

the hydrogen bonding between carboxylic functional group and the proton of the water molecules localized at the interface.

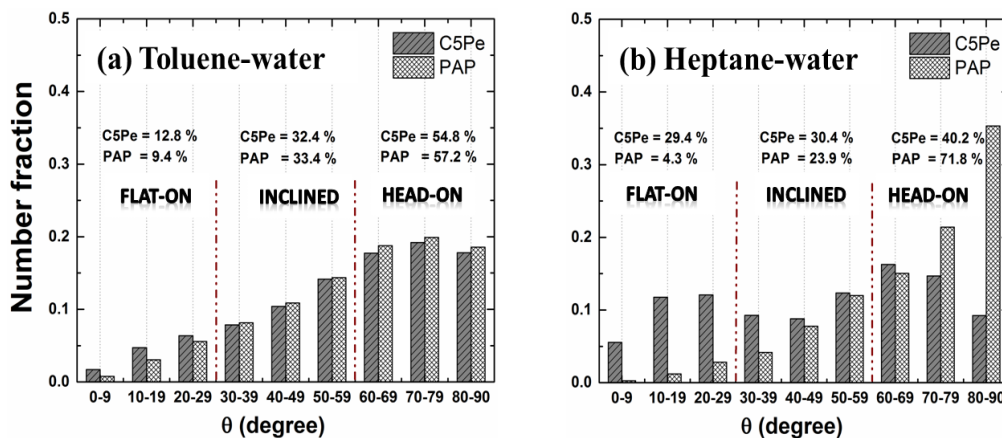


Figure 5.13 (a-b). The number fraction ($N_f = N_i / N_{Total}$) of polyaromatic molecules averaged over the last 2 ns of the simulation time in toluene-water (a) and heptane-water (b) 298 K.

Moreover, the results demonstrate that in toluene-water system C5 Pe and PAP molecules show similar angle distributions. However, at the heptane-water interface a large variation was observed between PAP and C5 Pe molecules. The polyaromatic plane of the PAP molecules at the heptane-water interface prefers more *head-on* (perpendicular to the oil-water interface) than C5 Pe molecules.

In order to gain a better insight into the rigidity of the nanoaggregates formed at the oil-water interface, we calculated the radial distribution function among the polyaromatic ring of the PAP and C5 Pe molecules. The results (Figure 5.15 a-b) show a strong π - π stacking among the interface-bound molecules at the interface.

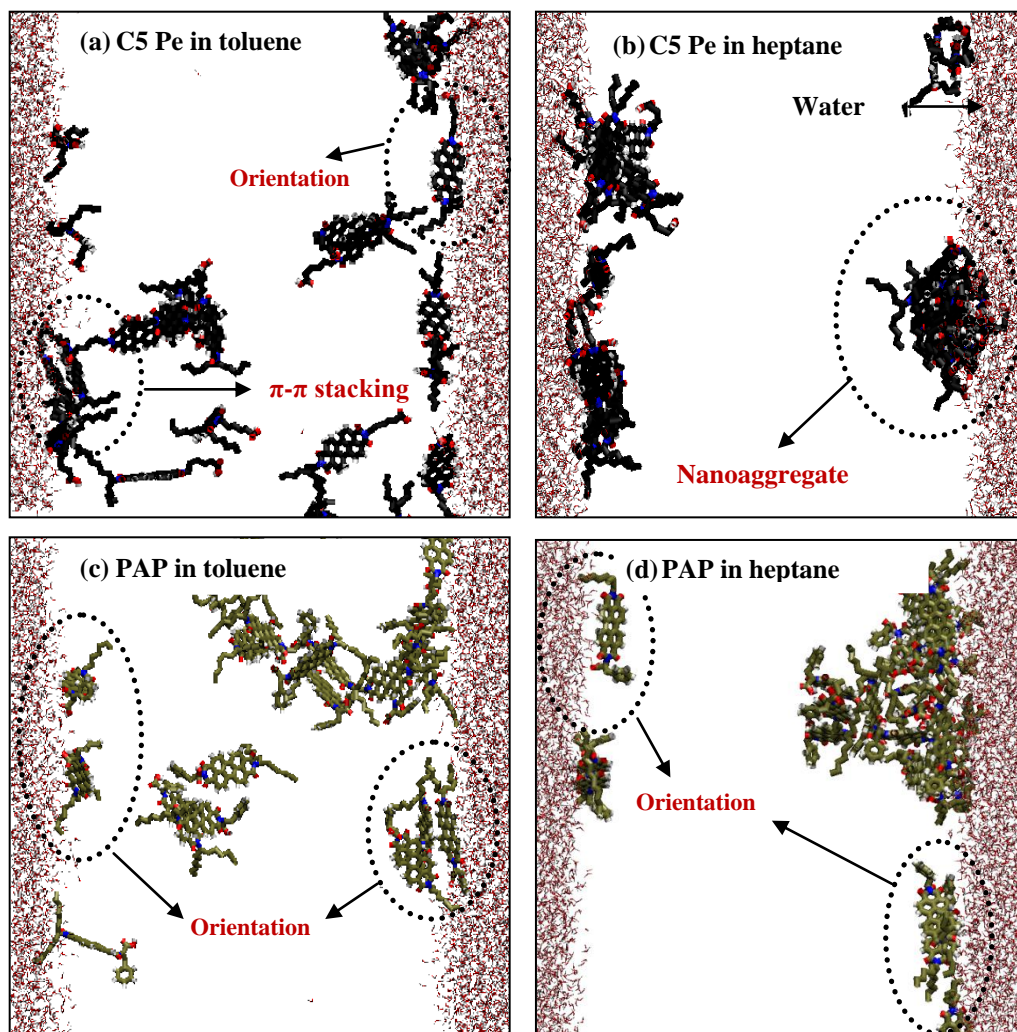


Figure 5.14 (a-d). Snapshots of molecular configurations of C5 Pe and PAP at the toluene-water and heptane-water interface at the end of 10 ns simulation time. Each molecule is shown in different colors to distinguish one from the other: PAP in tan and C5 Pe in black. In all structures, oxygen, nitrogen and hydrogen atoms are shown in red, blue and white, respectively. All the snapshots are top view of the simulation box. Toluene and heptane molecules have been removed for clarity.

The strong π - π stacking formed among C5 Pe and PAP molecules at the oil-water interface demonstrates the contribution of π - π interaction to the rigidity of the film formed. The snapshots in Figure 5.15b (inset) were taken at the end of 10 ns simulation time at heptane-water interface. It is important to highlight that the *head-on* or *side-on* molecular orientation predicted by our simulation for C5 Pe molecules at the toluene-water interface agrees well with the results of vibrational spectroscopy obtained using sum frequency generation (SFG) by Andrews, *et al.*⁴⁰

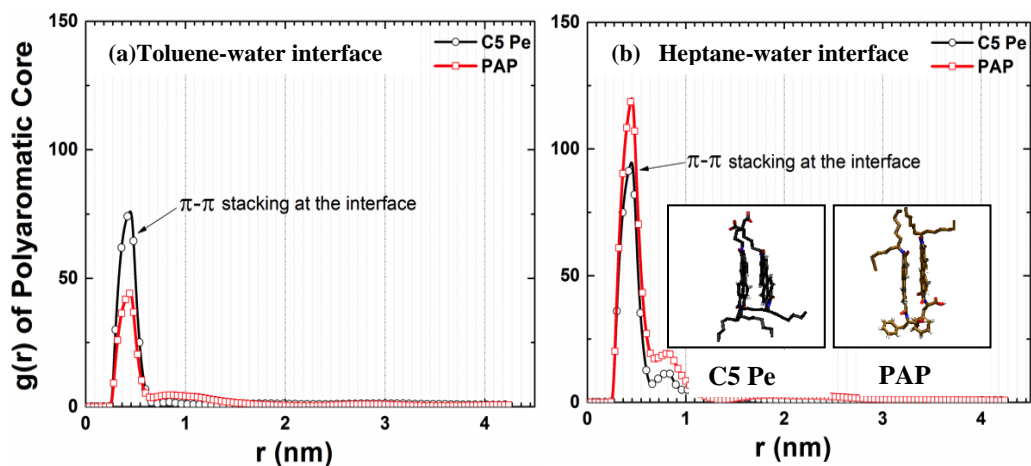


Figure 5.15 (a-b). The radial distribution function of polyaromatic cores of the interfacial-bound molecules at the oil-water interface averaged over the last 2 ns of the simulation time (8 ns – 10 ns) in toluene-water system (a) and heptane-water system (b) at 298 K. The snapshots of strong π - π stacking at the heptane-water interface of C5 Pe and PAP molecules are also shown (Inset). The snapshot was taken at the end of the simulation time.

5.3.5 Migration of PA Molecules from the Bulk Oil Phase to the Oil-Water Interface Assisted by Anionic Side-Chain Moieties

As mentioned in section 5.1 of this chapter, interfacially active molecules are often assigned charges to the functional groups (-COOH) that protonate or deprotonate in water. Initially PA molecules are mostly uncharged (i.e., protonated) in the oil phase, and the charges (i.e., deprotonation) are acquired only when they come in contact with the water molecules at the oil-water interface. Consequently, the initial migration of oil-dispersed PA molecules from bulk oil to the oil-water interface is most likely dictated by polarity, $\pi\cdots\pi$, dipole-dipole interactions, etc. in the absence of a charge on the PA molecules (-COO⁻). The contribution of all these factors that dictate the migration of PA molecules to the oil-water interface in the absence of a charge in the PA molecules was characterized in detail in the previous sections. The results indicate that the partition of the various protonated PA molecules at the oil-water interface was found to be highly sensitive to the variations of the side chain functional group and polarity of the oil phase. However, in this section we will only focus on the adsorption of PA molecules assisted by anionic moieties (deprotonated carboxylic functional group) to the oil-water interface to investigate only the molecular orientation and arrangements of deprotonated PA molecules at the oil-water interface. Previous studies have shown that deprotonated moieties exhibit strong interfacial activity in oil-water systems.^{34,35} In oil-water systems, deprotonated PA molecules are always drawn to the interface with the charged functional groups (-COO⁻) of the molecules remaining strongly associated with the water phase until

all the interfaces are occupied.^{34,35} Hence, simulating deprotonated PA molecules can provide a glimpse of the long-time adsorption phenomena (i.e., molecular orientation of the PA molecules after they come in contact with water), which evolve through an extremely slow processes. Therefore, we simulated three deprotonated PA molecules (C5 Pe⁻, PAP⁻ and TP⁻) in both toluene-water and heptane-water systems. The only difference between the protonated and deprotonated PA molecules are the charge distribution around the carboxylic functional groups and the removal of all acidic hydrogens from the carboxylic functional groups. In this study, all PA molecules are in the fully deprotonated form.

5.3.5.1 Density Profiles of PA Molecules with Anionic Side-Chain Moieties

We observe that deprotonated (-COO⁻) PA molecules have a higher tendency to adsorb at the interface than that of its protonated PA molecule (-COOH) counterpart. The results indicate that once a carboxylic moiety on the PA molecules is deprotonated, the impact of the functional group variations at the side chain of the aromatic core on the adsorption tendency and amount of adsorbed molecules becomes negligible. Deprotonated PA molecules possess stronger intermolecular interactions between the water molecules and the deprotonated carboxylic terminal group, altering the amount of adsorbed molecules at the interface. For example, PAP molecules with deprotonated side-chain moieties show a high tendency to adsorb to the interface than PAP molecules with fully protonated form in both toluene-water and heptane-water

binary systems. Figure 5.16 shows the density profiles of the deprotonated PA molecules at the toluene-water and heptane-water systems.

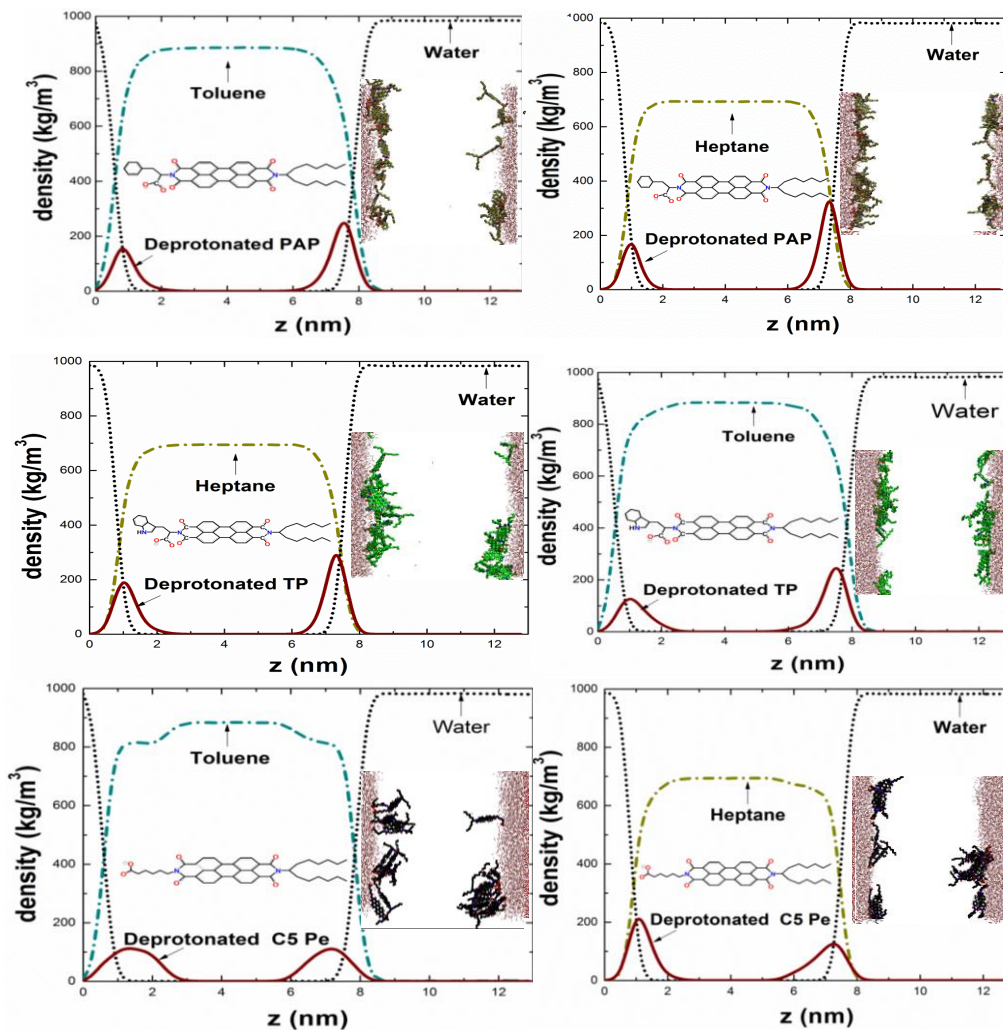


Figure 5.16. Density profiles of toluene-water and heptane-water systems containing various deprotonated PA molecules averaged over the last 2 ns of the simulation time at 298 K. The carboxylic acid functional groups in all of the PA molecules in the bulk oil phase are deprotonated ($-\text{COO}^-$).

Regardless the solvent polarity of the oil phase and side-chain variations of the PA molecule, all deprotonated PA molecules migrated quickly to the oil-water interface (24 molecules). This is confirmed by large peaks at the two interfaces, and the absence of any peaks in the bulk oil phase. Upon deprotonation of the PA molecules in the bulk oil phase, the PA-PA intermolecular interactions contributing to nanoaggregation in the bulk diminish drastically while PA-water interaction increases rapidly. This phenomenon is due to the strong electrostatic interaction between the PA and water molecules. This strong interaction between the deprotonated carboxyl functional group of the PA molecules and the water molecules are confirmed further by the radial distribution function of the oxygen atom of the carboxyl functional group (O_{-COO^-}) and the oxygen atom of the water molecules (O_{H_2O}) in the system as shown in Figure 5.17.

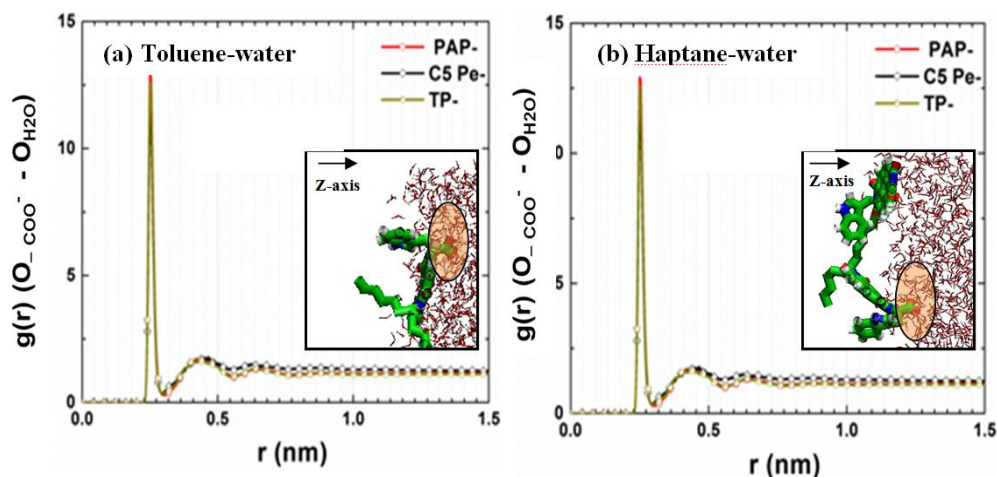


Figure 5.17. The radial distribution function between the oxygen atom of the deprotonated carboxyl functional group (O_{-COO^-}) and the oxygen atom of the water molecules (O_W) averaged for the last 2 ns of the simulation time. A snapshot of TP^- molecule tethered at the oil-water interface is shown in the inset.

All deprotonated PA molecules show very similar radial distribution functions irrespective of the polarity of the oil phase and the side-chain variation in the PA molecules. The sharp peak at a distance of 0.18 – 0.21 nm reflects the strong hydration of the carboxyl functional group of the PA molecules at the oil-water interface. Our MD results revealed that the tight-binding between the anionic carboxyl functional group ($-\text{COO}^-$) and the water molecules at the oil-water interface could alter the orientation of the PA molecules at the oil-water interface and thereby affects the π - π interactions between the aromatic core of the PA molecules.

In Table 5.5 we report the ratio of the number of protonated (N_{pro}) to deprotonated (N_{depro}) interface-bound PA molecules, and the ratio of the number of PA molecules in the large nanoaggregate cluster of protonated (AGG_{pro}) to deprotonated (AGG_{depro}) interface-bound molecules at the oil-water interface. The criterion for determining the number of associated PA molecules in the large aggregate cluster at the oil-water interface is determined by the linkage algorithm in GROMACS with a cutoff distance of 0.5 nm. The hydrogen bonds between deprotonated PA molecules and interfacial water molecules are also shown in Table 5.5. To calculate the average number of intermolecular hydrogen bonds in the system, a geometric criterion described in section 5.3.3 were applied.

In both toluene-water and heptane-water systems, all deprotonated PA molecules exhibit comparable hydrogen bond tendency irrespective of the nature and size of the side-chain moiety. Results show that all deprotonated PA molecules approximately form six hydrogen bonds per molecule with water, a

higher proportion compared to their protonated counterparts. These findings suggest that a strong intermolecular interaction between deprotonated PA molecules and the water molecules at the vicinity of the interface.

The ratio of the number of protonated to deprotonated interface-bound PA molecules adsorbed to the oil-water interface show a significant variation from one another in both heptane-water and toluene-water interface. The $R_{p/d}$ ratio of C5 Pe molecules, for example, show a larger value than the ratio calculated for TP molecules in both toluene-water and heptane-water interface. The results clearly indicate that protonation or deprotonation state of TP molecules has a stronger effect on adsorption (i.e., number of molecules) to the oil-water interface than C5 Pe molecules.

The results obtained from the simulation of both protonated and deprotonated PA molecules qualitatively agree with the experimental observations that C5 Pe lowers the interfacial tension of the toluene-water system than TP, PAP and BisA.¹³⁰⁻¹⁰⁵ BisA molecules in toluene-water systems were also show poor adsorption to the interface and as a result the interfacial tension of the systems does not change much as compared to the other PA molecules at the toluene-water systems (except TP molecules). Experimentally,¹⁰³⁻¹⁰⁵ the two acidic PA molecules (C5 Pe and PAP) are interfacially active molecules with interfacial tension of 1 mN/m (C5 Pe) and 4 mN/m (PAP) at pH 9 in toluene-water system. In contrast, the nonacidic BisA surfactant molecules can barely be considered interfacially active PA molecules, with an interfacial tension close to the pure toluene-water system (~ 36 mN/m).^{103-105,222}

The ratio of the number of PA molecules in the large nanoaggregate cluster of protonated to deprotonated $R_{AGGp/AGGd} = \left(\frac{AGG_{Pro}}{AGG_{depro}} \right)$ were also calculated to determine qualitatively the effect of deprotonation of the side-chain carboxylic functional group on the nanoaggregate formation at the oil-water interface. Results show that deprotonation of PA molecules slightly enhance the number of PA molecules (except PAP) per aggregate at the oil-water interface.

Table 5. 4. The ratio of the number of protonated to deprotonated interface-bound PA molecules, the ratio of the number of PA molecules in the large nanoaggregate cluster of protonated to deprotonated at the oil-water interface, and the average number of intermolecular hydrogen bonds (H-bond) in the system.

PA molecules	$R_{p/d} = \left(\frac{N_{Pro}}{N_{depro}} \right)$	$R_{AGGp/AGGd} = \left(\frac{AGG_{Pro}}{AGG_{depro}} \right)$	H-bond PA-water
toluene-water			
C5 Pe	0.54	0.20	5.510 ± 0.068
PAP	0.42	1.00	5.710 ± 0.065
TP	0.21	0.83	5.170 ± 0.057
heptane-water			
C5 Pe	1	0.82	6.110 ± 0.060
PAP	0.46	1.11	6.200 ± 0.024
TP	0.21	0.63	5.860 ± 0.038

5.3.5.2 Preferential Orientation of Deprotonated PA Molecules at the Oil-Water Interface

The angle distributions for the deprotonated PA molecules in toluene-water and heptane-water systems are reported in Figure 5.18 (a-b). The results revealed that not only the protonation and deprotonation state of the molecules have an impact on the interfacial activity but also on the preferential orientation of the PA molecules at the interface. From the angle distribution results, it is evident that the protonation or deprotonation of carboxylic acid of the PA molecules has a greater impact on the orientation of the adsorbed molecules at the interface. For example, PAP molecules in protonated state prefer to adsorb in *head-on* orientation in both toluene-water and heptane-water systems. However, as soon as the PAP molecules deprotonate at the interface the preferential orientation of the PAP molecules start to shift towards *intermediate* and *flat-on* orientations at the toluene-water and heptane-water interface, respectively. C5 Pe molecules in both protonation and deprotonation states show a high tendency to adsorb in *head-on* orientation in all systems. The main reason for the favorable *head-on* orientation of the C5 Pe molecules at the interface could be due to the absence of a bulk hydrophobic aromatic moiety (unlike TP and PAP) adjacent to its aliphatic carboxylic acid side chain (i.e., β -alanine derivative).

Protonated TP molecules prefer to stay in the bulk oil phase rather than migrating to the oil-water interface. In contrast, deprotonated TP molecules prefer an *intermediate* and *flat-on* orientation at the toluene-water and heptane-water interface, respectively.

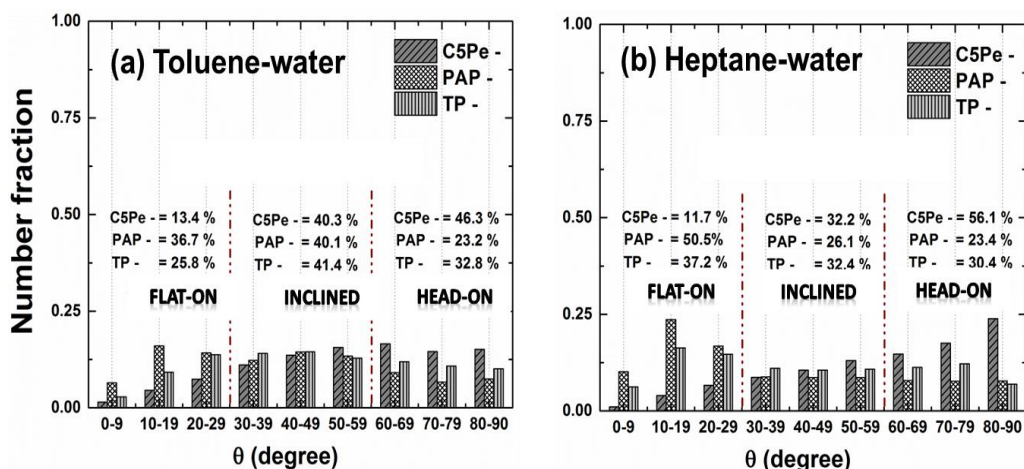


Figure 5.18. The number fraction of deprotonated PA molecules averaged over the last 2 ns of the simulation time in toluene-water (a) and heptane-water (b) 298 K.

Various other minor angle distributions of the deprotonated C5 Pe, TP and PAP molecules at the interface were also observed. PAP molecules, for example, partition into 36.7.8 % *flat-on*, 40.1% *intermediate*, and 23.2 % *head-on* angles at the toluene-water interface. In contrast, at heptane-water interface, PAP molecules exhibit a 50.5 % *flat-on*, 26.1 % *intermediate*, and 23.4 % *head-on* angle distribution. On the other hand, C5 Pe molecules show a 13.4 % *flat-on*, 40.3 % *intermediate* and 46.3 % *head-on* angle distribution at the toluene-water interface, in contrast to 11.7 % *flat-on*, 32.2 % *intermediate* and 56.1 % *head-on* angle distribution at heptane-water interface. For TP molecules, we have seen a dramatic difference between protonated and deprotonated TP molecules. Although protonated TP molecules prefer to stay at the bulk oil phase and shows poor adsorption tendency to the interface. Deprotonation of the TP molecules completely changed their interfacial activity in oil-water systems. Deprotonated

TP molecules show a 25.8 % *flat-on*, 41.8 % *intermediate* and 23.2 % *head-on* angle distribution at the toluene-water interface, in contrast to 37.2 % *flat-on*, 32.4 % *intermediate* and 30.4 % *head-on* angle distribution at heptane-water interface. Therefore, the protonation and deprotonation of the PA molecules have a great impact on the conformational preference of the PA molecules at the oil-water systems.

5.4 Conclusion

Adsorption of protonated PA molecules at oil-water interfaces from the bulk oil phase was studied using molecular dynamics simulations. In toluene-water systems, protonated PA molecules relatively prefer to stay in the bulk toluene phase, while in heptane-water system, the molecules approach the interface and promote the formation of larger nanoaggregate structures near the interface. The presence of carboxylic group on the side chain in the protonated PA molecules enhances their adsorption at the oil-water interface, mainly through hydrogen bond of carboxylic group with the water molecules. In toluene-water systems, fewer hydrogen bonds were observed than in heptane-water systems due to stronger interaction (solvation) of PA molecules with toluene. Bulky aromatic groups such as tryptophan in the PA molecules retard the adsorption process due to the strong π - π stacking in the system. Irrespective of the side-chain substituents and solvent polarity of the oil phase, protonated PA molecules prefer a *head-on* (*or side on*) configuration at the oil-water interface.

Finally, none of the protonated PA molecules was observed to partition to the aqueous phase. The protonation PA molecules always prefer to stay in the

nonaqueous phase. Our results also revealed that the protonation or deprotonation state of the PA molecules have a great impact on the interfacial activity, aggregation and preferential orientation of the PA molecules at the interface. Once the carboxylic moiety on the PA molecules is deprotonated, the impact of the functional group variations at the side chain of the aromatic core becomes negligible. The study sheds light on the molecular mechanisms of PA molecules portioning at oil-water interfaces, and provides considerable insight into key considerations necessary for the design of proper chemical demulsifiers for PA mediated emulsions (e.g., asphaltene at the oil-water interface) formed under specific process conditions of temperature, pressure and pH.

Chapter 6

The Influence of Naphthenic Acid on the Initial Partition and Aggregation of PA Molecules at the Toluene-Water Interface

6.1 Introduction

Although estimates vary considerably, recent research has consistently shown an increasingly higher content of complex polyaromatic (PA) and naphthenic acid (NA) molecules in several oil field operations and water treatment plants.^{44-48,98-100} As a result, there has long been an interest in understanding the influence of NA molecules on the initial adsorption and aggregation of PA molecules at the oil-water interface. Some of the problems associated with emulsion formation during crude oil production are believed to be linked to the collective behavior of both PA and NA molecules in the crudes.⁹⁸⁻¹⁰⁰ It should be noted, however, that bulky polyaromatic molecules (i.e., asphaltenes) in crude oil form an elastic interfacial film around water droplet, thereby, causing emulsion stability in water-in-crude oil emulsions.^{45,49,54-58}

Naphthenic acids (NA) are among the naturally occurring components in crude oil. The general chemical formula of NA is $C_nH_{2n+Z}O_2$, where n indicates the number of carbons in the naphthenic acid and Z is to the number of five or six

carbon rings in the naphthenic acid ($Z =$ between 0 to -12).⁹⁸⁻¹⁰⁰ These NA molecules tend to adsorb at the oil-water interface in such a way that the polar groups are incorporated into the water phase while the hydrophobic part of the NA molecules resides into the oil phase.⁹⁸ This phenomenon usually leads to the formation of interfacial films at the oil-water interface, which promotes emulsification and emulsion stabilization during oil production.

In Chapters 4 and 5, we have investigated in detail the aggregation and adsorption mechanism of various PA molecules (without NA) in the bulk oil phase and at the oil-water interface. Our results show that a subtle change in molecular structure and polarity of substituent side chain functional group has a significant impact on molecular association in the bulk oil phase and adsorption at the oil-water interface. The influence of naphthenic acid (NA) molecules on the initial adsorption and aggregation of PA molecules at the toluene-water interface. It should be noted, however, that the interaction between PA and NA molecules in the bulk oil phase and at the oil-water interface is generally discussed in this chapter in terms of the structure of NA and PA molecules in the simulated system.

6.2 Molecular Modeling and Simulation Methods

The structural characteristics of the PA molecules used in this study have been discussed in detail in Chapters 4 and 5 (see Tables 4.1 and 5.1). The topology and coordinate files of the PA molecules are similar to the ones developed and used in Chapter 5. In nature, PA molecules (e.g., asphaltenes) are often found as a mixture of many distinct compounds with different structures. Thus, in order to investigate their property using model compounds, an

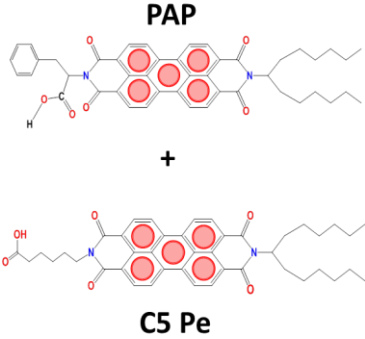
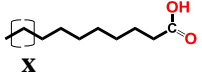
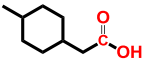
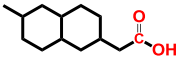
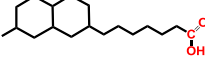
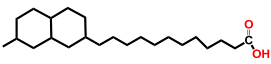
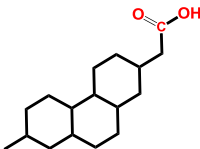
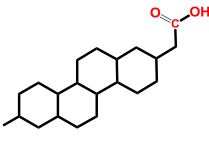
equimolecular mixture of various PA model compounds are commonly used to represent the average property of PA molecules in any given system. Based on the results obtained from Chapters 4 and 5, we selected PAP and C5 Pe mixtures to represent PA molecules in the system due to their diametrically opposite side chain constituents and relatively high adsorption tendency to the toluene-water interface (see Table 6.1). For example, our previous results showed that C5 Pe molecules tend to concentrate much closer to the toluene-water interface than PAP, TP and BisA molecules. The properties of the individual molecules (PAP and C5 Pe) in the bulk oil phase and at the oil-water interface were discussed at greater length in the previous two chapters. For the NA molecules, a new version of PRODRG was used to generate the coordinate and topology files. However, the initial molecular geometries (PDB coordinates) of these NA molecules were obtained using Chem 3D ultra 10.0 commercial software program.¹⁹⁴ Various NA molecules with different number of carbon (n) and rings (z) were used in this simulation to model naphthenic acids in nature (see Table 6.1b-h). Symbol x , a variable, is used to describe the length of alkyl side-chains with carboxyl terminal group.

In our simulations, toluene solvent molecules were used to model the oil phase. The topology and coordinate files of toluene was generated from phenylalanine amino acid fraction through the *pdb2gmx* routine in GROMACS software package. For the water model, the extended simple point charge (SPC/E) model was used in our simulation, as this water model adds the polarization correction to the potential energy function, and gives a reasonable properties of

water at ambient temperature (see Appendix A, for a detailed water model comparison).

In this study, a total of seven simulation boxes were constructed with each box containing 16 PA molecules (8 C5 Pe and 8 PAP molecules) and 8 NA molecules in an ordered placement in vacuum in a cubic box of 10 nm size (see Fig. 6.1). C5 Pe and PAP molecules were placed in the upper and lower layers of the simulated box, while NA molecules were positioned in the middle layer. In each simulation box a different type of NA molecules were added to examine the influence of different NA molecules with varying structures on partition and aggregation of PA molecules at the toluene-water interface. All the simulation boxes were then solvated with toluene molecules, followed by steepest descent energy minimization. The boxes were then stretched in the z -direction by 5 nm and filled with SPC/E water molecules. In order to compare the effect of various NA molecules on partition and aggregation of PA molecules at the toluene-water interface, we also performed an additional simulation without any NA molecules in the system (see Table 6.1a). In all the simulations, the carboxylic acid groups in the PA and NA molecules were maintained to be protonated. The detailed system setup is described in Table 6.2. All the simulations were done in an NPT ensemble at 298 K temperature and 1 bar pressure using Nosé-Hoover thermostat and Parrinello-Rahman pressure coupling algorithms implemented in GROMACS 3.3.3.^{154,155,156} The pressure and temperature coupling constants of $\tau_p = 3$ ps and $\tau_T = 0.3$ ps, respectively were used in all our simulations. All the simulations were performed for 10 ns simulation time.

Table 6.1. Structures of Polyaromatic and Naphthenic Acid Molecules

Polyaromatic molecules (PA)	Naphthenic acid (NA)	
 <p>PAP</p> <p>+</p> <p>C5 Pe</p>	(a) No NA	(b) $Z = 0, x = 9$  NA-1
	(c) $Z = - 2$ and $x = 1$	(d) $Z = - 4$ and $x = 1$
	 NA-2	 NA-3
	(e) $Z = - 4$ and $x = 6$	(f) $Z = - 4$ and $x = 11$
	 NA-4	 NA-5
(g) $Z = - 6$ and $x = 1$	(h) $Z = - 8$ and $x = 1$	
 NA-6	 NA-7	

The isothermal compressibility of water at room temperature ($k(T) = 4.5 \times 10^{-5} \text{ bar}^{-1}$) was used in all our MD simulations.¹⁶⁸ PBCs¹⁵² were applied in x, y, z dimensions of the simulation box. Long-range electrostatic interactions were

handled using the Particle-Mesh Ewald Summation (PME)¹⁹⁸ method with a fast Fourier transform (FFT) grid spacing of 0.16 nm and cutoff distance of 1.2 nm.

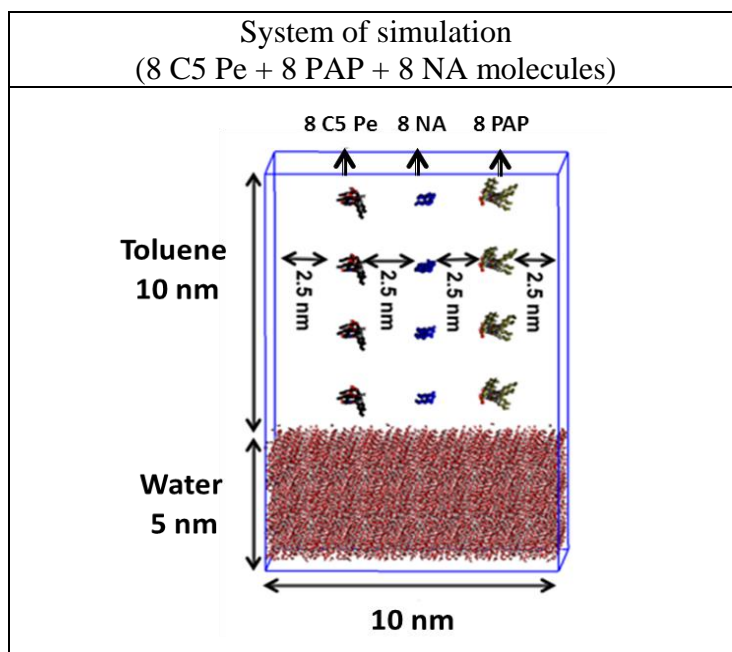


Figure 6.1. A schematic diagram showing the initial arrangements of PAP, C5 Pe and NA molecules in the toluene-water systems

A cutoff of 1.4 nm was used for the van der Waals interactions. The general MD simulation conditions and parameters used in this chapter were the same as the ones used in Chapters 4 and 5. Finally, GROMOS96 force field with a parameter set of 53a6 was used in all our systems. The time dependent structural evolution of the system was analyzed and visualized using both the GROMACS built-in analytical tools and the visual molecular dynamics software (VMD).²⁰⁰

Table 6. 2. System composition and simulation setup of PA and NA molecules in the toluene-water systems

system	simulation type	8 PAP + 8 C5 Pe + 8 NA molecules	
		N_{toluene}	N_{water}
S0	PA with no NA	3227	14150
S1	PA with NA-1	3206	14152
S2	PA with NA-2	3190	14161
S3	PA with NA-3	3207	14148
S4	PA with NA-4	3172	14151
S5	PA with NA-5	3154	14148
S6	PA with NA-6	3192	14146
S7	PA with NA-7	3206	14153

6.3 Results and Discussion

6.3.1 Density Profiles of PA and NA Molecules

Figure 6.2a-h shows the density profiles of the simulated species (C5 Pe, PAP, NA, water and toluene molecules) in the system averaged over the last 2 ns of simulation time. To compute the density distribution of the simulated species across the simulation box, the box was divided into 50 slabs of equal thickness along the z-direction, followed by computing the density of the desired molecule in each slab. It should be noted that, the toluene-water interfaces in these calculated density profiles were located at the position where toluene and water

lines in the system intersect. From these density profiles and molecular snapshots of the simulation box at $t = 10$ ns (see the insets in Figure 6.2) we can directly observe that the partition of PA molecules (PAP and C5 Pe) at the toluene-water interface is moderately sensitive to the presence of NA molecules in the simulated systems. For example, in the absence of NA molecules, most C5 Pe and PAP molecules in the system prefer to concentrate near the toluene-water interface than staying in the bulk toluene phase. This higher affinity towards the toluene-water interface was confirmed by the presence of relatively large and broad peaks at the two interfaces in the density profiles shown in Figure 6.2a (PA without NA). In contrast, PA molecules mixed with molecules of two fused hydrogenated rings with a moderate length of aliphatic carboxylic acid at the side chain ($x = 6$) create in the density profile a large and broad peak in the bulk toluene phase, indicating that the interfacial activity of these PA molecules significantly diminishes by the presence of NA molecules (i.e., NA-4) in the system. Thus, the presence of NA molecules in the system has the ability to influence or alter the partition of the PA molecules (C5 Pe and PAP) at the toluene-water interface.

To further examine the influence of the molecular structure, type and size of the NA molecules on partition of PA molecules at the toluene-water interface, we also compared qualitatively the density profiles of each NA-containing simulation with our reference simulation, which is a simulation without NA molecules in the system (Fig. 6.2a). Our results show that PA molecules mixed with NA-5 molecules tend to form large peaks at the two interfaces, indicating that NA molecules of two fused hydrogenated rings with a very long aliphatic

carboxylic acid at the side chain ($x = 11$) enhance only slightly the migration of PA molecules to the toluene-water interface (relative to the reference simulation). In contrast, NA-4 molecules of two fused hydrogenated rings with a moderate length aliphatic carboxylic acid at the side chain ($x = 6$) have a significant impact on the partition of PA molecules at the toluene-water interface. These results suggest that the length (x) of the aliphatic carboxylic acid at the side chain has a greater impact on partition and aggregation of PA molecules at the toluene-water interface. The larger the length of the aliphatic carboxylic acid at the side chain of the two fused hydrogenated rings, the more PA molecules migrate to the interface. In general, the number of hydrogenated ring (Z) and the length of the aliphatic carboxylic acid at the side chain (x) of the NA molecules have varying degrees of influence on the partition of PA molecules in the toluene-water systems. Conversely, most NA molecules used in this simulation have a tendency to disperse across the toluene-water systems (from the interface to the bulk phase), indicating that there exists a competing intermolecular interaction among the various species present in the system (e.g., PA, water, toluene and NA). These intermolecular interactions could be a reason to impede the migration of NA molecules to the toluene-water interface (see Fig. 6.2 b and f). In order to gain a better insight into the strength of the intermolecular interactions among the various species in the system, we calculated the radial distribution function between different species in the system. Figure 6.3 (a-f) depicts the pair correlation functions between PA and water, NA and water, PA and NA, and among NA and PA molecules in toluene-water systems.

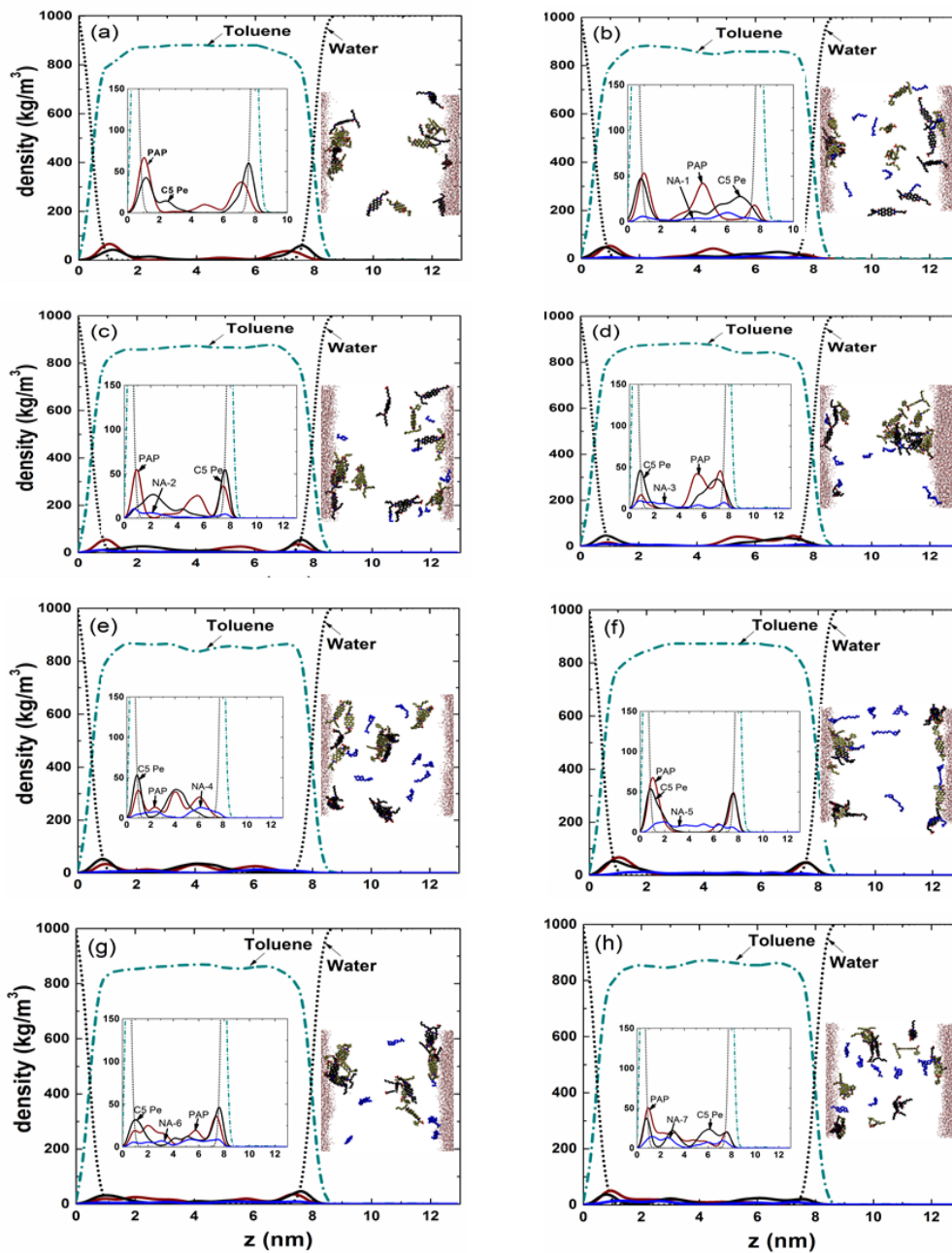


Figure 6.2. Density profiles of various protonated PA and NA molecules in the toluene-water systems averaged over the last 2 ns of the simulation time at 298 K.

As shown in Figure 6.3 (a-b), the pair correlation functions for all PA and NA molecules with water increase monotonically in toluene solvent, indicating

that the molecules are well-embedded in the bulk toluene phase with different molecular distributions across the system. With the exception of PA molecules mixed with NA-5 molecules, the radial distribution function of most PA molecules with water (Figure 6.3a) decreases by the presence of different NA molecules in the system (relative to our reference simulation). These results indicate that naphthenic acid molecules in the system generally hinder the adsorption of PA molecules to the toluene-water interface, except for NA of very long ($x=11$) aliphatic carboxylic acid at the side chain.

Among the simulations performed in this study, PA molecules mixed with NA-4 show the least increase in the radial distribution function (Figure 6.3a). This finding implies that NA molecules of two fused hydrogenated rings with a moderate ($x = 6$) aliphatic carboxylic acid at the side chain greatly influence the adsorption of the PA molecules to the toluene-water interface. It should be noted that, the difference in structure between NA-4 ($x = 6$) and NA-5 ($x = 11$) molecules is the length of the aliphatic carboxylic functional group at the side chain (i.e., x).

Our results indicate that NA molecules with very long aliphatic carboxylic functional group at the side chain enhance the adsorption of PA molecules to the toluene-water interface. The reason could be due to the large steric effect of NA-5 molecules in the system, which creates an unfavorable environment in the bulk for the PA molecules to associate or stay as an individual PA molecules. Compared to other NA molecules in the system (Fig. 6.3d), NA-5 molecules show the least associations.

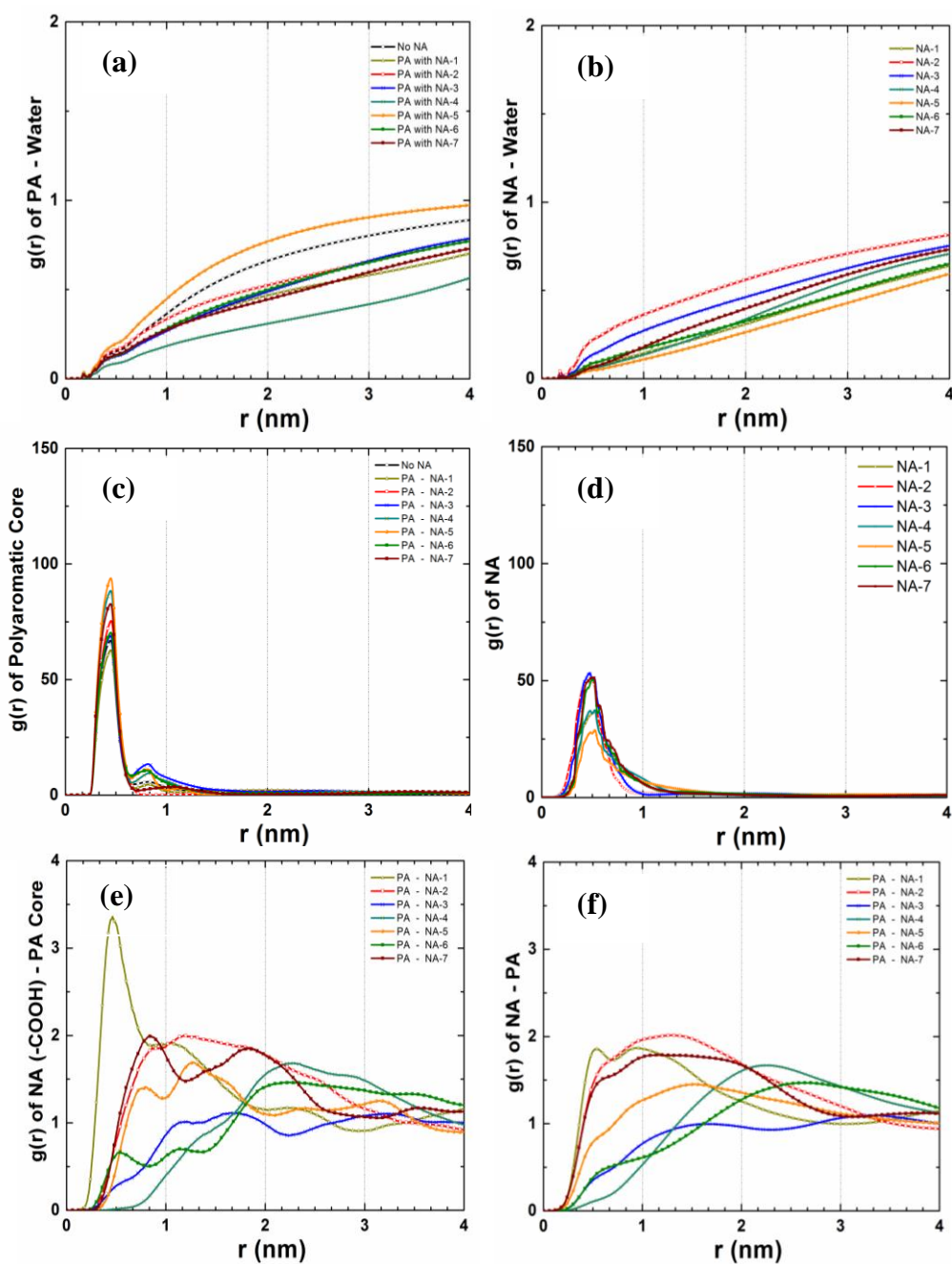


Figure 6.3. Radial distribution functions calculated from the center of mass between PA and water (a), NA and water (b), among the polyaromatic core of the PA molecules (c), among the NA molecules (d), between $-\text{COOH}$ of NA molecules and polyaromatic core (e), and between NA and PA molecules (f).

Our results further indicate that the adsorption of PA molecules at the toluene-water interface decreases slightly with the increase in the number of hydrogenated rings (Z) in the NA molecules (NA-2, NA-3, NA-6 and NA-7). The result implies that the influence of the size of the hydrogenated ring (Z) is very weak in comparison to the length of the aliphatic carboxylic acid side chain (x). As one can see in Figure 6.3 e and f, PA molecules interact more with NA-1 molecules. This implies that small linear NA molecules have a slightly higher tendency to weaken the molecular association and stacking of PA molecules at the toluene-water interface (see Fig.6.3c). Therefore, depending on the type and size of the NA molecules present in the system different interactions between PA and NA molecules were observed. This varying degree of interactions between PA and different NA molecules in the current system generally hinder the migration of PA molecules to the toluene-water interface.

6.3.2 Partition of PA and NA Molecules at the Toluene-Water Interface

The partition of mixed PA and NA molecules between the bulk toluene phase and toluene-water interface was investigated to explore the competition between PA and NA molecules when they migrate to the toluene-water interface. Our focus in this section is mainly on the quantification of the PA and NA molecules based on their affinity towards the interface. Figure 6.4 (a-c) shows the root mean square distance (RMSD) of PAP, C5 Pe and NA molecules from the toluene-water interface as a function of time. The root mean square distance of the PAP, C5 Pe and NA molecules from the nearest oil-water interface was calculated

using Equation 5.1, as described in section 5.3.2. Each line in the RMSD figure (Figure 6.4 a-c) represents the sum of the individual PAP, C5 Pe and NA molecules in each simulated systems. The data in Figure 6.4a, for instance, describes the root mean square distance of PAP molecules from the nearest oil-water interface in each simulation box as a function of time.

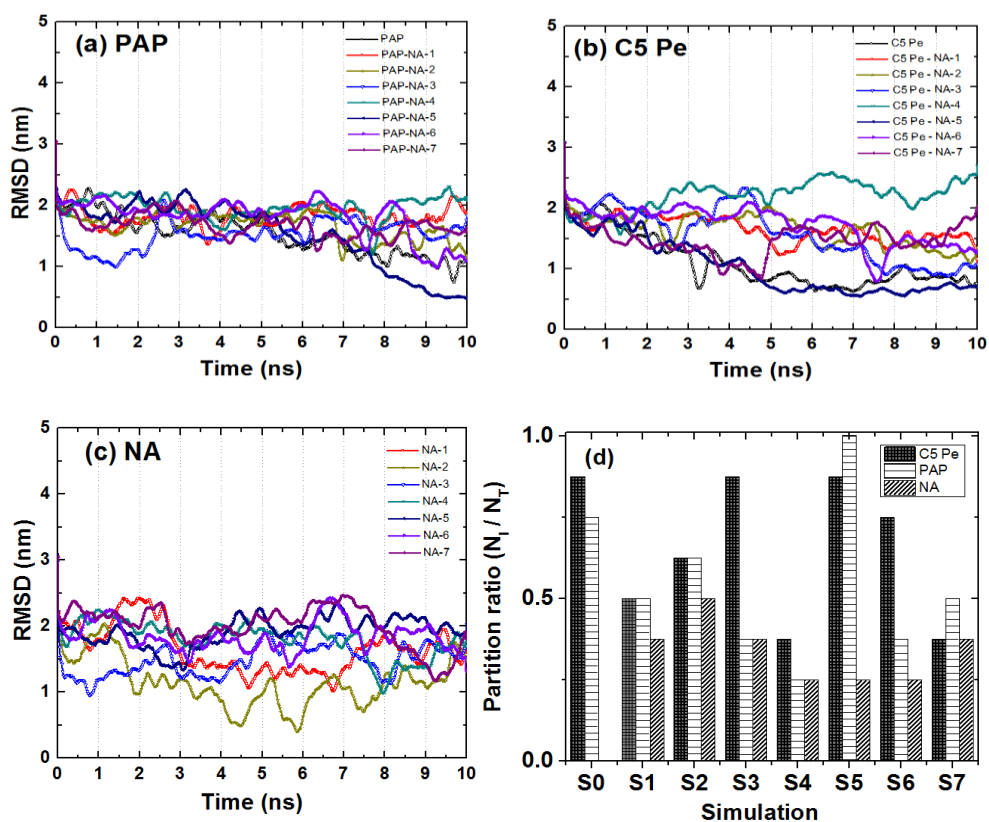


Figure 6.4. The root mean square distance of PAP (a), C5 Pe (b), NA (c) molecules from the toluene-water interface as a function of time. (d) Partition ratio of PAP, C5 Pe and NA molecules in toluene-water systems averaged over the last 2 ns (8 -10 ns) of the simulation time at 298 K.

As shown in Figure 6.4 (a-b), the rate of PA molecules approaching the toluene-water interface varied greatly in the simulation systems, indicating that

the type and size of the NA molecules present in the system greatly influence the interfacial affinity of PA molecules in toluene-water systems. Compared with our reference simulation, PAP and C5 Pe molecules approaching the toluene-water interface is reduced by the presence of NA molecules exception for NA-5 molecules. Our results further indicate that the presence of NA molecules in the system has greater influence on the molecular trajectories of C5 Pe molecules migrating to at the toluene-water interface than PAP molecules. It is important to note, however, that in the presence of PA molecules most protonated NA molecules in the system generally exhibit lower interfacial affinity to the toluene-water interface. Figure 6.4d shows the partition of PAP, C5 Pe and NA molecules between bulk (core-bound) and toluene-water interface (interface-bound). The partition ratio ($P_{I/T} = N_I / N_T$) of PAP, C5 Pe and NA molecules between the bulk toluene and toluene-water interface is also calculated in this section to compare the competition between these molecules to the interface. To calculate the number of molecules near the toluene-water interface we followed the same methodology mentioned in section 5.3.2. As can be seen in Figure 6.3d, both PAP and C5 Pe molecules show a higher tendency to concentrate near the toluene-water interface than NA molecules. Furthermore, PA (C5 Pe and PAP) molecules mixed with NA-5 molecules show the highest partition ratio while those PA molecules mixed with NA-4 exhibit the lowest ratio at the toluene-water interface.

Various partition ratios of PAP and C5 Pe molecules were observed in our simulations, indicating that the preference of adsorption at the interface changes due to the presence of NA molecules. The variation in partition coefficient

observed in our simulation indicates that the adsorption of PA molecules to the interface decreases when NA molecules of two hydrogenated rings with a moderate ($x = 6$) aliphatic carboxylic acid at the side chain is present in the system.

6.3.3 The influence of NA Molecules on the Self-Association of PA Molecules

In the previous section, the partition ratio of both NA and PA molecules was computed to examine the effect of structural feature and size of the NA molecules on the adsorption of PA molecules at the toluene-water interface. Interestingly, our results in the previous sections clearly show a profound effect of the molecular size and length of the aliphatic carboxylic functional group at the side chain (i.e., x) of the NA molecules have on the adsorption of PA molecules at the toluene-water interface. Such effect is a result of change in interactions among the species present in the system (e.g., hydrophobic interactions, steric repulsion, etc.).

In this section, the mean aggregate number of clusters (N_{clusters}) and the number of molecules ($N_{\text{Molecules}}$) in the large aggregate cluster are calculated to determine the impact of the NA molecules on the self-association of PA molecules in the system in the absence or presence of a water phase. It should be noted that, when water phase (in toluene-water systems) is present in the system some of the PA and NA molecules migrate to the toluene-water interface, resulting in the formation of aggregates both in the bulk toluene phase and at the toluene-water interface. However, in the absence of a water phase in the system

(i.e. pure toluene phase) the aggregates of PA molecules reside in the bulk toluene phase. Therefore, our objective in this section is to examine the influence of different NA molecules on the aggregation size and number of aggregate clusters in the system in the presence and absence of a water phase. By comparing the simulations of PA and NA molecules in pure toluene phase and toluene-water interface, the effect of NA molecules on the self-association of PA molecules in a wide range of scenarios was tested.

For the simulation of bulk toluene phase, everything kept the same except that the 5 nm water layer in this simulation was removed from the initial simulation setup and the box size were reduced to 10 nm \times 10 nm \times 10 nm (see Table 6.2). Therefore, a total of 16 simulations were performed in this section, 8 simulations in pure toluene phase and 8 simulations at the toluene-water interface.

Figure 6.5 (a-b) shows the pair correlation functions among the polyaromatic core of the PA molecules, and PA and NA molecules in pure toluene phase. The radial distribution function calculated for the polyaromatic core of the PA molecules in pure toluene (Fig. 6.5a) and at the toluene-water interface (Fig. 6.3c) exhibits similar trend. The results obtained for the π - π stacking between the polyaromatic rings of PA molecules in the system in the presence and absence of the water phase show a similar pattern. However, the presence of different NA molecules in the system causes a small change in the peak height of the radial distribution functions, indicating that the NA molecules (except NA-1) in the system slightly enhance the π - π stacking of PA molecules. In contrast, the RDFs between PA and NA molecules in pure toluene phase (Fig.

6.5b) and toluene-water interface (Fig. 6.3f) are very different in the RDF peak heights and shape. These results indicate that PA molecules interact more with NA molecules in the presence of water phase than in bulk toluene phase, in particular when the NA molecules are very small (NA-1 and NA-2), and very large (NA-5 and NA-7) in size.

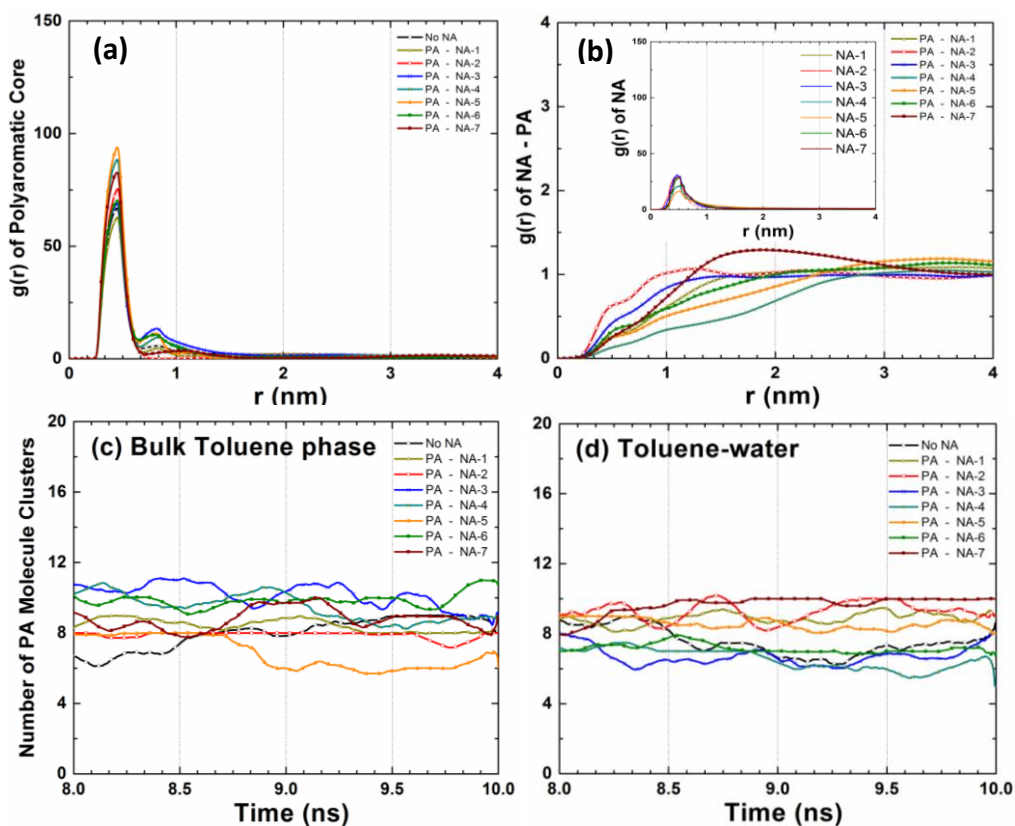


Figure 6.5 Radial distribution functions calculated from the center of mass among the polyaromatic core of the PA molecules (a), between NA and PA (b), and the mean aggregate number of clusters (N_{clusters}) in pure toluene phase (c) and at the toluene-water interface (d).

Furthermore, the RDFs among NA molecules in pure toluene phase and toluene-water interface also show the same trend, indicating that water phase does

not have an influence on the association of protonated NA molecules in the system (inset of Fig 6.5b and Fig. 6.3d).

In Table 6.3 we report the number of aggregated molecules in a large nanoaggregate cluster ($N_{\text{Molecules}}$) and the mean aggregate number of clusters (N_{clusters}) in the bulk toluene and at the toluene-water interface.

Table 6.3. The Number of Aggregated Molecules of the Large Nanoaggregate Cluster ($N_{\text{Molecules}}$) and the Mean Aggregate Number of Clusters (N_{clusters}) in the Simulated Systems

PA molecules				
bulk toluene phase			toluene-water system	
system	(N_{cluster}) aggregates	$(N_{\text{molecules}})$ Large aggregate	(N_{cluster}) aggregates	$(N_{\text{molecules}})$ Large aggregate
S0	9	4	7	6
S1	8	4	9	5
S2	8	4	9	3
S3	10	4	7	5
S4	9	3	6	4
S5	6	6	8	4
S6	10	3	7	4
S7	9	3	10	4

The number of associated molecules per aggregate is determined by the linkage algorithm with a cutoff distance of 0.5 nm between the atoms of any two given molecules. In both bulk toluene and toluene-water interface, the number of PA molecules in the large aggregate is in the range of 3-5 molecules (except for the case with NA-5 at the toluene-water interface). This finding suggests that the

presence of NA molecules in the system has only a marginal influence on the aggregation size of the PA molecules. Similar conclusions were drawn in for number of clusters of aggregates in pure toluene and at the toluene-water interface.

The total number of clusters of aggregates in both pure toluene and toluene-water interface ranges between 7-10 clusters (except for the case with NA-4 at the toluene-water interface and NA-5 at the bulk toluene phase). Only PA molecules mixed with NA-5 in pure bulk toluene phase exhibit the formation of large aggregates in the system, up to 6 PA molecules per the large aggregate in the system.

Figure 6.4 shows the molecular snapshots of the system at the end of simulation time. In the presence of NA molecules no significant variation in the number of clusters or molecules per aggregate was observed. Visual inspection of the MD snapshots also qualitatively reveals that all PA molecules show smaller and less structured aggregates in both pure toluene phase and at the toluene-water interface. It is interesting to note, however, that molecular association and stacking between C5 Pe and PAP were observed in the simulated system.

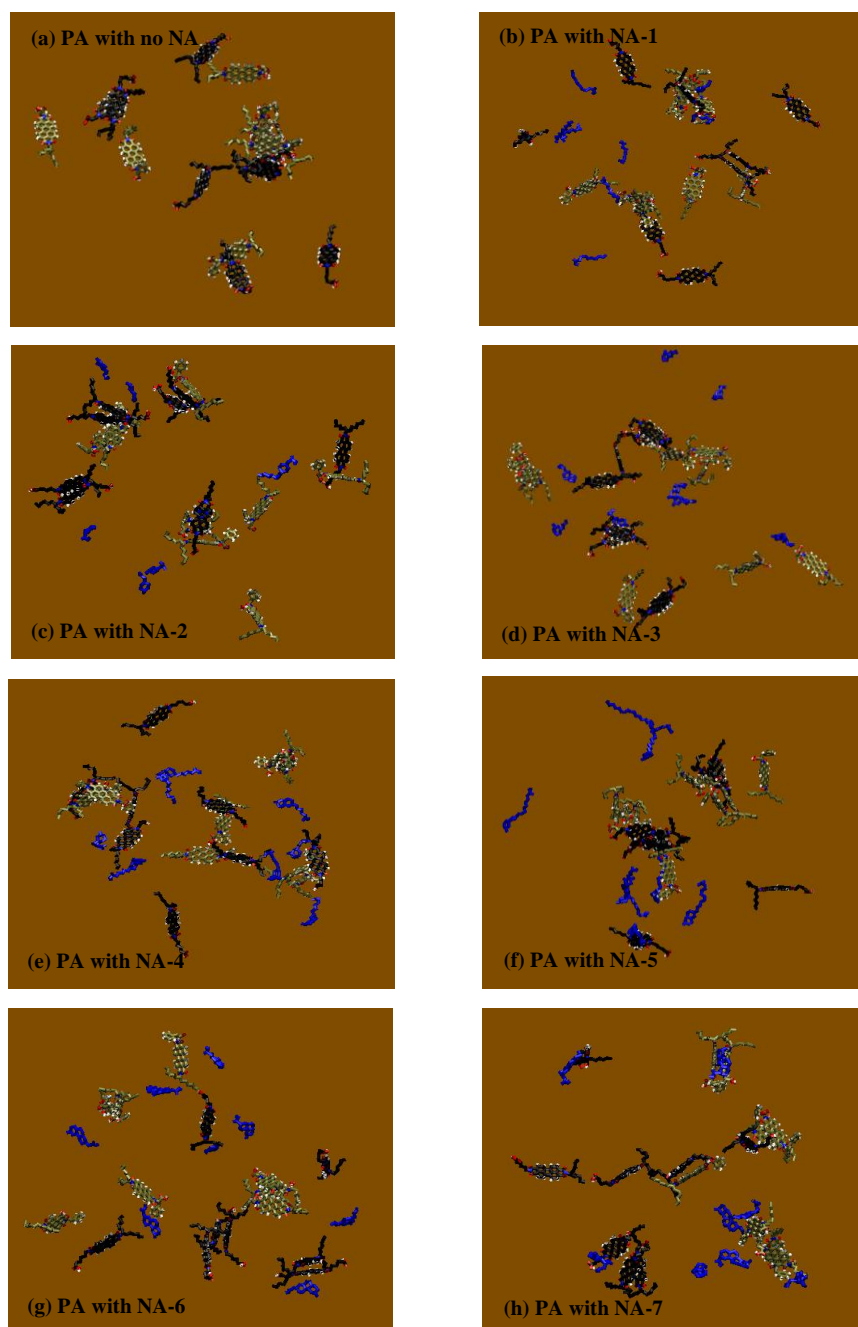


Figure 6.6. Snapshots of PA molecules at the end of the simulation time in bulk toluene. Each molecule is presented by a different color to distinguish one from the other: C5 Pe in black, PAP in tan, and NA in blue. All the molecular snapshots are taken along z-axis.

6.4 Conclusions

The partition of PA molecules at the toluene-water interface was found to be sensitive to the presence of NA molecules in the simulated systems. Our results indicate that naphthenic acid molecules in the system generally hinder the adsorption of PA molecules to the toluene-water interface except for the case when the length of the aliphatic carboxylic acid at the side chain is very long. The presence of NA molecules of two fused hydrogenated rings with a very long aliphatic carboxylic acid at the side chain enhances the migration of PA molecules to the toluene-water interface. These results imply that in comparison to the length of the aliphatic carboxylic acid side chain, the size of the hydrogenated ring has a negligible effect on migration of PA molecules to toluene-water interface.

Depending on the type and size of the NA molecules present in the system different interactions between PA and NA molecules were observed in toluene-water systems. With the exception of NA-5 molecules, the rate of approach of PAP and C5 Pe molecules to the toluene-water interface is reduced by the presence of NA molecules in all simulation systems. The presence of NA molecules in the system has only marginal effect on the size of the large aggregates and total number of aggregate clusters in pure toluene and at the toluene-water interface.

Finally, the results obtained from this work supplements earlier report by song *et al.* (2010)²³⁰. They found that the presence of naphthenic acid molecules in bitumen can destabilize, moderately, the water-in-oil emulsion by lowering the

interfacial tension. Therefore, reduces the rigidity of diluted asphaltene-water interface due to weaker adsorption of polyaromatic molecules at the oil-water interface.

Chapter 7

Summary and Conclusions

Several research scientists and engineers in the area of petroleomics, emulsion systems, thermodynamics of fluid-fluid interfaces, interfacial phenomena, transport phenomena and fluid-particles devoted much of their time trying to understand the fundamental governing physico-chemical properties of complex systems and their dynamical behavior over a range of process conditions.²²⁻²⁷ The reason is that most of the fundamental static and dynamic properties in these area are usually related to a number of engineering problems such as heavy organic deposition, suspensions, corrosion, fluidized beds, lubricated transport and refinery poisoning, etc.^{22-27,44-48,52,53} However, despite the enormous progress made, so far our basic understanding of the underlying system dynamics in these problems are severely limited or hampered due to the intrinsic complexity of the system exhibited and inadequate instrumentations.²²⁻²⁷

Consequently, computational approaches are increasingly being integrated with the available experimental techniques to explore the time-dependent behavior of the system dynamics over an enormous range of spatio-temporal domain. Not only that but also the experimental assessment of these systems are too expensive and much restricted by the high cost and unsatisfactory resolution.²²⁻²⁵ However, in the last decade, most of the attempts so far made to

model such systems are based on the continuum computational modeling approaches in which it overlook the microscale system interactions despite the fact that the macroscopic properties of the system emerges from the interaction at the microscale or local interactions.²²⁻²⁵ Several of the continuum based model studies had to resort to simplifying assumptions of the physics of the interactions governing the molecular associations of the compositions in the systems. This limitation place significant restrictions on the validity of the derived solutions and sometimes leads to inaccurate results or predictions.²²⁻²⁵

In this thesis, the molecular association, nanoaggregate formation and molecular dynamics of an in-house synthesized asphaltene-like or polyaromatic model compounds were explored to understand and detect the influence of molecular fingerprint on the first steps of molecular association into nanoaggregates, where these aggregates represent the first level of molecular clusters or building blocks in 3D structures. Furthermore, the initial migration of oil-dispersed PA molecules from bulk oil to the oil-water interface was also examined under two extreme solvent conditions to understand the influence of the polarity, $\pi\cdots\pi$, dipole-dipole interactions in the absence of a charge on the PA molecules. The role of different functional group substituents on molecular orientations, layering arrangements and dynamics at the oil-water interface were also explored. The interaction between naphthenic acids and polyaromatic molecules in a bulk oil phase and at the oil-water interface was also examined.

To explore the detailed molecular level time-dependent behavior of the asphaltene-like and naphthenic acid molecules over an enormous range of spatio-

temporal domain, extensive MD simulations were used throughout the research project. From the extensive computational studies the following significant conclusions were made about the physico-chemical properties of polyaromatic and naphthanic acid sub-fractions of the crude oil in a bulk oil phase and at the oil-water interface.

7.1 Major Conclusions and Contributions

- I. Our extensive computational results show that a variation in the nature of side chains attached to the polyaromatic core of the PA molecules has a significant impact on molecular association, nanoaggregation dynamics, nanoaggregate structure and aggregate stability in both heptane and toluene. PA molecules containing functional groups such as double aliphatic in both side chains (BisA) or phenylalanine (PAP) show smaller, less structured aggregates while molecular moieties such as tryptophan (TP) and aliphatic carboxylic acid (C5 Pe) at the side chains form larger aggregates in both solvents. In particular, BisA with an aliphatic functional group in both side chains does not form polyaromatic π - π stacking in both solvents due to its strong steric hindrance.
- II. The polarity of the oil phase (toluene or heptane) has significant impact on the nanoaggregate formation of the PA aggregates in bulk oil phase. PA molecules tend to form large aggregates in heptane than in toluene.
- III. During PA molecules association and π - π stacking formation the solvent molecules are excluded from the interstices of the stacked polyaromatic cores in nanoaggregates.

- IV. The substituent side chain change in the molecular structure of the PA surfactants has a negligible impact on their self-diffusivity, but a profound impact on their intermolecular interactions, leading to different aggregate diffusion coefficients. PA molecules exhibit a higher self-diffusivity in heptane than in toluene.
- V. The strong polyaromatic π - π stacking is the main driving force for molecular aggregation of PA molecules in the bulk, which is greatly influenced by the steric hindrance and polarity of its side chains. The more steric barriers the compound possesses, the less likely they stack, in particular, in the presence of aliphatic or alkyl side chains in its good solvent environment.
- VI. The concept of critical molecular packing parameter widely accepted for predicting geometry of molecular aggregates in aqueous solutions is inapplicable to predicting molecular aggregation of the PA surfactants in an organic solvent.
- VII. In toluene-water systems, uncharged PA molecules prefer to stay in the bulk toluene phase, while in heptane-water system, the molecules approach the interface and promote the formation of larger nanoaggregate structures near the interface. The results indicate that the polarity of the oil phase hinders the adsorption of the PA molecules to the oil-water interface.
- VIII. The presence of carboxylic group on the side chain in the uncharged PA molecules enhances adsorption to the oil-water interface, mainly through hydrogen bond of carboxylic group with the water molecules.

- IX. Bulky aromatic groups such as tryptophan in the PA molecules retard the adsorption process due to the strong π - π stacking in the system. In contrast, aliphatic carboxylic acid in the PA molecules enhances the adsorption process.
- X. Irrespective of the side-chain substituents and solvent polarity of the oil phase, uncharged PA molecules prefer a head-on (or side-on) orientation at the oil-water interface.
- XI. Irrespective of the charge state of the carboxylic acid on the PA molecules, the polyaromatic core of the PA molecules always prefers to stay in the nonaqueous phase.
- XII. Deprotonation of the carboxylic functional group at the side chain have a higher tendency to adsorb at the interface than that of its protonated counterpart due strong electrostatic interaction. Once the carboxylic moiety on the PA molecules is deprotonated, the impact of the functional group variations at the side chain of the aromatic core becomes negligible.
- XIII. The partition of PA molecules at the toluene-water interface was found to be sensitive to the presence of NA molecules in the simulated systems.
- XIV. Naphtanic acid molecules in the system generally hinder the adsorption of PA molecules to the toluene-water interface except when the length of the aliphatic carboxylic acid at the side chain is very long.
- XV. Our findings also revealed that NA molecules have the ability to perturb or change the adsorption behavior of the PA molecules at the toluene-water interface. Depending on the type and size of the NA molecules present in the

system different interactions between PA molecules and NA were also observed in toluene-water systems.

- XVI. The presence of NA molecules in the system has a small effect on the size of a large aggregate and total number of aggregate clusters in the system in both pure toluene and at the toluene-water interface.

The major contribution of this thesis is the successful atomic-scale exploration of the mechanism of polyaromatic molecules association, nanoaggregates formation and adsorption in organic solvent and at the oil-water interface by using molecular dynamics simulation (MD). We have showed for the first time the chemical and structural modification on the side-chain functional groups (aliphatic, steric, polarity, aromaticity, etc.) of the PA molecules leads to significant variations in molecular association, dynamics of molecular nanoaggregation and structure of resultant nanoaggregates in organic solvents and at the oil-water interface. The initial migration process to the oil-water interface or the first steps of molecular association into nanoaggregates are crucial in preventing asphaltene deposition, flocculation and emulsion formation in crude oil systems. These initial stages are usually difficult to probe experimentally because of the different association steps and inadequate instrumentations. In this research we have successfully connected the microscopic information to macroscopic observables for PA molecules or asphaltene-like model compounds in organic solvents and at the oil-water interface. The results obtained from this work could help:

- 1) In predicting the precipitation onset of asphaltene molecules during froth treatment processes and crude oil transportations.
- 2) In the rational design of appropriate chemical demulsifiers under specific process conditions. Chemical demulsifiers are interfacial active species, and when added to emulsion systems, they tend to adsorb to the oil-water interface and partly dislodge the PA molecules adsorbed at the interface.
- 3) In developing and enriching structural and molecular databases of crude oil components which eventually will be connected with the process engineering databases that can provide significant insight in optimizing the upstream and downstream process conditions.

Other contribution of the thesis lies in the development of experimentally validated computational MD simulation protocols and molecular topologies for the prediction of the molecular dynamics of asphaltene-like molecules in organic solvents and at the oil-water interface. The use of appropriate molecular topologies, simulation setup, simulation time and force field is crucial in the successful MD simulation of a desired system. Finally, although it is fascinating to see the capabilities of mathematical models in predicting the physico-chemical properties of a system, however, we have to remind ourselves always that, when using any kind of model it is imperative to know about the model and how it works rather than just use it and get some data and interpret. This means knowing what assumptions the model uses and what is missing in the model, all the approximations, and the advantages and disadvantages and look back at the

mathematical formulations will always help us interpreting the experimental or computational findings, and setting the time frame of using it.

7.2 Suggestions for Future Research

As this research work has shown, the chemical and structural modification on the side-chain functional groups of the PA molecules have a significant impact on the first steps of molecular association into nanoaggregates and initial migration process to the oil-water interface. Based on our findings a number of conclusions were made as listed in section 7.1. In order to better understand and comprehend the dynamics and molecular associations of crude oil constitutes the following research works are suggested in this area.

- I. Synthesize several polyaromatic molecules based on perylene bisimide moieties (PBI) containing various side chain functional groups. These functional groups include thiophenic, sulfide, pyridinic, pyrrolic, different polyaromatic core ring size, and a variety of other basic groups which are known to present in the asphaltene. It is well-known that asphaltenes contain a wide range of functional groups. Examine the effect of these side-chain substituents in bulk organic phase and at the oil-water interface. These functional groups could be obtained from the petroleomics data bases.
- II. Study the effect of these various side chain functional groups of asphaltenes on the solubility, thermodynamic properties, propensity of aggregation, interfacial activities, etc. The petroleum industry is in need of these approximations in order to optimize the upstream and downstream process conditions.

- III. It is important to note that, the extent to which the asphaltenes are solvated by resins is one of the most important factors controlling the asphaltene aggregations at the oil-water interface. The addition of resin to a constant asphaltene concentration increases the resin-asphaltene ratio, and hence decreasing the emulsion stability. Using both asphaltene (such as PA molecules) and resin model compounds explore the mechanism of their free energy change of the resin-solvated asphaltenic aggregates.
- IV. Study the effect of the presence of anionic and cationic species such as Ca^{+2} , Cl^{-1} , Na^{+1} and Mg^{+2} in the aqueous phase on the interfacial activities of the above mentioned asphaltene model compounds. The polar sites of the asphaltene model compounds need to be in protonation and de-protonation state.
- V. In fact it is believed that naphthenic acids compete with surface-active asphaltenes during crude oil production in the formation of emulsions. In this thesis, we have investigated the influence and interaction of various types of naphthenic acids (NAs) on the adsorption of PA molecules at the toluene-water interface. However, as we have seen in Chapters 4 and 5 of this thesis the oil aromaticity has a great impact on the aggregation and partitioning to the oil-water interface. Thus, investigating the effect of various types of naphthenic acids (NAs) on the adsorption of PA molecules at the heptane-water interface is essential to determine the influence of the oil aromaticity.
- VI. Study the mechanism of the molecular re-arrangements of the interface bound PA molecules when they come in contact with the water at the oil-water interface. PA

molecules are mostly uncharged in the oil phase, and the charges are acquired only through protonation/deprotonation of the molecules at the interface.

References

- (1) Hirsch, R. L.; Bezdek, R.; Wendling, R. *Peaking of World Oil Production: Impacts, Mitigation, and Risk Management*. US Department of Energy. National Energy Technologies Laboratory, 2005.
- (2) Höök, M.; Hirsch, R. L.; Aleklett, K. *Energy Policy* **2009**, 37, 2262-2272.
- (3) Canada's Oil Sands: Opportunities and Challenges to 2015: *An Update, An energy market assessment*, National Energy Board, Calgary, Alta., 2004.
- (4) Manar El-Sayed Abdel-Raouf (2012). *Factors Affecting the Stability of Crude Oil Emulsions, Crude Oil Emulsions- Composition Stability and Characterization*, Prof. Manar El-Sayed Abdul-Raouf (Ed.), ISBN: 978-953-51-0220-5, InTech. Retrieved from <http://www.intechopen.com/books/crude-oil-emulsions-compositionstability-and-characterization/factors-affecting-the-stability-of-crude-oil-emulsions>.
- (5) Masliyah, J. H.; Murray, R. G. *Extraction and Upgrading of Oilsands Bitumen*, Short Course, 2009.
- (6) Marshall, G. A.; Rodgers, R. P. *Acc. Chem. Res.* **2004**, 37, 53-59.
- (7) Marshall, G. A.; Rodgers, R. P. *P Natl Acad Sci.* **2008**, 105, 18090-18095.
- (8) Hsu, C. S.; Hendrickson, C. L.; Rodgers, R. P.; McKenna, A. M.; Marshall, G. A. *J Mass Spectrom* **2011**, 46, 337-43.
- (9) Hammami, A.; Ratulowski, J. *Asphaltenes in Production Systems: A Flow Assurance Overview*. In *Asphaltenes, Heavy Oils, and Petroleomics*; Mullins, O. C.; Sheu, E. Y.; Hammami, A.; Marshall, G. A., Eds.; Springer, New York, USA, 2007.
- (10) Marshall, A. G.; Blakney, G. T.; Beu, S. C.; Hendrickson, C. L.; McKenna, A.M.; Purcell, J. M.; Rodgers, R. P.; Xian, F. *Eur J Mass Spectrom* **2010**, 16, 367-71.
- (11) Rogel, E. *Colloids and Surfaces A: Physicochem. Eng. Aspects* **1995**, 104, 85-93.
- (12) Boduszynski, M. M. *Am. Chem. Soc.* **1979**, 24, 935-948.

- (13) Buenrostro-Gonzalez, E.; Groenzin, H.; Lira-Galeana, C.; Mullins, O. C. *Energy & Fuels* **2001**, 15, 972- 972.
- (14) Ralston, C. Y.; Mitra-Kirtley, S.; Mullins, O. C. *Energy & Fuels* **1996**, 10, 623-630.
- (15) Akbarzadeh, K.; Hammami, A.; Kharrat, A.; Zhang, D.; Allenson, S.; Creek, J.; Kabir, S.; Jamaluddin, A.; Marshall, A. G.; Rodgers, R. P.; Mullins, O. C.; Solbakken, T. *Oilfield Review* **2007**, 19, 22-43.
- (16) Mullins, O. C. *Energy & Fuels* **2010**, 24, 2179-2207.
- (17) Lamia Goual (2012). *Petroleum Asphaltenes, Crude Oil Emulsions-Composition Stability and Characterization*, Prof. Manar El-Sayed Abdul-Raouf (Ed.), ISBN: 978-953-51-0220-5, InTech, Retrieved from <http://www.intechopen.com/books/crude-oil-emulsions-composition-stability-and-characterization/petroleumasphaltenes>.
- (18) Allen, P. M. *Introduction to Molecular Dynamics Simulation*. In Computational soft matter: From synthetic polymers to proteins; Attig, N.; Binder, K; Grubmueller, H.; Kremer. K., Eds.; Computational Soft Matter, Gustav-Stresemann-Institut Bonn, Jülich NIC Series, 2004.
- (19) Allen, P. M.; Glenn. T. E.; Daan. F.; Bela, M. *Adv. Chem. Phys.* **1993**, 86, 1-166.
- (20) Allen, P. M.; Tildesley, D. J. *Computer Simulation of Liquids*. Clarendon Press, Oxford, 1986.
- (21) Connell, S. T.; Thompson, P. *Physical Review E - PHYS REV E* **1995**, 52, R5792-R5795.
- (22) Leach. A. R. *Molecular Modelling: Principles and Applications*. Prentice Hall, 2nd edition, 2001.
- (23) Cook, K.; Nobel, D.; Williams, J. *Engineering Computations* **2004**, 21, 151-168.
- (24) Han, K.; Feng, Y.; Owen, D. *Computers and Structures* **2007**, 85, 1080-1088.
- (25) Chen, S.; Doolen, G. *Annu. Rev. Fluid Mech.* **1998**, 30, 329-364.
- (26) Kadanoff, L.P. *Phys. Today* **1986**, 39, 7-9.

- (27) Feng, Z.; Michaelides, E. *Journal of Hydraulic engineering* **2003**, 129, 985-994.
- (28) Frisch, U.; Hasslacher, B.; Pomeau, Y. *Phys. Rev. Lett.* **1986**, 56, 1505-1508.
- (29) Chen, S.; Doolen, G. D.; Eggert, K. G. *A versatile tool for multiphase and other complicated flows*. Lattice-Boltzmann Fluid Dynamics. Los Alamos Science, 1994. Retrieved from <http://www.fas.org/sgp/othergov/doe/lanl/pubs/00285550.pdf>.
- (30) Keyes, D. E.; McInnes, L. C.; Woodward, C.; Gropp, W.; Myra, E.; et al. *Multiphysics Simulations: Challenges and Opportunities*. International Journal of High Performance Computing Applications, 2012. Retrieved from http://scholar.harvard.edu/files/efthimios_kaxiras/files/ijhpc_a_icisreport_2012.pdf.
- (31) McNamara, G.; Zannetti, G. *Physical Review Letters* **1988**, 61, 2332-2335.
- (32) Zhou, W. J.; Luan, H. B.; Sun, J.; He, Y. L.; Tao, W. Q. *NUMER HEAT TRANSFER PT B-FUND* **2012**, 61, 369-386.
- (33) Park, S. J.; Mansoori, G. A. *Int. J. Energ. Sources* **1988**, 10, 109-125.
- (34) Kuznicki, T.; Masliyah, J. H.; Bhattacharjee, S. *Energy & Fuels* **2008**, 22, 2379-2389.
- (35) Kuznicki, T.; Masliyah, J. H.; Bhattacharjee, S. *Energy & Fuels* **2009**, 23, 5027-5035.
- (36) Boek, E. S.; Yakovlev, D. S.; Headen, T. F. *Energy & Fuels* **2009**, 23, 1209-1219.
- (37) Headen, T. F.; Boek, E. S.; Skipper, N. T. *Energy & Fuels* **2009**, 23, 1220-1229.
- (38) Diallo, M.S.; Cagin, T.; Faulon, J. L.; Goddard, III W. A. *Thermodynamic Properties of Asphaltene Constituents: A Predictive Approach Based on Computer Assisted Structure Elucidation and Atomistic Simulations*. In *Asphaltene Constituents and Asphalts, Developments in Petroleum Science*; Yen, T. F.; Chilingarian, G. V., Eds.; Amsterdam, The Netherlands, 1994.

- (39) Rakotondradany, F.; Fenniri, H.; Rahimi, P.; Gawryls, K. L.; Kilpatrick, P. K.; Gray, M. R. *Energy & Fuels* **2006**, 6, 2439-2447.
- (40) Andrews, A. B.; McClelland, A.; Korkeila, O.; Demidov, A.; Krummel, A.; Mullins, O. C.; Chen, Z. *Langmuir* **2011**, 27, 6049-6058.
- (41) Gonzalez, M. F.; Stull, C. S.; Linares, F. L.; Almaso, P. P. *Energy & Fuels* **2007**, 21, 234-241.
- (42) Gafonova, O. V.; Yarranton, H. W. *J. Colloid and Interface Science* **2001**, 241, 469-478.
- (43) Spiecker, P. M.; Gawryls, K. L.; Trail, C. B.; Kilpatrick, P. K. *Colloids and Surfaces A: Physicochem. Eng. Aspects* **2003**, 220, 9-27.
- (44) McLean, J. D.; Spiecker, P. M.; Sullivan, P. A.; Kilpatrick, K. P. *The Role of petroleum asphaltenes in the stabilization of water-in-oil emulsions*. In Structure and Dynamics of Asphaltenes; Mullins, O. C.; Sheu, E. Y., Eds.; Plenum Press, New York, 1998.
- (45) Strassner, J. E. *Journal of Petroleum Technology* **1968**, 20, 303-312.
- (46) McLean, J. D.; Kilpatrick, P. K. *J. Colloid Interface Sci.* **1997**, 189, 242-253.
- (47) Speight, J. G. *Oil Gas Sci. and Technol. - Rev.IFP* **2004**, 59, 467-477.
- (48) Kilpatrick, P. K.; Spiecker, P. M. *Asphaltene Emulsions*. In Encyclopedic Handbook of Emulsion Technology; Sjöblom, J., Ed.; Marcel Dekker, New York, 2001.
- (49) Zulkania, A. *M.Sc thesis*, Faculty of Chemical and Natural Resources Engineering, Universiti Teknologi Malaysia, 2004.
- (50) CLI HOUSTON, *Dispersion of heavy organics in petroleum fluids*, Corrosion and Materials Technology, 2013. Retrieved from <http://www.clihouston.com/knowledge-base/dispersion-of-heavy-organics-in-petroleum-fluids.html>.
- (51) Mansoori, G. A. *Molecular Based Study of Arterial Blockage/Fouling in Petroleum and Natural Gas Industries*, 2013. Retrieved from http://tigger.uic.edu/~mansoori/HOD_html.
- (52) Sjöblom, J.; Johnsen, E. E.; Westvik, A.; Ese, M.-H.; Djuve, J.; Auflem, I. H.; Kallevik, H. *Demulsifiers in the Oil Industry*. In Encyclopedic

Handbook of Emulsion Technology; Sjöblom, J., Ed.; Marcel Dekker, New York, 2001.

- (53) Yarranton, H.W.; Fox, W. A.; Svrcek, W. Y. *Can. J. Chem. Eng.* **2007**, 85, 635-642.
- (54) Kilpatrick, P. K.; Sullivan, A. P. *Ind. Eng. Chem. Res.* **2002**, 41, 3389-3404.
- (55) Blair, C. M. *Chem. Ind.* **1960**, 20, 538-544.
- (56) Johansen, E. J.; Skjarvo, I. M.; Lund, T.; Sjöblom, J.; Soderlund, H.; Bostrom, G. *Colloids Surf.* **1989**, 34, 353-370.
- (57) Sjöblom, J.; Soderlund, H.; Lindblad, S.; Johansen, E. J.; Skjarvo, I. M. *Colloid Polym. Sci.* **1990**, 268, 389- 398.
- (58) Menon, V. B.; Nagarajan, R.; Wasan, D. T. *Sep. Sci. Technol.* **1987**, 22, 2295- 2322.
- (59) Andrew, B. A.; Mullins, O. C.; Pomerantz, E. A.; Elshahawi, H.; Dong, C.; Petro, D.; Seifert, D.; Zeybek, M.; Zuo, J. *Oilfield Review*, Schlumberger, 2013. Retrieved from http://www.slb.com/~media/Files/resources/oilfield_review/ors12/win12/2_asphaltene.pdf.
- (60) Mostowfi, F.; Indo, K.; Mullins, O. C.; McFarlane, R. *Energy & Fuels* **2009**, 23, 1194-1200.
- (61) Sheu, E.Y.; De Tar, M. M.; Storm, D.A.; DeCanio, S.J. *Fuel* **1992**, 71, 299-302.
- (62) Veil, J. A.; Quinn, J. J. *Water Issues Associated with Heavy Oil Production, ANL/EVS/R-08/4*, Environmental Science Division, Argonne National Laboratory, 2008.
- (63) Energy Resources Conservation Board (ERCB), *Alberta's Energy Reserves 2007 and Supply/Demand Outlook 2008-2017: ERCB ST-98*, 2008.
- (64) Deutsch, C. V.; McLennan, J. A. *Guide to SAGD (Steam Assisted Gravity Drainage) Reservoir Characterization using Geostatistics*. Center for Computational Geostatistics. Marking/CNRL Natural Resource Engineering Facility, Edmonton, Canada, 2005.

- (65) Vargas-Vasquez, S. M.; Romero-Zerón, L. B. *Petroleum Science and Technology* **2007**, 25, 1447-1463.
- (66) The google view satellite map of the oil sands extraction and tailing pond [Map]. (2009). Retrieved from <http://www.uofaweb.ualberta.ca/cme//pdfs/Drs.%20Xu%20&%20Masliyah%20-%20Oil%20Sands%20Presentation%20March%202009.pdf>.
- (67) The diluted bitumen crude oil [Picture]. (2010). Retrieved from <http://www.chrinikap.co.za/Butimen.html>.
- (68) Eley, D. D.; Hey, M. J.; Symonds, J.D.; Willison, J. H. M. *J. Colloid Interface Science* **1976**, 54, 462-466.
- (69) McLean, L. D.; Kilpatrick, P. K. *J. Colloid Interface Sci.* **1997**, 196, 23-34.
- (70) Xu, Y.; Dabros, T.; Hamza, H.; Shelfantook, W. *Pet. Sci. and Tech.* **1999**, 17, 1051-1070.
- (71) Shelfantook, W. E.; Long, Y. C.; Tipman, R. N. Solvent Process for Bitumen Separation from Oil Sands Froth. Canadian Patent No. CA 2217300; filed Sep. 29, 1997, issued Aug. 20, 2002.
- (72) Czarnecki, J.; Moran, K. *Energy & Fuels* **2005**, 19, 2074-2079.
- (73) Groenzin, H.; Mullins, O. C. *J. Phys. Chem. A* **1999**, 103, 11237-1245.
- (74) Groenzin, H.; Mullins, O. C. *Energy & Fuels* **2000**, 14, 677-684.
- (75) Strausz, O.P.; Mojelsky, L.W.; Lown, E. M. *Fuel* **1992**, 71, 1355-1363.
- (76) Goual, L.; Sedghi, M.; Zeng, H.; Mostowfi, F.; McFarlane, R.; Mullins, O.C. *Fuel* **2011**, 90, 2480-2490.
- (77) Pfeiffer, J. P.; Saal, R.N. *J. Phys. Chem.* **1940**, 44, 139-149.
- (78) Klein, C. G. *Bulk Asphaltene Analysis by negative-mode ESI FT-ICR MS*. *Petroleomics and Asphaltenes*, 2013. Retrieved from <https://sites.google.com/a/cnu.edu/klein-research/research-projects/petroleomics-and-asphaltenes>.
- (79) Goncalves, S.; Castillo, J.; Fernandez, A.; Hung, J. *Fuel* **2004**, 83, 1823-1828.

- (80) McKenna, A. M.; Donald, L.J.; Fitzsimmons, J. E.; Blakney, G.T.; Juyal, P.; Hendrickson, C. L.; Spicer, V.; Standing, K. G.; Marshall, A. G.; Rodgers, R. P., *Energy & Fuels* **2013**, 27, 1246-1256.
- (81) Rodgers, R. P.; Marshall, A. G. *Petroleomics: Advanced Characterization of Petroleum-Derived Materials by Fourier-Transform Ion Cyclotron Resonance Mass Spectrometry (FT-ICR MS)*. In *Asphaltenes, Heavy Oils and Petroleomics*; Mullins, O. C.; Sheu, E.Y.; Hammami, A.; Marshall, A. G., Eds.; Springer, New York, USA. 2007.
- (82) Qian, K.; Edwards, K.E.; Siskin, M.; Olmstead, W. N.; Mennito, A. S.; Dechert, G. J.; Hoosain, N. E. *Energy & Fuels* **2007**, 21, 1042-1047.
- (83) Hortal, A. R.; Martínez-Haya, B.; Lobato, M. D.; Pedrosa, J. M. & Lago, S. *Journal of Mass Spectrometry* **2006**, 41, 960-968.
- (84) Akbarzadeh, K.; Alboudwarej, H.; Svrcek, W.Y.; Yarranton, H.W. *Flu. Phase Equi.* **2005**, 232, 159-170.
- (85) Hirschberg, A.; de Jong, L. N. J.; Schipper, B. A.; Meijer, J. G. *Soc. Pet. Eng. Journal* **1984**, 24, 283-293.
- (86) Danielsson, I.; Lindman, B. *Colloids Surf. A.* **1981**, 3, 391-392.
- (87) Sjöblom, J.; Lindberg, R.; Friberg, S. E. *Adv. Colloid Interface Sci.* **1996**, 95, 125-287.
- (88) Kumar, S. H.; Singh, V. *Journal of Drug Delivery & Therapeutics* **2012**, 2, 40-45.
- (89) Xiaohu, L.; Kalman, B.; Redelius, P. *Fuel* **2008**, 87, 1543-1551.
- (90) Lu, X.; Redelius, P. *Energ & Fuel* **2006**, 20, 653-60.
- (91) Carbognani, L.; DeLima, L.; Orea, M.; Ehrmann, U. *Petrol Sci Technol.* **2000**, 18, 607-634.
- (92) Kane, M.; Djabourov, M.; Volle, J. L.; Lechaire, J. P.; Frebourg, G. *Fuel* **2003**, 82,127-135.
- (93) Al-Sahhaf, T. A.; Fahim, M. A.; Elsharkawym, A. M. *Journal of Dispersion Science and Technology* **2009**, 30, 597-604.
- (94) Mouraille, O.; Skodvin, T.; Sjöblom, J.; Peytavy, J-L. *J. Dispersion Sci. Technol.* **1998**, 19, 339-367.

- (95) Al-Sahhaf, T. A.; Fahim, M. A.; Elsharkawym, A. M. *Petroleum Science and Technology* **2008**, 26, 2009-2022.
- (96) Førdedal, H.; Midttun, Ø.; Sjöblom, J.; Kvalheim, O. M.; Schildberg, Y.; Volle, J-L. A *J. Colloid Interface Sci.* **1996**, 182, 117-125.
- (97) Li, M.; Xu, M.; Ma, Y.; Wu, Z.; Christy, A. A. *Colloids and Surfaces A: Physicochem. Eng. Aspects* **2002**, 197,193-201.
- (98) Auflem, I. H.; Havre, T. E.; Sjöblom, J. *Colloid Polym Sci.* **2002**, 280, 695-700.
- (99) Havre, T. E.; Sjöblom, J.; Vindstad, J. E. *Journal of Dispersion Science and Technology* **2003**, 24, 789-801.
- (100) Havre, T. E.; Ese, M.-H.; Sjöblom, J.; Blokhus, A. M. *Colloid Polym Sci.* **2002**, 280, 647-652.
- (101) Ese, M-H.; Kilpatrick, K. P. *Journal of Dispersion Science and Technology* **2004**, 25, 253-261.
- (102) Mullins, O. C. *Annu. Rev. Anal. Chem.* **2011**, 4, 393-418.
- (103) Nordgård, L. E.; Sjöblom, J. *J. Dispersion Sci. Technol.* **2008**, 29, 1114-1122.
- (104) Nordgård, L. E.; Landsem, E.; Sjöblom, J. *Langmuir* **2008**, 24, 8742-8751.
- (105) Nordgård, L. E.; Sørland, G.; Sjöblom, J. *Langmuir* **2010**, 26, 2352-2360.
- (106) Sabbah, S.; Morrow, A. L.; Pomerantz, A. D.; Zare, R. N. *Energy & Fuels* **2011**, 25, 1597-1604.
- (107) Zajac, G. W.; Sethi, N. K.; Joseph, J. T. *Scan. Microsc.* **1994**, 8, 463-470.
- (108) Headen, T. F.; Boek, E. S.; Stellbrink, J.; Scheven, U. M. *Langmuir* **2009**, 25, 422-428.
- (109) Mason, T.; Lin, M. *Phys. ReV. E: Stat., Nonlinear, Soft Matter Phys.* **2004**, 67, 050401.
- (110) Mason, T.; Lin, M. J. *Chem. Phys.* **2003**, 119, 565-571.
- (111) Pacheco-Sánchez, J. H.; Zaragoza, I. P.; Martínez-Madagán, J. M. *Energy & Fuels* **2003**, 17, 1346-1355.

- (112) Pacheco–Sánchez, J. H.; Zaragoza, I. P.; Martínez–Madagán, J. M. *Energy Fuels* **2004**, 18, 1676-1686.
- (113) Gray, M. R.; Tykwinski, R. R.; Stryker, J. M.; Tan, X. *Energy & Fuels* **2011**, 25, 3125-3134.
- (114) Facchetti, A. *Chem. Mater.* **2011**, 23, 733-758.
- (115) Huang, Y.; Quan, B.; Wei, Z.; Liu, G.; Sun, L. *J. Phys. Chem. C* **2009**, 113, 3929-3933.
- (116) Li, C.; Liu, M.; Pschirer, N. G.; Baumgarten, M.; Müllen, K. *Chem. Rev.* **2010**, 110, 94, 6817-6855.
- (117) Hippus, C.; Schlosser, F.; Vysotsky, O. M.; Böhmer, V.; Würthner, F. *J. Am. Chem. Soc.* **2006**, 128, 3870-3871.
- (118) Mizoshita, N.; Tani, T.; Inagaki, S. *Adv. Funct. Mater.* **2011**, 21, 3291-3296.
- (119) Law, K.-Y. *Chem. Rev.* **1993**, 93, 449-486.
- (120) Díaz-García, M. A.; Calzado, E. M.; Villalvilla, J. M.; Boj, P. G.; Quintana, J. A.; Céspedes-Guirao, F. J.; Fernández-Lázaro, F.; Sastre-Santos, A. *Synth. Met.* **2009**, 159, 2293-2295.
- (121) Choi, H.; Paek, S.; Song, J.; Kim, C.; Cho, N.; Ko, J. *Chem. Commun.* **2011**, 47, 5509-5511.
- (122) Würthner, F.; Sautter, A. *Chem. Commun.* **2000**, 6, 445-446.
- (123) Lee, M.; Cho, B.; Jang, Y.; Zin, W. *J. Am. Chem. Soc.* **2000**, 122, 7449-7455.
- (124) Ke-Rang, W.; Dong-Sheng, G.; Bang-Ping, J.; Zhan-Hu, S.; Yu, L. *J. Phys. Chem. B* **2010**, 114, 101-106.
- (125) Suhrit, G.; Xue-Qing, L.; Vladimir, S.; Würthner, F. *Chem. Eur. J.* **2008**, 14, 11343-11357.
- (126) O'Neil, M. P.; Niemczyk, M. P.; Svec, W. A.; Gosztola, D.; Gaines, G. L.; Wasielewski, M. R. *Science* **1992**, 257, 63-65.
- (127) Würthner, F.; Hanke, B.; Lysetska, M.; Lambright, G.; Harms, G. S. *Org. Lett.* **2005**, 7, 967-970.

- (128) Yongjun, L.; Liang, X.; Taifeng, L.; Yanwen, Y.; Huibiao, L.; Yuliang, L.; Daoben, Z. *Org. Lett.* **2011**, 13, 5692-5695.
- (129) Chang-Cheng, Y.; Würthner, F. *Org. Lett.* **2004**, 6, 2401-2404.
- (130) Würthner, F.; You, C. C.; Saha-Möller, C. R. *Chem. Soc. Rev.* **2004**, 33, 133-146.
- (131) Alder, B. J.; Wainwright, T. E. *J. Chem. Phys.* **1957**, 27, 1208-1209.
- (132) Alder, B. J.; Wainwright, T. E. *J. Chem. Phys.* **1959**, 31, 459-466.
- (133) Rahman, A. *Phys Rev.* **1964**, 136, A405-A411.
- (134) Stillinger, F. H.; Rahman, A. *J. Chem. Phys.* **1974**, 60, 1545-1577.
- (135) McCammon, J. A.; Gelin, B. R.; Karplus, M. *Nature* **1977**, 267, 585-590.
- (136) Hehre, W. A. *Guide to Molecular Mechanics and Quantum Chemical Calculations*. Wavefunction, Inc, CA, 2003.
- (137) Cramer, C. *Essentials of Computational Chemistry: Theories and Models*. 2nd ed.; Wiley & Sons, New York, 2004.
- (138) Momany, F.; Rone, R. *J. Comput. Chem.* **1992**, 13, 888-900.
- (139) Davie, E. K.; Murrall, N. W. *Comput. Chem.* **1989**, 13, 149-156.
- (140) Allinger, N.; Yuh, Y.; Lii, J. *J. Am. Chem. Soc.* **1989**, 111, 8551-8566.
- (141) Mayo, S. L.; Olafson, B. D.; Goddard, W. J. *J. Phys. Chem.* **1990**, 94, 8897-8909.
- (142) Daura, X.; Mark, A. E.; van Gunsteren, W. J. *Comput. Chem.* **1998**, 19, 535-547.
- (143) Hagler, A. T.; Huler, E.; Lifson, S. *J. Am. Chem. Soc.* **1977**, 96, 5319-5327.
- (144) Halgren, T. A. C. *Opin. Struct. Bio.* **1995**, 5, 205-210.
- (145) Halgren, T. A. *J. Comput. Chem.* **1996**, 17, 520-552.
- (146) Halgren, T. A. *J. Comput. Chem.* **1996**, 17, 553-586.
- (147) Clark, M.; Cramer III, R.; Opdench, N. *J. Computational Chem.* **1989**, 10, 982-1012.

- (148) Weiner, S.; Kollman, P.; Nguyen, D.; Case, D. *J. Comput. Chem.* **1986**, *7*, 230-252.
- (149) van Gunsteren, W. F.; Billeter, S. R.; Eising, A. A.; Hünenberger, P. H.; Krüger, P.; Mark, A. E.; Scott, W. R. P.; Tironi, I. G. *Biomolecular Simulation: The GROMOS96 Manual and User Guide*, Vdf Hochschulverlag AG an der ETH Zürich, Zürich, Switzerland, 1996.
- (150) Burkert, U.; Allinger, N. *Molecular Mechanics*. ACS Monograph 177, American Chemical Society, Washington, DC, 1982.
- (151) Lewars, E. G. *Computational Chemistry: Introduction to the Theory and Applications of Molecular and Quantum Mechanics*, Springer, London, 2003.
- (152) van der Spoel, D.; van Buuren, A. R.; Apol, E.; Meulenhoff, P. J.; Tieleman, D. P.; Sijbers, A.; Feenstra, K. *The GROMACS Manual (version 3.3)*; Groningen University: Groningen, The Netherlands, 2004.
- (153) Berendsen, C. J. H.; Postma, M. P. J.; DiNola, A.; Haak, R. J. *J. Chem. Phys.* **1984**, *81*, 3684-3690.
- (154) Nosé, S. *Mol. Phys.* **1984**, *52*, 255-268.
- (155) Hoover, W.G. *Phys. Rev. A.* **1985**, *31*, 1695-1697.
- (156) Parrinello, M.; Rahman, A. *J. Appl. Phys.* **1981**, *51*, 7182-7190.
- (157) van der Spoel, D.; Lindahl, E.; Hess, B.; Groenhof, G.; Mark, A. E.; Berendsen, H. J. C. *J. Comp. Chem.* **2005**, *26*, 1701-1718.
- (158) Berendsen, H.; van der Spoel, D.; Drunen, V. R. *Comp. Phys. Comm.* **1995**, *91*, 43-56.
- (159) Lindahl, E.; Hess, B.; van der Spoel, D. *J. Mol. Mod.* **2001**, *7*, 306-317.
- (160) Oostenbrink, C.; Villa, A.; Mark, A.; van Gunsteren, W. *J. Comp. Chem.* **2004**, *25*, 1656-1676.
- (161) Yudin, I. K.; Anisimov, M. A. *Dynamic Light Scattering Monitoring of Asphaltene Aggregation in Crude Oils and Hydrocarbon Solutions*. In *Asphaltenes, Heavy Oils, and Petroleomics*; Mullins, O. C.; Sheu, E. Y.; Hammami, A.; Marshall, G. A., Eds.; Springer, New York, USA, 2007.
- (162) Yevgeniy, G. B.; Yudin, I. K.; Dechabo, V. A.; Kosov, V. I.; Anisimov, M. A. *APPLIED OPTICS* **2001**, *40*, 4028-4035.

- (163) Hadavi, S. M.; Sharifi, S.; Jafari, S. *Soft Nanoscience Letters* **2012**, 2, 77-80.
- (164) Cheng, H.; Zhang, G. *Thermally Sensitive Microgels: From Basic Science to Applications*. Hydrogel Micro and Nanoparticles; Lyon, A. L.; Serpe, J. M., Eds.; Wiley-VCH Verlag GmbH & Co. KGaA, 2012.
- (165) Natalia, V. L.; Denise, E. F.; Pabitra, N. S.; Yi-Qiao, S. *Energy & Fuels* **2009**, 23, 1189-1193.
- (166) Jean-Pierre, K.; Alain, L.; Lyès, B. *J. Phys. Chem. B* **2013**, 117, 7002-7014.
- (167) Atul, S.; Henning, G.; Akira, T.; Mullins, O. C. *Energy & Fuels* **2002**, 16, 490-496.
- (168) Knovel Critical Tables, 2nd ed.; Knovel: New York, NY, USA, 2008; Available online: http://www.knovel.com/web/portal/browse/display?_EXT_KNOVEL_DISPLAY_bookid=761&VerticalID=0 (accessed on 20 May 2011).
- (169) Antalek, B.; Williams, J. A.; Texter, J. *Phys. Rev. E* **1996**, 54, 5913-5916.
- (170) Zhao, L.; Choi, P. *The Journal of Chemical Physics* **2004**, 120, 1935-1942.
- (171) Lee, S. H.; Lee, H.; Pak, H. *Bull. Korean Chem. Soc.* **1997**, 18, 478-485.
- (172) Moore, J.; Wellek, R. *Journal of Chemical and Engineering data* **1974**, 19, 136-139.
- (173) Hvidsten, T. R.; Lægreid, A.; Kryshtafovych, A.; Andersson, G.; Fidelis, K.; Komorowski, J. *PLoS ONE* **2009**, 4, e6266.
- (174) Song, K. B.; Damodaran, S. *J. Agric. Food Chem.* **1987**, 35, 236-241.
- (175) Klebe, G. *J Mol Med.* **2000**, 78, 269-281.
- (176) Kim, H. S.; Hartgerink, J. D.; Ghadiri, M. R. *J. Am. Chem. Soc.* **1998**, 120, 4417-4424.
- (177) Ryu, J. H.; Hong, D. J.; Lee, M. *Chem. Commun.* **2008**, 9, 1043-1054.
- (178) Hoeben, F. J. M.; Jonkheijm, P.; Meijer, E. W.; Schenning, A. P. H. *J. Chem. Rev.* **2005**, 105, 1491-1546.

- (179) Müllen, K.; Jürgen P, R. *Acc. Chem. Res.* **2008**, 4, 511-520.
- (180) Schenning, A. P. H. J.; Jonkheijm, P.; Hoeben, F. J. M.; van Herrikhuyzen, J.; Meskers, S. C. J.; Meijer, E. W.; Herz, L. M.; Daniel, C.; Silva, C.; Phillips, R. T.; Friend, R. H.; Beljonne, D.; Miura, A.; De Feyter, S.; Zdanowska, M.; Uji-i, H.; De Schryvere, Chen, Z.; Würthner, F.; Mas-Torrent, M.; den Boer, D.; Durkut, M.; Hadley, P. *Synthetic Met.* **2004**, 147, 43-48.
- (181) Mikami, Y.; Liang, Y.; Matsuoka, T.; Boek, E. S. *Energy & Fuels* **2013**, 27, 1838-1845.
- (182) Oh, K.; Ring, T. A.; Deo, M. D. *J. Colloid Interface Sci.* **2008**, 271, 212-219.
- (183) Mackie, I. D.; Dilabio, G. A. *J. Phys. Chem. A* **2008**, 112, 10968-10976.
- (184) Avlasevich, Y.; Li, C.; Müllen, K. *J. Mater. Chem.* **2010**, 20, 3814-3826.
- (185) Fischer, M. K. R.; Kaiser, T. E.; Würthner, F.; Bäuerle, P. *J. Mater. Chem.* **2009**, 19, 1129-1141.
- (186) Reghu, R. R.; Bisoyi, H. K.; Grazulevicius, J. V.; Anjukandi, P.; Gaidelis, V.; Jankauskas, V. *J. Mater. Chem.* **2011**, 21, 7811-7819.
- (187) Ilhan, F.; Tyson, D. S.; Stasko, D. J.; Kirschbaum, K.; Meador, M. A. *J. Am. Chem. Soc.* **2006**, 128, 702-703.
- (188) Rybtchinski, B. *ACS Nano* **2011**, 9, 6791-6818.
- (189) Zhang, X.; Rehm, S.; Safont-Sempere, M.; Würthner, F. *Nature Chemistry* **2009**, 1, 623-629.
- (190) Baram, J.; Shirman, E.; Ben-Shitrit, N.; Ustinov, A.; Weissman, H.; Pinkas, I.; Wolf, S. G.; Rybtchinski, B. *J. Am. Chem. Soc.* **2008**, 130, 14966-14967.
- (191) Wang, K.; Guo, D.; Jiang, B.; Sun, Z.; Liu, Y. *J. Phys. Chem. B* **2010**, 114, 101-106.
- (192) Zhang, X.; Chen, Z.; Würthner, F. *J. Am. Chem. Soc.* **2007**, 129, 4886-4887.
- (193) Oostenbrink, C.; Soares, T. A.; van der Vegt, N. F. A.; van Gunsteren, W. F. *Eur Biophys J.* **2005**, 34, 273-284.

- (194) Chem3D Ultra 10.0. *Cambridge Scientific Software: CambridgeSoft Corporate Headquarters*, 100 Cambridge Park Drive Cambridge, MA 02140, USA, 2006.
- (195) Schuettelkopf, A. W.; van Aalten, D. M. F. *Acta Cryst.* **2004**, D60, 1355-1363.
- (196) Verlet, L. *Phys. Rev.* **1967**, 159, 98-103.
- (197) Hockney, R. W. *The potential calculation and some applications*. In *Methods of computational Physics*; Alder, B.; Frnback, S.; Rotenberg, M., Eds.; Academic press: New York, 1970.
- (198) Essman, U.; Perela, L.; Berkowitz, L. M.; Darden, T.; Le, H.; Pedersen, G. *J. Chem. Phys.* **1995**, 103, 8577-8592.
- (199) Hess, B.; Bekker, H.; Berendsen, C. J. H.; Fraaije, M. E. G. J. *J. Comp. Chem.* **1997**, 18, 1463-1472.
- (200) Humphrey, W.; Dalke, A.; Schulten, K. *J. Molec. Graphics* **1996**, 14, 33-38.
- (201) Sztukowski, D. M.; Jafari, M.; Alboudwarej H.; Yarranton H. W. *J. Colloid Interface Sci.* **2003**, 265, 179-186.
- (202) Yarranton, H. W.; Hussein, H.; Masliyah, J. H. *J. Colloid Interface Sci.* **2000**, 196, 52-63.
- (203) Horváth-Szabó, G.; Masliyah, J. H.; Elliott, J. A.; Yarranton, H. W.; Czarnecki, J. *J. Colloid Interface Sci.* **2005**, 283, 5-17.
- (204) Verruto, V. J.; Kilpatrick, P. K. *Langmuir* **2008**, 24, 12807-12822.
- (205) Gu, G.; Xu, Z.; Nandakumar, K.; Masliyah, J. H. *Fuel* **2002**, 81, 1859-1869.
- (206) Hannisdal, A.; Orr, R.; Sjöblom, J. *J. Dispersion Sci. Technol.* **2007**, 28, 81-93.
- (207) Dicharry, C.; Arla, D.; Sinquin, A.; Graciaa, A.; Bouriat, P. *J. Colloid Interface Sci.* **2006**, 297, 785-791.
- (208) Fortuny, M.; Oliveira, C. B. Z.; Melo, R. L. F. V.; Nele, M.; Coutinho, R. C. C.; Santos, A. F. *Energy & Fuels* **2007**, 21, 1358-1364.

- (209) Langevin, D.; Poteau, S.; Hénaut, I.; Argillier, J. F. *Oil Gas Sci. Technol. - Rev.IFP*. **2004**, 59, 511-521.
- (210) Smit, B. *Physical & review A*. **1988**, 37, 3431-3433.
- (211) Mulqueen, M.; Blankschtein, M. *Langmuir* **2002**, 18, 365-376.
- (212) Pereira, C. J.; Delgado-Linares, J.; Scorzza, C.; Rondón, M.; Salager, J. *Energy & Fuels* **2011**, 25, 1045-1050.
- (213) Staples, E.; Penfold, J.; Tucker, I. *J. Phys. Chem. B* **2000**, 104, 606-614.
- (214) Zdziennicka, A.; Jańczuk, B. *J Surfact Deterg*. **2011**, 14, 257-267.
- (215) Wangab, L.; Wang, H.; Zhu, Y.; Song, X.; Liu, S.; Liu, X.; Jianga, S. *J. Dispersion Sci. Technol.* **2012**, 33, 374-379.
- (216) Kamenka, N.; Haouchea, G.; Lindman, B. *Colloids and Surfaces*. **1987**, 25, 287-296.
- (217) Xu, Q.; Nakajima, M.; Liu, Z.; Shiina, T. *Int. J. Mol. Sci.* **2011**, 12, 462-475.
- (218) Teklebrhan, R. B.; Ge, L.; Bhattacharjee, S.; Xu, Z.; Sjöblom, J. *J. Chem. Phys. B* **2012**, 116, 5907-5918.
- (219) Nenningsland, A. L.; Gao, B.; Simon, S.; Sjöblom, J. *Energy & Fuels* **2011**, 25, 5746-5754.
- (220) Wang, J.; van der Tuuk Opedal, N.; Lu, Q.; Xu, Z.; Zeng, H.; Sjöblom, J. *Energy & Fuels* **2011**, 26, 2591-2599.
- (221) Grimes, B. A.; Dorao, C. A.; Simon, S.; Nordgård, E. L.; Sjöblom, J. *J. Colloid Interface Sci.* **2010**, 348, 479-490.
- (222) Kunieda, M.; Nakaoka, K.; Liang, Y.; Miranda, C. R.; Ueda, A.; Takahashi, S.; Okabe, H.; Matsuoka, T. *J. Am. Chem. Soc.* **2010**, 132, 18281-18286.
- (223) Gragson, E. D.; Richmond, G. L. *J. Am. Chem. Soc.* **1998**, 120, 366-375.
- (224) Rane, P. J.; Harbottle, D.; Pauchard, V.; Couzis, A.; Banerjee, S. *Langmuir* **2012**, 28, 9986-9995.
- (225) Zhang, Y. L.; Breen, P.; Xu, Z.; Masliyah, M. H. *Energy & Fuels* 2007, 21, 274-285.

- (226) Poteau, S.; Argillier, J. *Energy & Fuels* **2005**, 19, 1337-1341.
- (227) Martin, C. Water structure and Science, 2014. Retrieved from <http://www1.lsbu.ac.uk/water/models.html>.
- (228) Mark, P.; Nilsson, L. *J. Phys. Chem. A* 2001, 105, 9954-9960.
- (229) Zielkiewicz.; J. *J. Chem. Phys.* 2005, 123, 104501- 104506.
- (230) Gao, S.; Moran, K.; Xu, Z.; Masliyah, J. *J. Phys. Chem. B* 2010, 114, 7710-7718.

Appendix A

Over the past few decades, advances in complex mathematical methods and powerful computer hardware are now assisting us in narrowing the gap between the actual property of a system and quantitative models.²¹⁻³² For example, numerous water molecular models such as SPC, SPC/E, TIP3P, TIP4P, etc. have been developed in the last few decades in order to reproduce the actual properties of a liquid water at different conditions.²²⁷ The applicability of these developed water models depend on their strength to reasonably predict the actual physical properties of the liquid water (e.g., structure of water, surface tension, hydrogen bonding, etc.). However, each of these water models has its own strengths and weaknesses. The detailed description and comparison of most of the existing water models can be found on Martin Chaplin's website.²²⁷ In this appendix, however, we compared the applicability and sensitivity of two water models (SPC and SPC/E) implemented in GROMACS software package in our study. To compare the sensitivity of the water model used in our study, we simulated C5 Pe molecules with both SPC and SPC/E water models. Figure A1 (a and b) shows the root mean square distance of C5 Pe molecules as a function of time from the oil-water interface. Our results show that the rate of C5 Pe molecules approaching the oil-water interface of both SPC and SPC/E containing systems gave similar trends, indicating that the use of either SPC or SPC/E water models in our study is reasonable. The partition ratio ($P_{I/T} = N_I / N_T$) results also shows similar results. C5 Pe molecules exhibit the highest partition coefficient to

the interface when the oil phase is heptane than toluene. However, the value of the partition ratio deviates slightly with water model change when the oil phase is toluene.

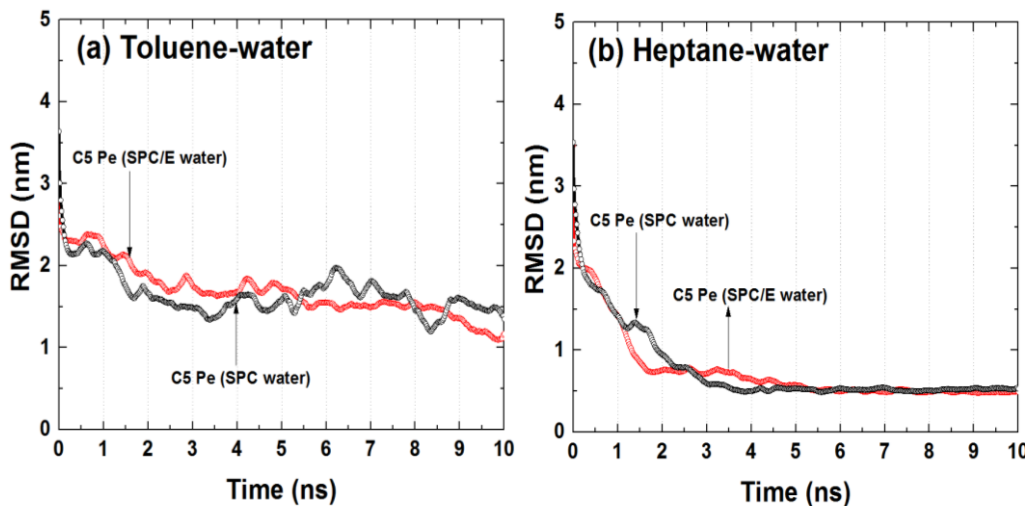


Figure A.1 The root mean square distance of C5 Pe molecules from the oil-water (SPC or SPC/E) interface as a function of time in toluene-water and heptane-water systems at 298 K.

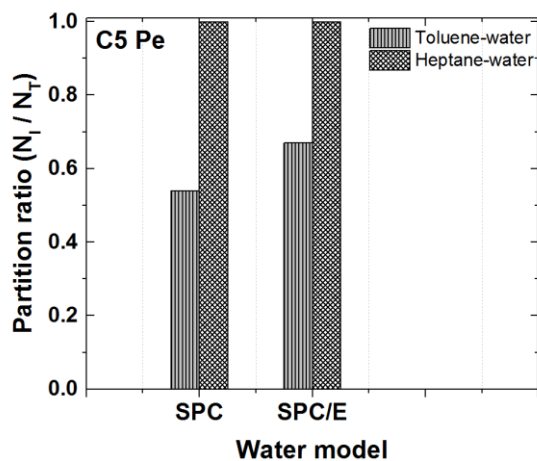


Figure A.2 Partition ratio of the C5 Pe molecules in oil-water (SPC or SPC/E) systems averaged over the last 2 ns of the simulation time at 298 K.

The hydrogen bonding between C5 Pe and water (SPC and SPC/E) are also calculated in this section to examine the sensitivity of the water model in the system (see Table A1). The results show that SPC and SPC/E gave comparable results, indicating that both SPC and SPC/E water models are reasonable to use simultaneously in our study. The sensitivity and applicability of the SPC model of water in our current study was also tested further by carrying out two simulations on pure toluene-water and pure heptane-water systems (without C5 Pe molecules). The simulations were run for 10 ns to calculate toluene-water and heptane-water interfacial tension (IFT) using the SPC model of water. At ambient temperature, the calculated interfacial tension of 36.8 and 47.0 mN/m is in reasonable agreement with the previously published experimental value of 36.1 and 50.2 mN/m for the toluene-water and heptane-water interface, respectively.²²² The computational study reported earlier also confirmed that the hydrocarbon and SPC/E model of water could reasonably reproduce the bulk and interfacial properties of the simulated systems.²²² The IFTs of heptane with the SPC/E water are around 50 mN/m, whereas the aromatics with SPC/E water are around 35 mN/m.²²²

Table A.1 The average number of intermolecular hydrogen bonds per C5 Pe molecule (N_{H-Bond}) at 298 K temperature and 1 bar over the last 2 ns simulation time

C5 Pe molecules	toluene-water system	heptane-water system
	N_{H-Bond}	N_{H-Bond}
SPC	1.3 ± 0.1	2.6 ± 0.1
SPC/E	1.4 ± 0.2	2.7 ± 0.3